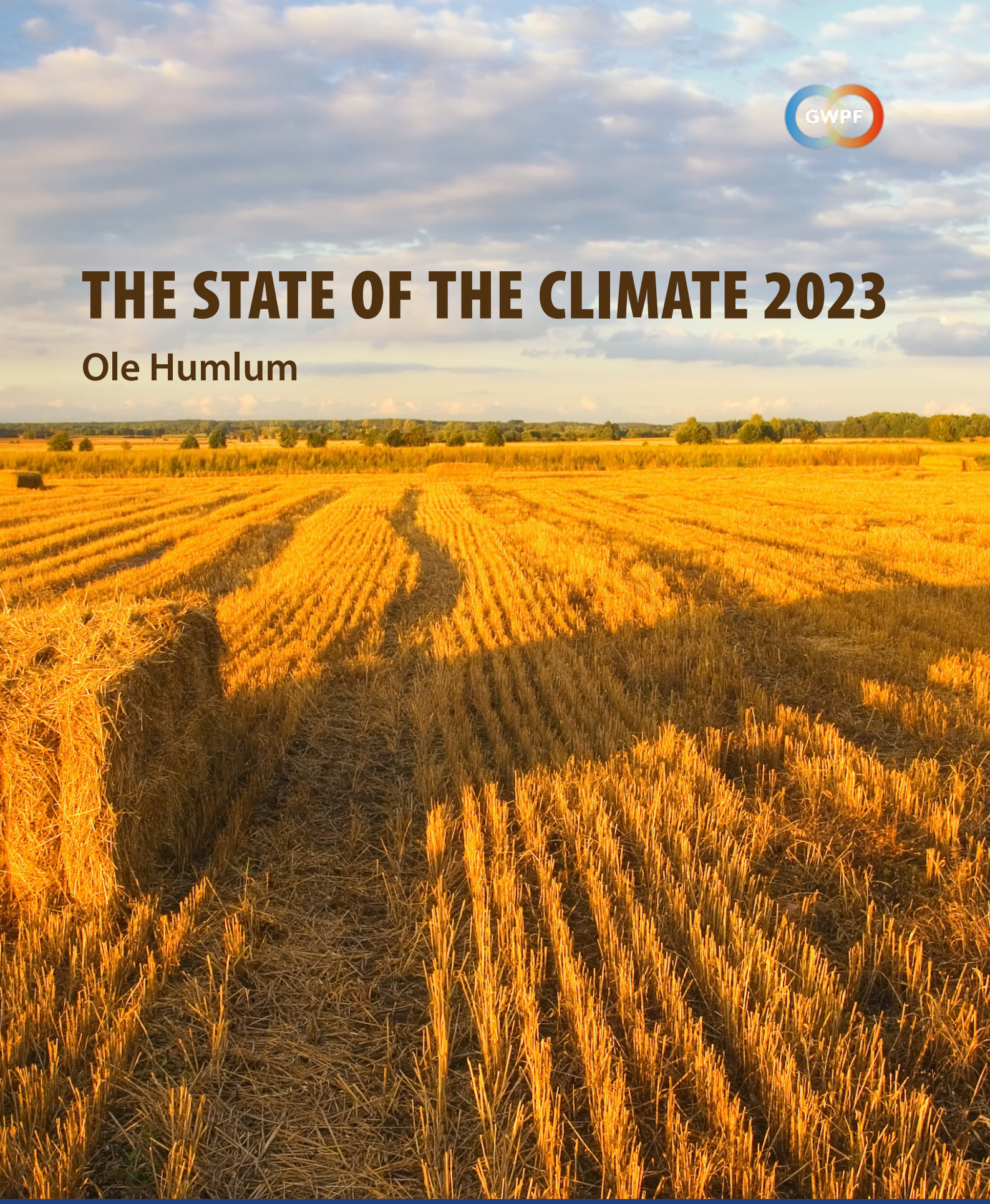

THE STATE OF THE CLIMATE 2023

Ole Humlum

The Global Warming Policy Foundation
Report 61

The State of the Climate 2023
Ole Humlum
Report 61, The Global Warming Policy Foundation

About the author

Ole Humlum is former Professor of Physical Geography at the University Centre in Svalbard, Norway, and Emeritus Professor of Physical Geography, University of Oslo, Norway.

Contents

THE STATE OF THE CLIMATE 2023

Ole Humlum

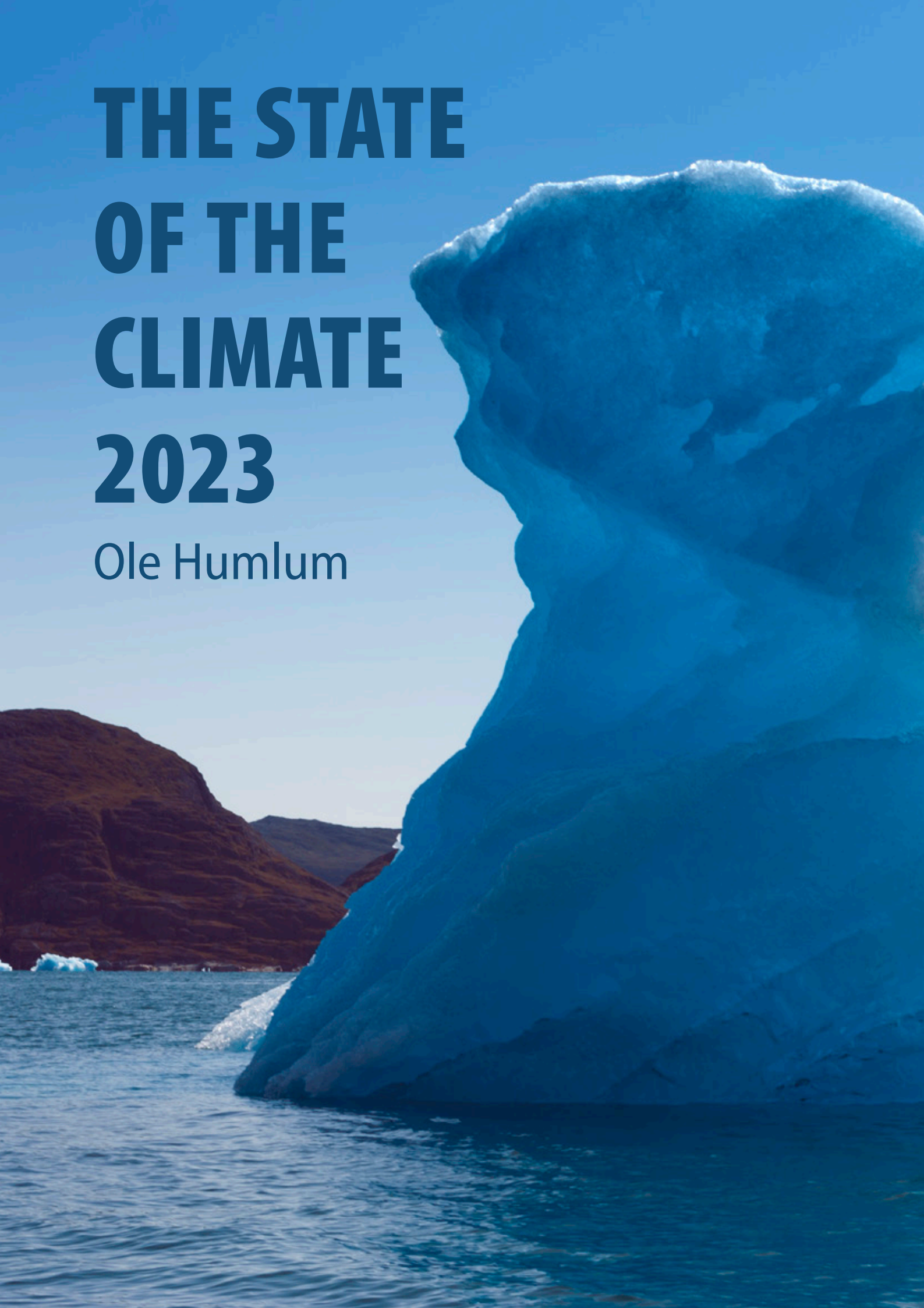

1. Introduction

This report is written for people wishing to form their own opinion on issues relating to climate. Its focus is on publicly available observational datasets, and not on the output of numerical models, although there are a few exceptions, such as Figure 42. References and data sources are listed at the end.

The observational data presented here reveal a vast number of natural variations, some of which appear in more than one series. The existence of such natural climatic variations is not always fully acknowledged, and therefore generally not considered in contemporary climate conversations. The drivers of most of these climatic variations are not yet fully understood, but should represent an important focus for climatic research in future.

In this report, meteorological and climatic observations are described according to the following overall structure: atmosphere, oceans, sea level, sea ice, snow cover, precipitation, and storms. Finally, in the last section, the observational evidence as at 2023 is briefly summarised.

2. Ten facts about the year 2023

1. Air temperatures in 2023 were the highest on record (since 1850/1880/1979, according to the particular data series). Recent warming is not symmetrical, but is mainly seen in the Northern Hemisphere (Figures 1 and 13).

2. Arctic air temperatures have increased during the satellite era (since 1979), but Antarctic temperatures remain essentially stable (Figure 14).

3. Since 2004, globally, the upper 1900 m of the oceans has seen net warming of about 0.037°C. The greatest warming (of about 0.2°C) is in the uppermost 100 m, and mainly in regions near the Equator, where the greatest amount of solar radiation is received (Figure 28).

4. Since 2004, the northern oceans (55–65°N) have, on average, experienced a marked cooling down to 1400 m depth, and slight warming below that (Figure 29). Over the same period, the southern oceans (55–65°S) have, on average, seen some warming at most depths (above 1900 m), but mainly near the surface.

5. Sea level globally is increasing at about 3.4 mm per year or more according to satellites, but only at 1–2 mm per year according to coastal tide gauges (Figures 39 and 41). Local and regional sea-level changes usually deviate significantly from such global averages.

6. Global sea-ice extent remains well below the average for the satellite era (since 1979). Since 2018, however, it has remained quasi-stable, perhaps even exhibiting a small increase (Figure 43).

7. Global snow cover has remained essentially stable throughout the satellite era (Figure 47), although with important regional and seasonal variations.

8. Global precipitation varies from more than 3000 mm per year in humid regions to almost nothing in deserts. Global average precipitation exhibits variations from one year to the next, and from decade to decade, but since 1901 there has been no clear overall trend (Figure 57).

9. Storms and hurricanes display variable frequency over time, but without any clear global trend towards higher or lower values (Figure 51).

10. Observations confirm the continuing long-term variability of average meteorological and oceanographic conditions, but do not support the notion of an ongoing climate crisis.

3. Air temperatures

The spatial pattern of global surface air temperatures in 2023

The global average surface air temperature for 2023 was the highest on record for all databases considered in this report (Figure 1). The year was affected by a warm El Niño episode (Pacific Ocean; see Section 5).

The Northern Hemisphere was characterised by regional temperature contrasts, especially north of 30°N. The most pronounced temperature events were the high average temperatures seen in Canada and in parts of western Russia. In contrast, the western USA, much of the North Atlantic, northern Europe, Siberia, and Alaska had relatively low average temperatures (compared to the last 10 years).

In the Arctic, the Canadian and Russian sectors were relatively warm, while the Greenland, Atlantic and Siberian sectors were relatively cool (Figure 2a).

Near the Equator, surface air temperatures were generally above the average for the previous 10 years, reflecting the ongoing El Niño episode in the Pacific Ocean. This explains 2023's high average global temperature; no less than 50% of the planet's surface is located between 30°N and 30°S.

In the Southern Hemisphere, average surface air temperatures were near or below the average for the previous 10 years. In particular, South America and most of southern Africa and Australia were cool.

Above the oceans, temperatures were near or below the 10-year average, with the exception of the southern parts of the South Atlantic, which were relatively warm.

The ocean around the Antarctic continent was generally characterised by relatively high annual surface air temperatures in 2023 (Figure 2b). Only the ocean beyond parts of West Antarctica was relatively cold. Most of the Antarctic continent was relatively cold. Only parts of the Atlantic sector of East Antarctica were relatively warm.

The influence of the Hunga Tonga-Hunga Ha'apai eruption on 2023 meteorological conditions is still uncertain. The eruption, which occurred in the southern Pacific Ocean in January 2022,

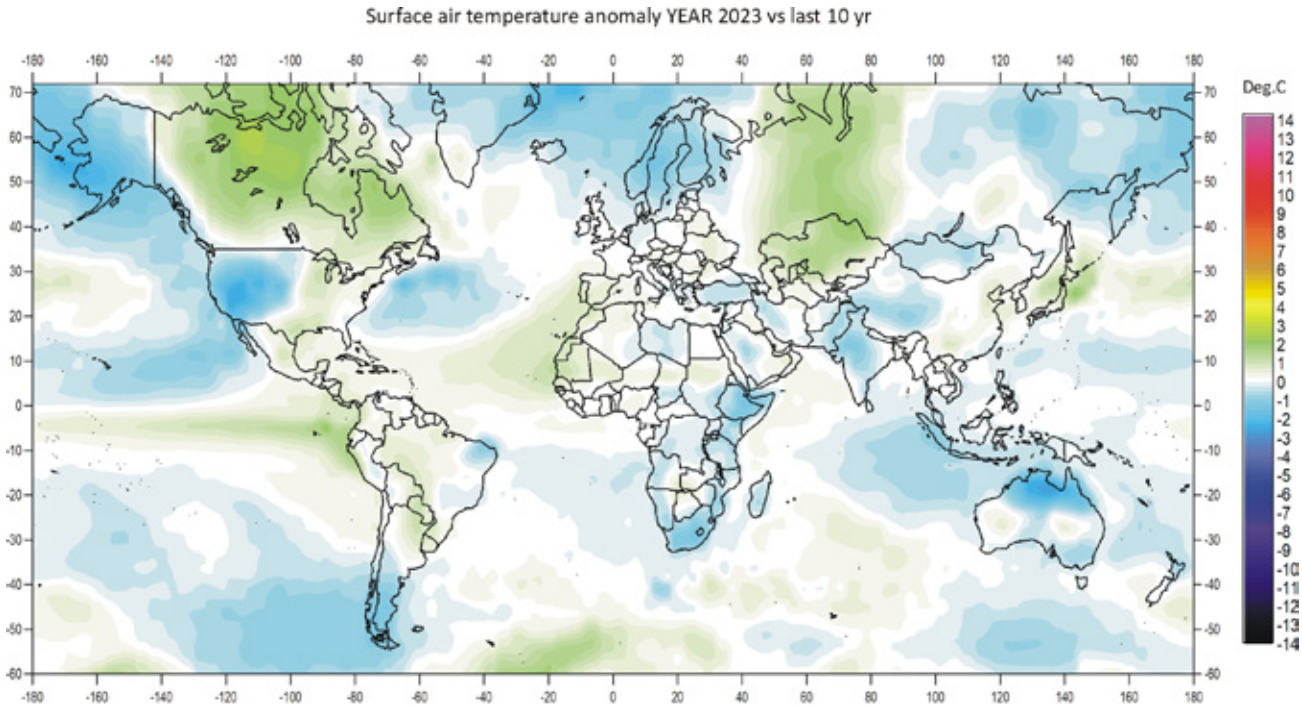

Figure 1: 2023 surface air temperatures compared to the average for the previous 10 years.

Green-yellow-red colours indicate areas with higher temperature than the average, while blue colours indicate lower than average temperatures. Data source: Remote Sensed Surface Temperature Anomaly, AIRS/Aqua L3 Monthly Standard Physical Retrieval 1-degree x 1-degree V006 (https://airs.jpl.nasa.gov/), obtained from the GISS data portal (https://data.giss.nasa.gov/gistemp/maps/).

released an enormous plume of water vapour into the Stratosphere, but there is little evidence that this had an influence on atmospheric temperatures (see also Figure 16).

Summing up, global average surface air temperatures in 2023 were at record highs relative to long instrumental records (since 1850), a result of the still ongoing El Niño episode. In contrast, the two previous years, 2021 and 2022, were influenced by a cold La Niña in the Pacific Ocean. Thus the global surface air temperature record in 2023 continues to be significantly influenced by oceanographic phenomena.

In the maps displayed in Figures 1 and 2, a 10-year reference period is used for comparison. A 30-year reference period is often used for such comparisons, and this is supposed to be updated through to the end of each decade ending in zero (1951–1980, 1961–1990, etc). The concept of a normal climate goes back to the first part of the 20th century. At that time, and until about 1960, it was generally believed that for all practical purposes climate could be considered constant, no matter how obvious year-to-year fluctuations might have been. Meteorologists therefore decided to work with an average or 'normal' climate, defined by a 30-year period, named the 'normal' period, assuming that it was of sufficient length to iron out all intervening variations. In fact, a 30-year normal is an unfortunate choice, because several observational datasets demonstrate that there are global climate parameters that are influenced by periodic changes of 50–70 years' duration (see, e.g., comments to Figures 8–10 and 52). The traditional 30-year reference period is roughly half this time interval, and is therefore most unsuitable as a reference period. Deciding the optimal length of a reference period is clearly not straightforward, and requires knowledge of the natural cycles embedded in the data. The decadal approach taken for the maps here corresponds to the memory span for many people, and is also adopted as reference period by other institutions, such as the Danish Meteorological Institute.

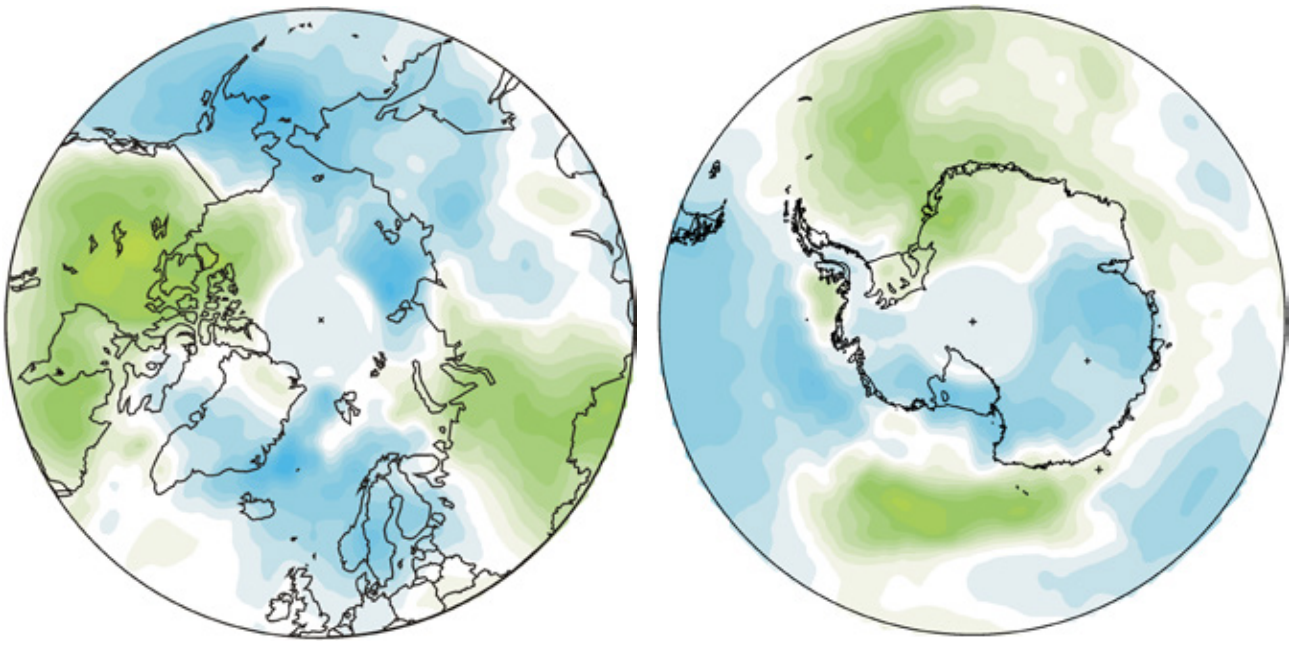

Figure 2: 2023 polar surface air temperatures compared to the average for the previous 10 years.
Details as per Figure 1.

Global monthly lower Troposphere air temperature since 1979

The satellite temperature records for the lower Troposphere show temperature spikes associated with the 2015–16 and the 2019–20 El Niños, with temperature drops after each, due to the succeeding La Niñas (Figure 3). The latest development is a renewed temperature increase since May–June 2023, due to a new and still ongoing El Niño (Figure 29). Many El Niños culminate during the Northern Hemisphere winter. From the two diagrams in Figure 4, however, it looks as if the present episode terminated somewhat earlier, during the Northern Hemisphere autumn and early winter of 2023.

The overall temperature variation in the diagrams (Figures 3 and 4) is similar for the two data series, but the overall temperature increase from 1979 to 2023 is larger for the RSS record than for the UAH one (Figure 5). Before the rather substantial adjustment of the RSS series in 2017, the temperature increase was almost identical for the two datasets. Figure 4 illustrates similarities and differences between them.

A Fourier analysis (not shown here) reveals that both the UAH and the RSS records have a significant 3.6-year oscillation.

(a) UAH

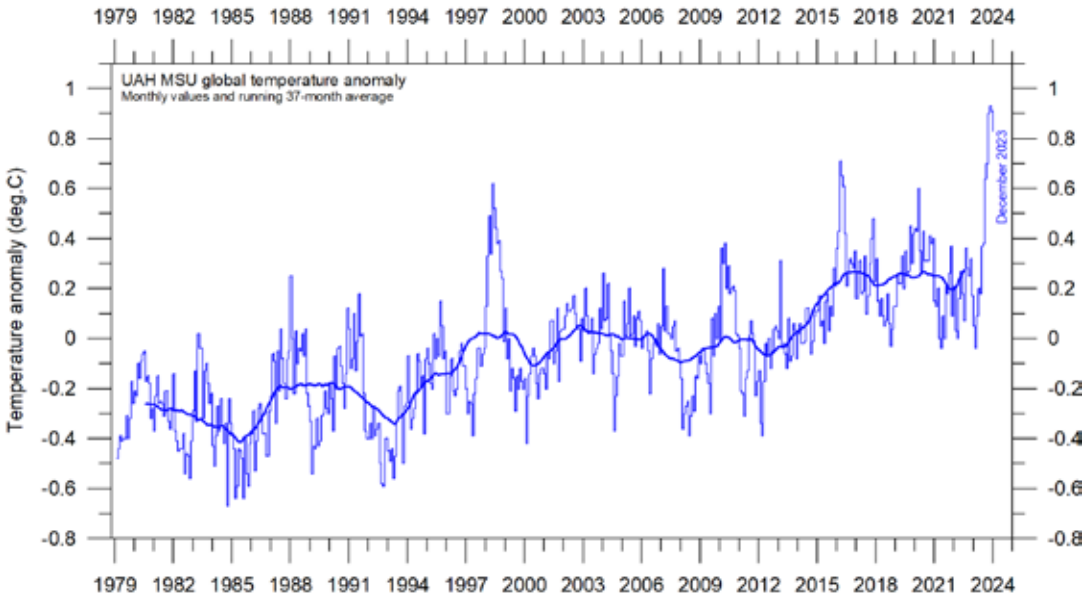

(b) RSS

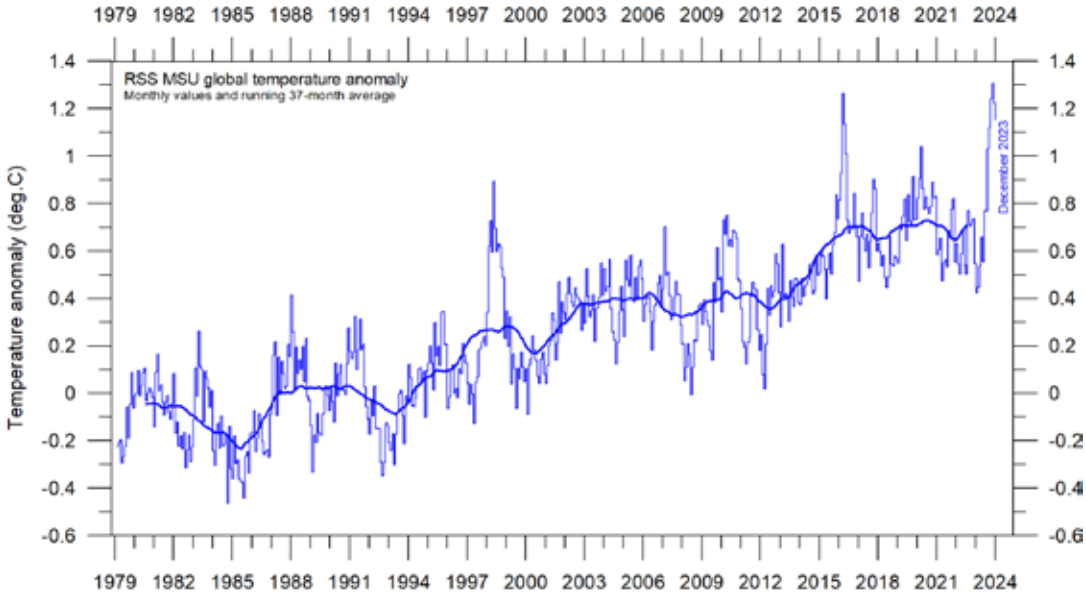

Figure 3: Global monthly average lower troposphere temperatures since 1979.

The chart represents temperatures at around 2 km altitude. (a) UAH and (b) RSS. The thick line is the simple running 37-month average, approximately corresponding to a 3-year running average.

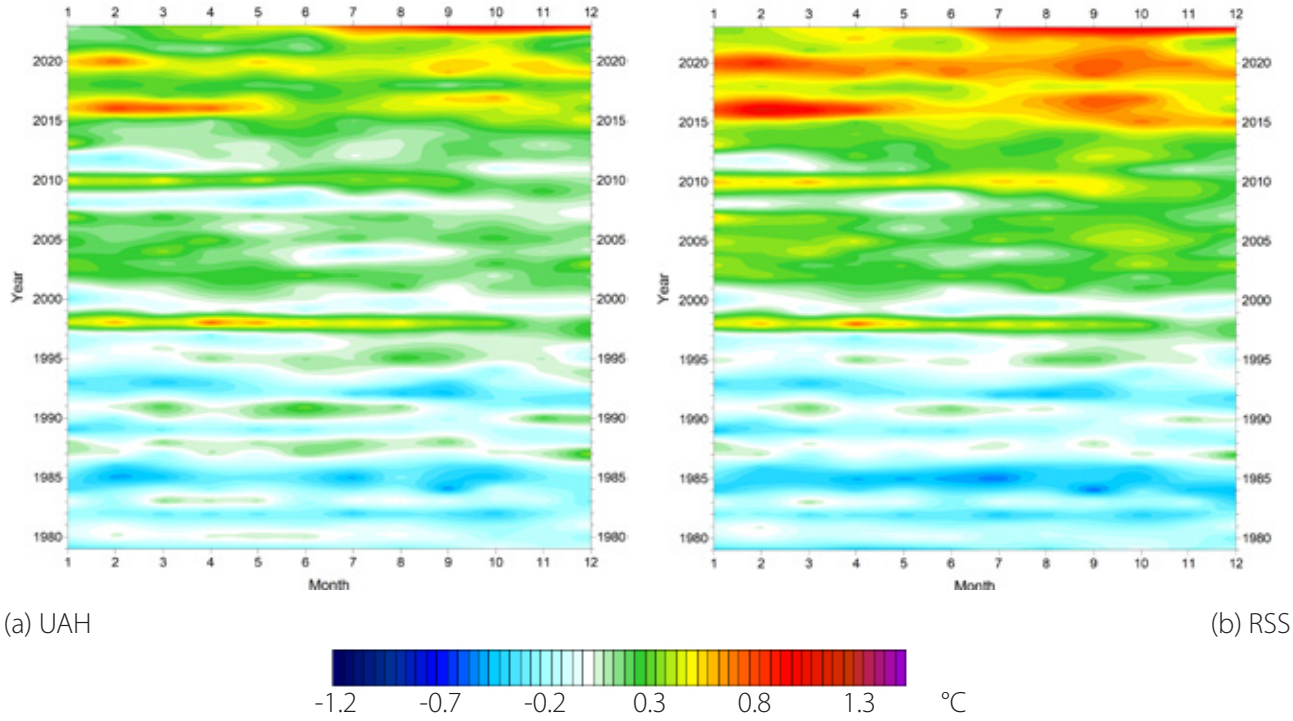

Figure 4: Temporal evolution of global lower troposphere temperatures since 1979.

Temperature anomaly versus 1979–2008. The effects of the El Niños of 1998, 2010,2015–2016 and 2023 are clearly visible as 'warm' bands, as is the tendency for many El Niños to culminate during the Northern Hemisphere winter. As the different temperature databases use different reference periods, the series have been made comparable by setting their individual 30-year average for 1979–2008 to zero.

Lower Troposphere: annual means

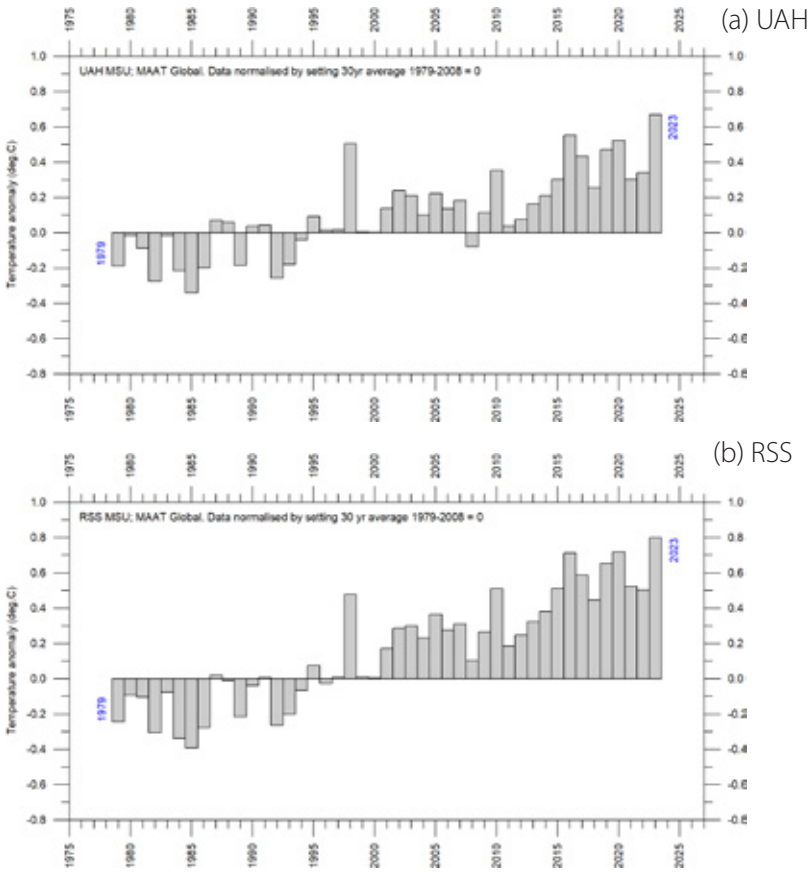

Figure 5: Global mean annual lower troposphere air temperatures since 1979.

Satellite data interpreted by (a) the University of Alabama at Huntsville (UAH), and (b) Remote Sensing Systems (RSS), both in the USA.

Global mean annual lower Troposphere air temperature since 1979

Figure 6: Global mean monthly surface air temperatures since 1979.

(a) HadCRUT5 (b) NCDC (c) GISS. The thick line is the simple running 37-month average, nearly corresponding to a running 3-year average.

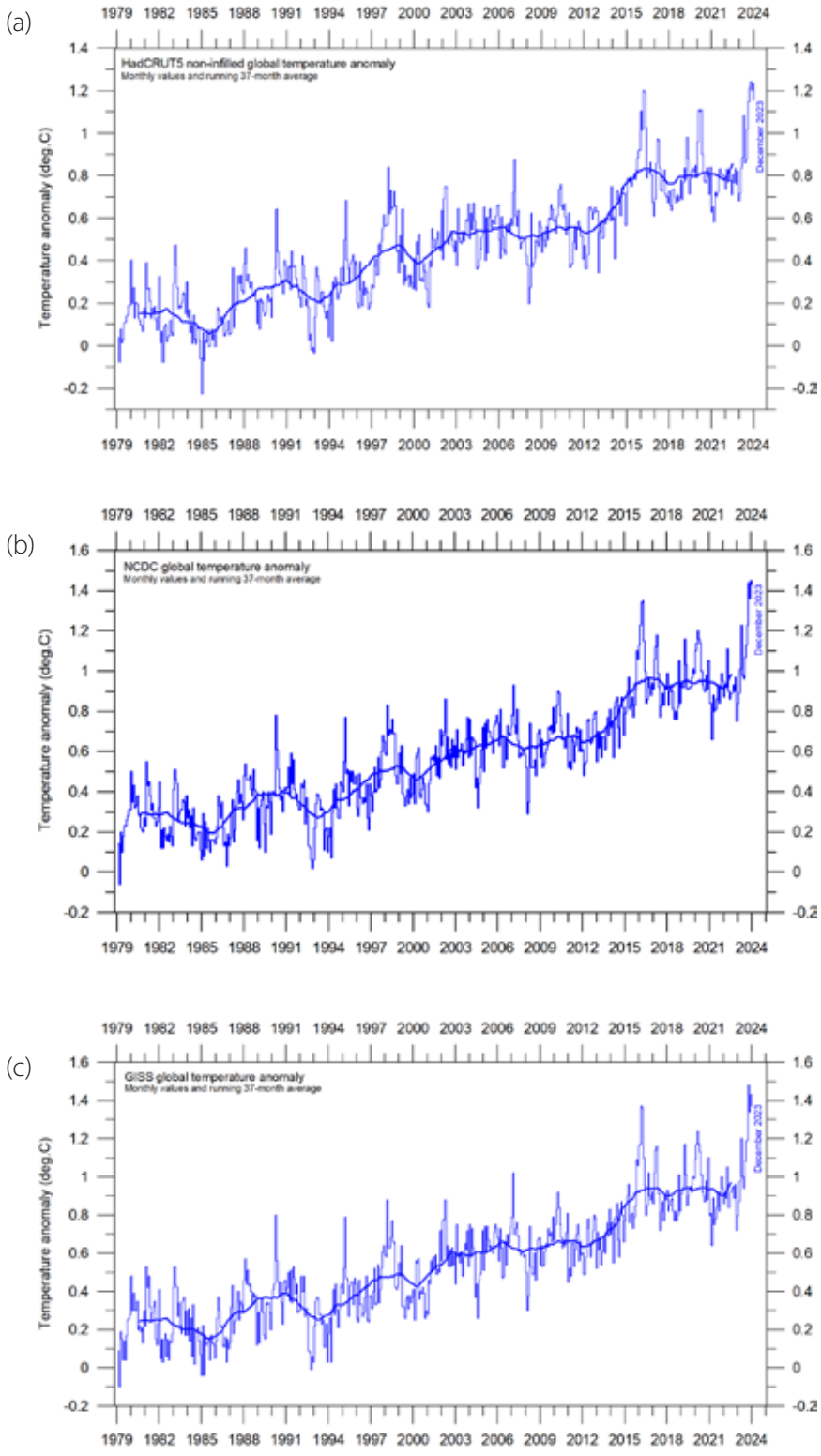

Global monthly surface air temperature since 1979

All three surface air temperature records clearly show variations in concert with El Niños and La Niños playing out in the Pacific Ocean (Section 5). The latest development is a renewed temperature increase since May–June 2023 due to a new and still ongoing El Niño. Global surface air temperature is greatly influenced by this oceanographic phenomenon. Figure 7 illustrates similarities and differences between the three data series.

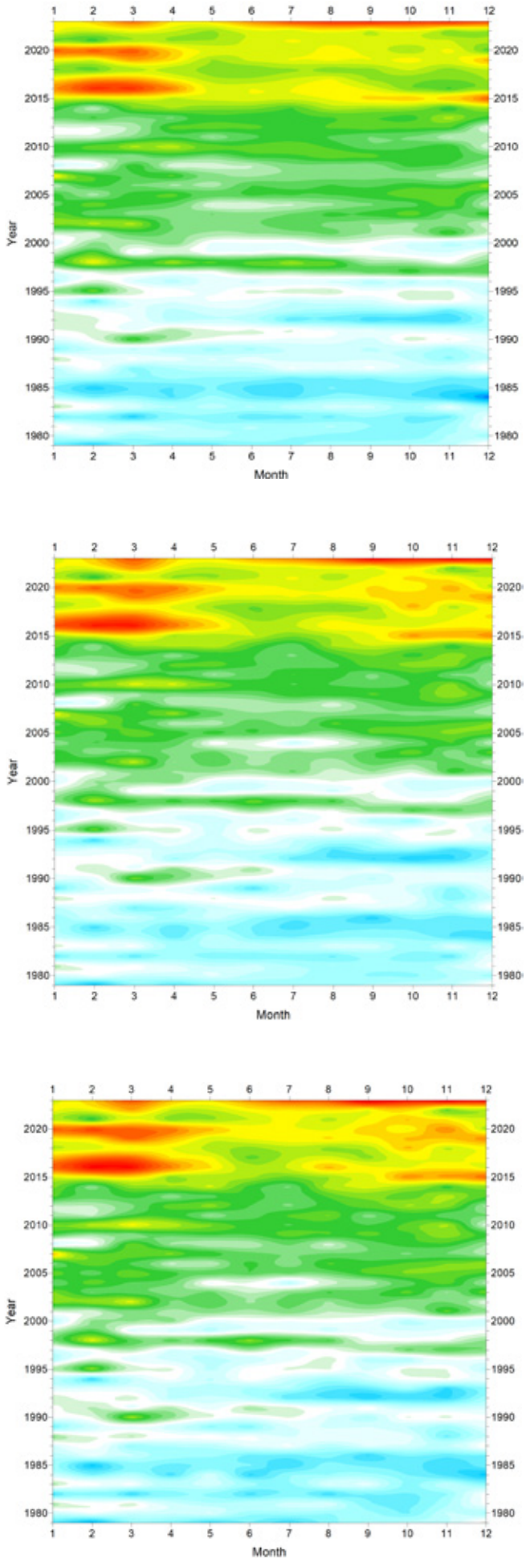

Figure 7: Temporal evolution of global mean monthly surface air temperatures.

(a) HadCRUT (b) NCDC (c) GISS. Temperature anomaly (°C) versus 1979–2008. As the different temperature databases are using different reference periods, the series have been made comparable by setting their individual 30-year averages for 1979–2008 to zero.

Global mean annual surface air temperature

All three average surface air temperature estimates show that 2023 was the warmest year on record. The year was influenced by a strong El Niño in the Pacific Ocean (see Section 5).

A Fourier analysis (not shown here) reveals that both the HadCRUT and NCDC records have a significant 74-year oscillation, while the equivalent period in the GISS record is 64 years long.

(a) HadCRUT

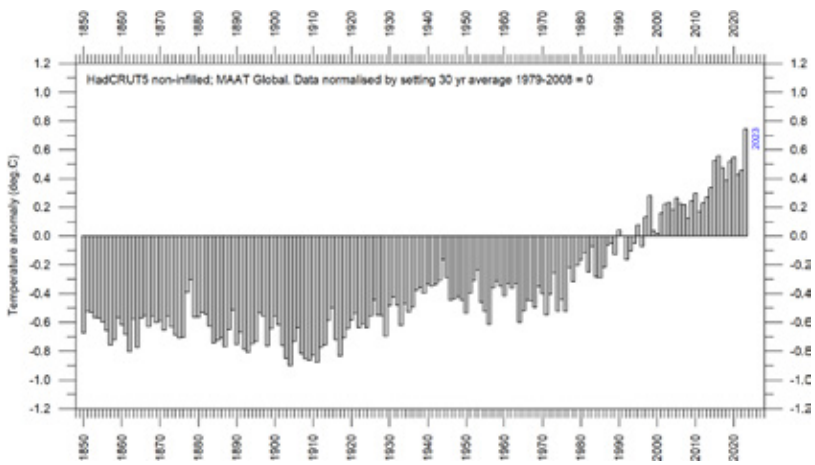

(b) NCDC

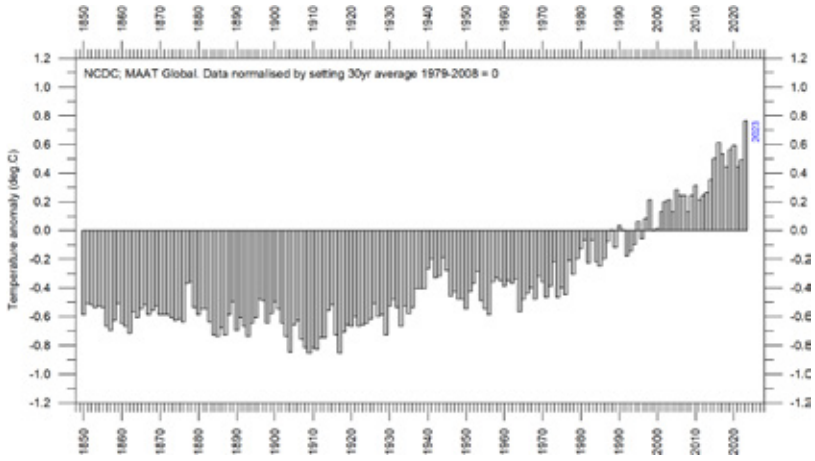

(c) GISS

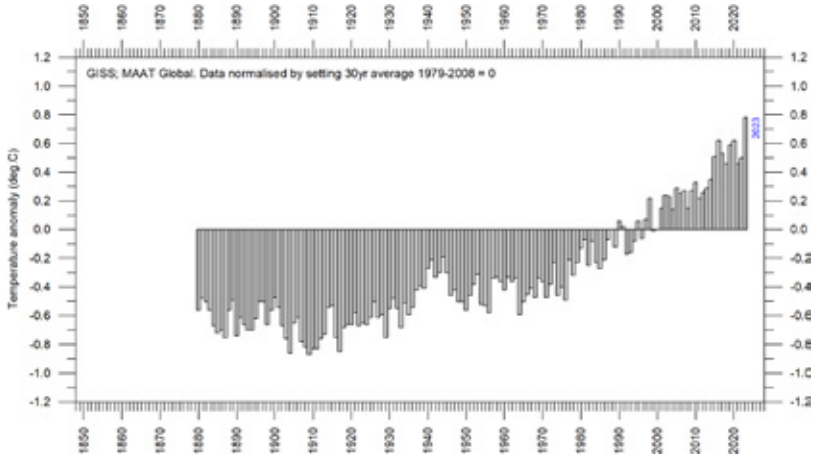

Figure 8: Global mean annual surface air temperatures.

(a) HadCRUT (b) NCDC (c) GISS temperature anomaly (°C) versus 1979–2008.

Reflections on the margin of error, constancy, and quality of temperature records

The surface records represent a blend of sea-surface data, collected from ships or by other means, and data from land stations, of partly unknown quality and unknown representativeness for their region. Many of the land stations have also been moved geographically during their periods of operation, instrumentation has been changed, and most have been influenced by ongoing changes in their surroundings (vegetation, buildings, and so on).

The satellite temperature records have their own problems, but these are generally of a more technical nature and therefore are probably easier to rectify. In addition, the temperature sampling by satellites is more regular and complete on a global basis than in the surface records. It is also important to note that the sensors on satellites measure temperature directly, by emitted radiation, while most modern surface temperature measurements are indirect, using electronic resistance.

All temperature records are affected by at least three different sources of error, which differ between the individual station records used for calculation of a global average temperature estimate. 1) The *accuracy* is the degree of closeness of measurements to the actual (true) values. 2) The *precision* is the degree to which repeated measurements under unchanged conditions show an identical value, true or not. In addition, we have 3) the measurement *resolution*, which is the smallest change in temperature that produces a response in the instrument. Combined, these represent the *margin of error* for temperature records. The margin of error has been thoroughly examined and is probably at least ±0.1°C for modern average global surface air temperatures, and feasibly higher for older data. This often makes it statistically impossible to classify any year as representing a global temperature record: several other years may be within the ±0.1°C range of the value considered.

In addition, two other issues relating to the margin of error for surface records have not been widely discussed. First, as an example, it will not be possible to conclude much about the actual value of the December 2023 global surface air temperature before March–April 2024, when data not yet reported (in January 2024) are finally incorporated into the databases. This is what might be described as the effect of *delayed reporting*. Secondly, surface air temperature records often display *administrative changes* over time, which makes it even more difficult to draw conclusions about the significance of any recently reported values.

The administrative issue arises from the apparently perpetual adjustments applied to the temperature records. These mean that the value reported as the average global temperature for a particular point in time will gradually change in the years following its first reporting. These adjustments appear to have little or nothing to do with delayed reporting of missing data. Of particular concern are the GISS and NCDC databases, which have changes applied to periods far back in time, even before the year 1900, for which the possibility of reporting delays is exceedingly small. Most likely, such administrative changes are the result of alterations in the way average monthly values are calculated, in an attempt to enhance the resulting record.

As an example, Figure 9 shows the accumulated effect since May 2008 of administrative changes in the GISS global surface air temperature record, which extends back to 1880. This is just an example taken from this particular record to illustrate the effect; any of the other datasets would show something similar. The overall net effect of adjustments applied to the GISS record since May 2008 is a warming of the early and modern part of the record and cooling of the period in between, roughly from 1900 to 1970. Several of the net changes introduced since 2008 are quite substantial, ranging from about +0.20 to –0.20°C.

To illustrate the effect of administrative changes in a different way, Figure 10 shows how the global surface air temperature for January 1910 and January 2000 (selected two months indicated in Fig. 15) has changed since May 2008, again exemplified by the GISS record.

The administrative uplift to the global surface air temperature (GISS) from January 1915 to January 2000 has grown from 0.45°C (as reported in May 2008) to 0.67°C (as reported in January 2024). This

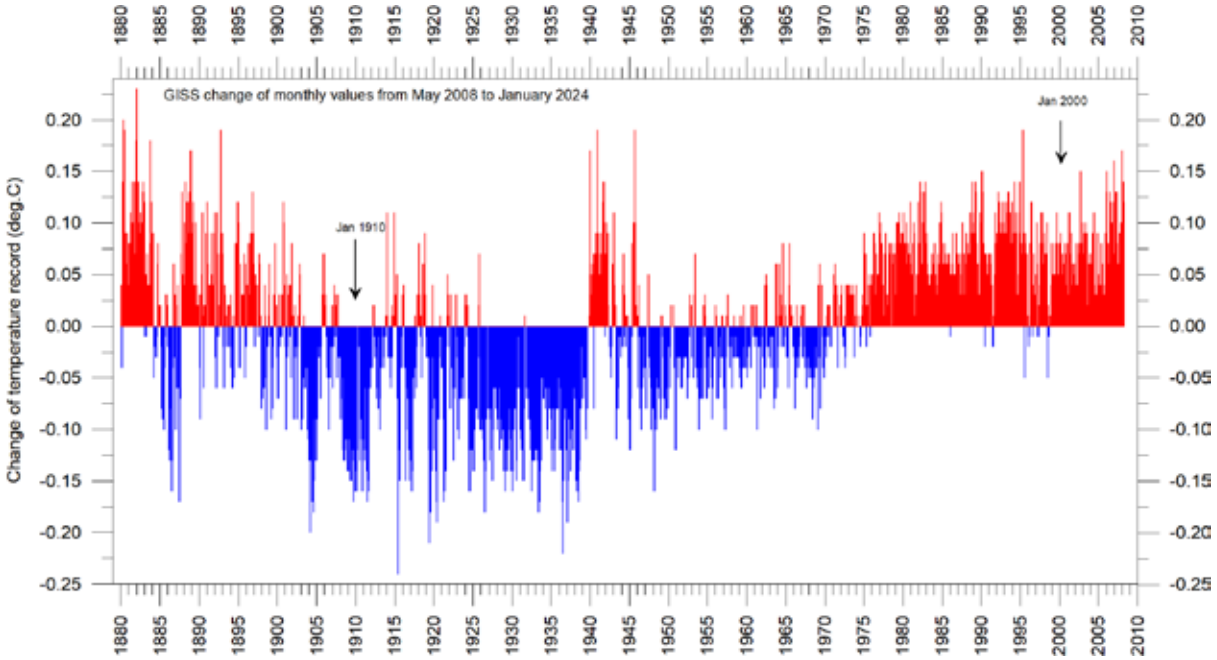

Figure 9: Adjustments since 17 May 2008 in the GISS surface temperature record.

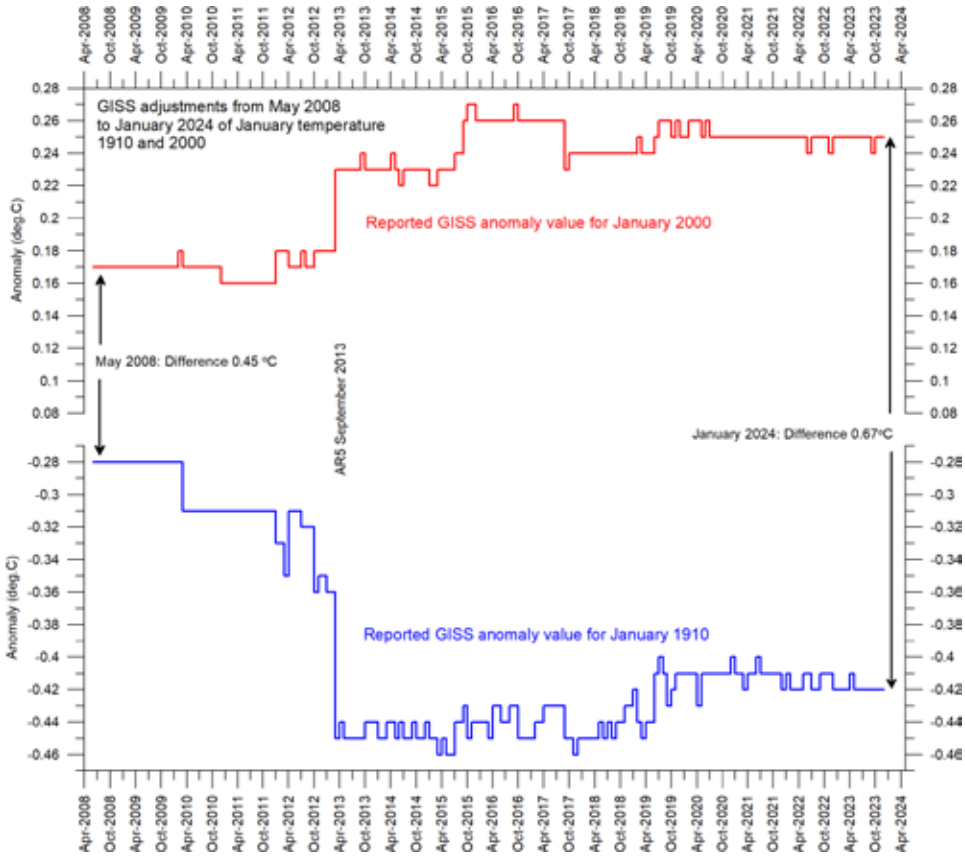

Figure 10: Adjustments made since May 2008 to GISS anomalies for the months January 1910 and January 2000.

'AR5' indicates the publication of IPCC report AR5 Climate Change 2013: The Physical Science Basis.

represents an increase of about 49%, meaning that about half of the apparent global temperature increase from January 1910 to January 2000 (as reported by GISS in January 2024) is due to administrative changes to the original data. Clearly such adjustments are important when evaluating the overall quality of the various temperature records, along with other standard sources of error. In fact, the magnitude of administrative changes may often exceed the formal margin of error.

For obvious reasons, as the past does not change, any record undergoing continuous change cannot describe the past correctly all the time. Frequent and large corrections in a database invariably signal a fundamental uncertainty about the correct values.

Nevertheless, everybody interested in climate science should acknowledge the efforts put into maintaining the different temperature databases referred to in the present report. At the same time, however, it is also important to realise that all temperature records cannot be of equal scientific quality. The simple fact that they all, to some degree, differ shows that they cannot all be completely correct.

Comparing surface and lower Troposphere temperatures

In general, there is fair agreement between the the surface and satellite records, as shown in Figure 11. However, before a major adjustment of the RSS satellite record in 2017, there was a significant discrepancy, with the average in the surface records drifting in a warmer direction than the average of satellite records. Again, this illustrates the importance of ongoing administrative changes of the individual temperature records.

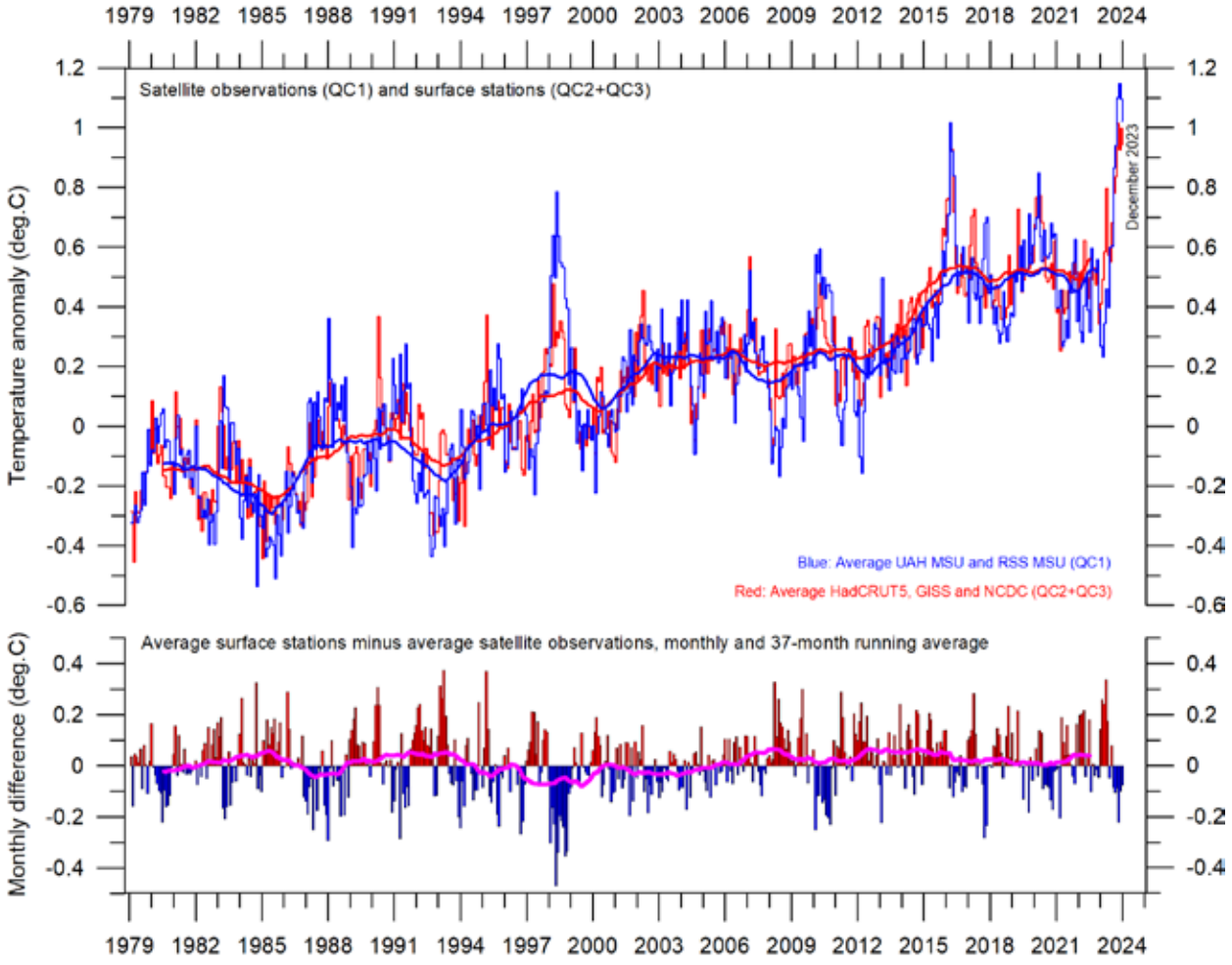

Figure 11: Surface temperatures versus lower Troposphere temperatures.

Average of monthly global surface air temperature estimates (HadCRUT, NCDC and GISS) and satellite-based lower Troposphere temperature estimates (UAH and RSS). The thin lines indicate the monthly value, while the thick lines represent the simple running 37-month average, nearly corresponding to a running 3-year average. The lower panel shows the monthly difference between surface air temperature and satellite temperatures. As the base period differs for the different temperature estimates, they have all been normalised by comparing to the average value of 30 years from January 1979 to December 2008.

Comparing temperature change over land and oceans; lower Troposphere air temperature

Since 1979, the lower Troposphere has warmed much more over land than over the oceans (Figure 12). There may be several reasons behind this, including differences in surface heat capacity, and variations in incoming solar radiation, cloud cover and land use.

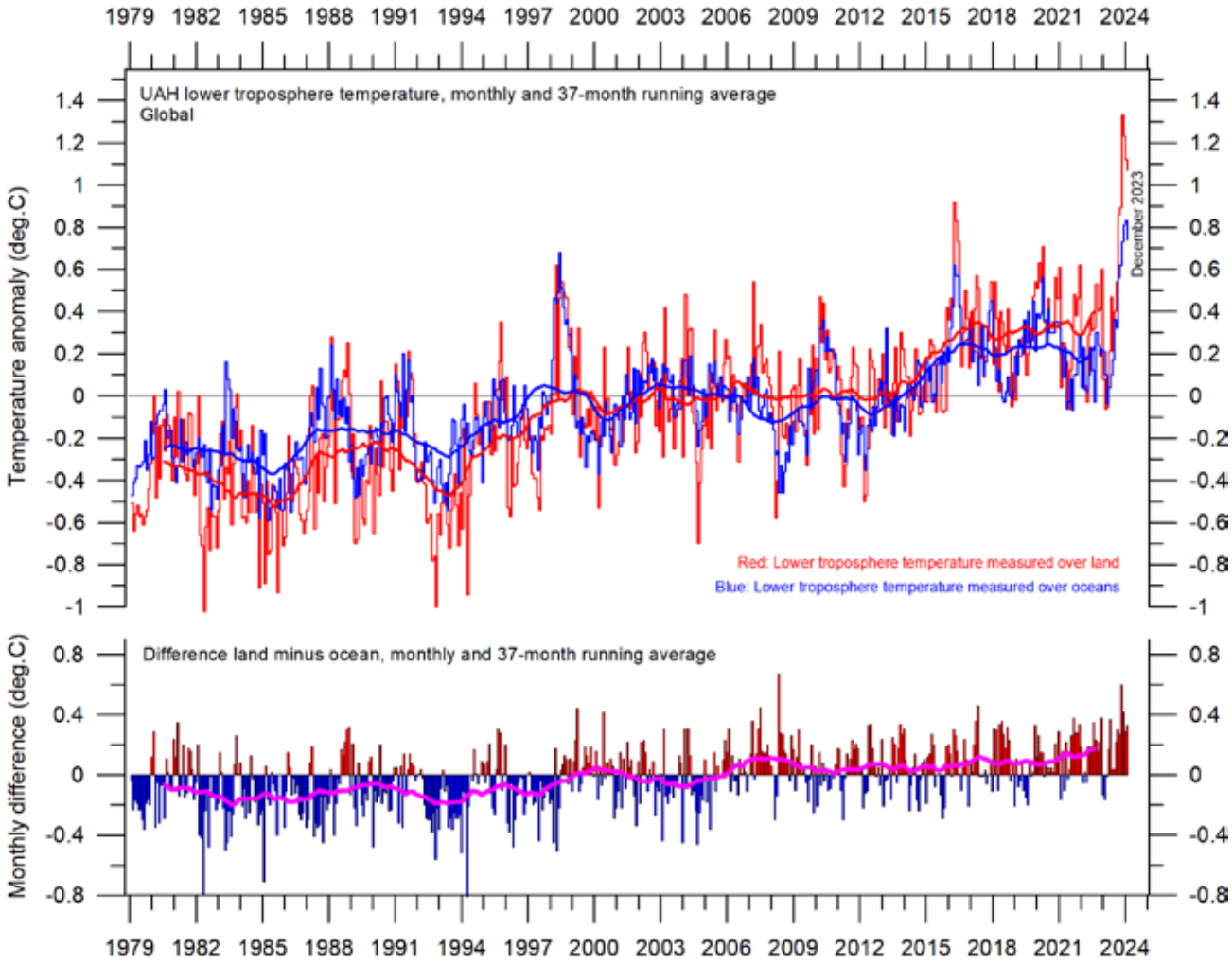

Figure 12: Lower Troposphere temperatures over land and ocean

Global monthly average lower troposphere temperature since 1979 measured over land and oceans, shown in red and blue, respectively, according to University of Alabama at Huntsville (UAH), USA. The thin lines represent the monthly average, and the thick line the simple running 37-month average, nearly corresponding to a running 3-year average.

Zonal air temperatures

Figure 13 shows that the 'global' warming seen since 1980 has predominantly been a Northern Hemisphere phenomenon. In addition, it mainly played out as two step changes: in 1994–1999 and 2015–2016. The first of these was, however, influenced by the Mount Pinatubo eruption of 1992–93 and the 1997 El Niño episode.

Figure 13 also reveals that the temperature effects of the strong El Niños of 1997 and 2015–16, as well as the recent one in 2023, spread to higher latitudes in both hemispheres, although with some delay. The effect was, however, mainly seen in the Northern Hemisphere, and only to lesser degree in the Southern Hemisphere. This is true in general of most temperature variations in the tropics, which are therefore clearly very important for understanding meteorological and climatic dynamics.

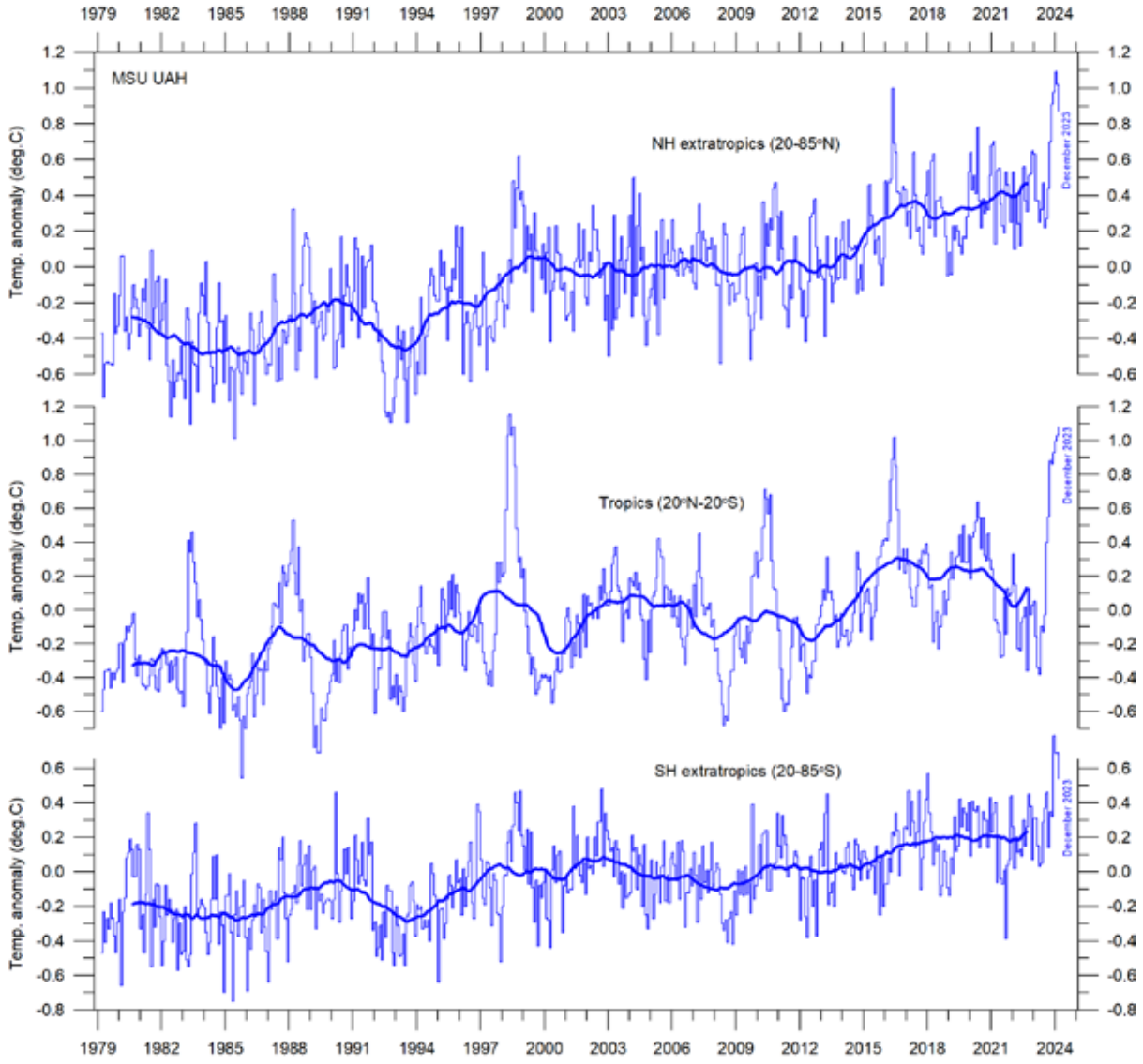

Figure 13: Zonal air temperatures.

Global monthly average lower troposphere temperature since 1979 for the tropics and the northern and southern extra-tropics, according to University of Alabama at Huntsville, USA. Thin lines: monthly value; thick lines: 3-year running mean.

Polar air temperatures

In the Arctic, warming was rapid in the period 1994–96, but slower subsequently (Figure 14). In 2016, however, temperatures peaked for several months, presumably because of oceanic heat given off to the atmosphere during the 2015–16 El Niño (Figure 25) and subsequently partly advected to higher latitudes. There was a small temperature decrease after 2016, but in 2023 a new temperature peak was seen, presumably derived from the ongoing El Niño.

In the Antarctic, temperatures have essentially remained stable since the onset of the satellite record in 1979. In 2016–17 and in 2023, a small temperature peak is visible in the monthly record and this might be interpreted as the subdued effect of El Niño episodes.

Arctic and Antarctic temperature peaks derived from El Niño episodes, as outlined above, are paradoxically due to heat ventilating out from the Pacific Ocean near the Equator. Polar temperature peaks result in increased radiation loss to space, and therefore represent incidents associated with cooling of the Earth, when considered in a broader context.

These developments are confirmed by the long polar surface air temperature series (Figure 15). At this station level, however, conditions specific for each site are apparent, demonstrating the amount of variability in temperatures around both poles.

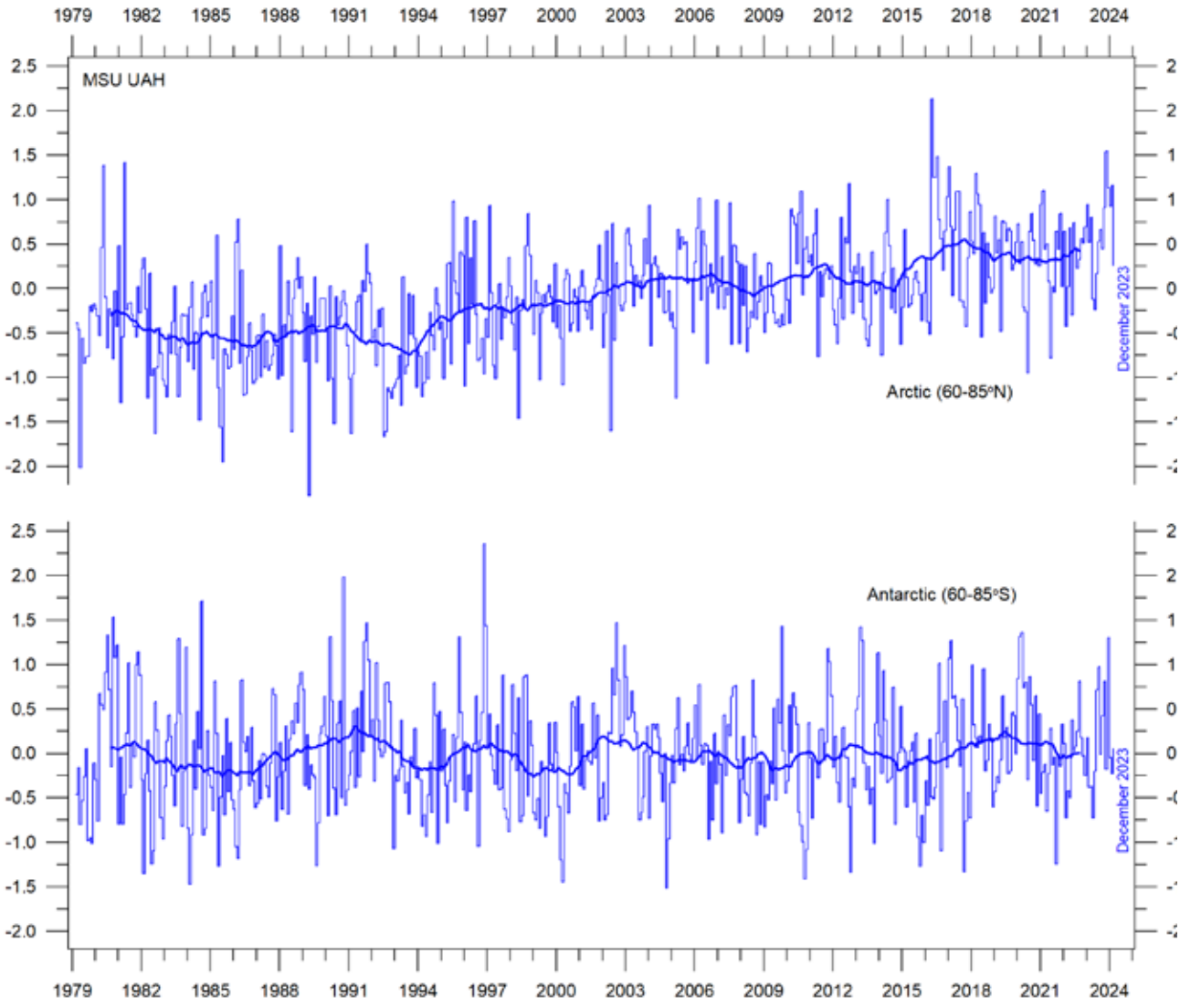

Figure 14: Polar temperatures

Global monthly average lower troposphere temperature since 1979 for the North and South Pole regions, according to University of Alabama at Huntsville (UAH), USA. Thick lines are the simple running 37-month average.

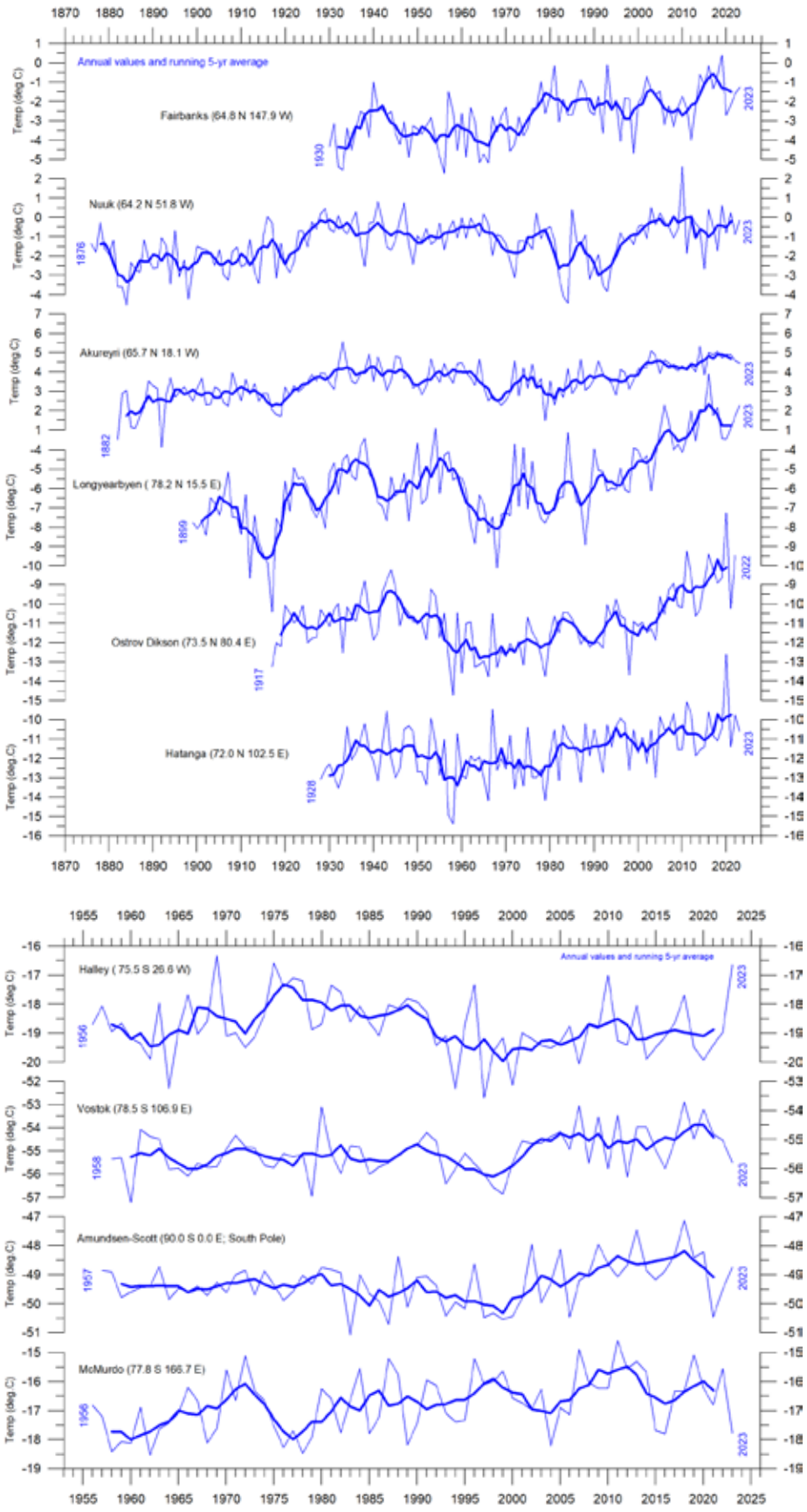

Figure 15: Long polar annual surface air temperature series

Annual values were calculated from monthly average temperatures. Almost unavoidably, some missing monthly data were encountered in some of the series. In such cases, the missing values were generated as either 1) the average of the preceding and following monthly values, or 2) the average for the month registered the preceding year and the following year. The thin blue line represents the mean annual air temperature, and the thick blue line is the running 5-year average. Data source: Goddard Institute for Space Studies (GISS)..

Temperatures by altitude

Changes in the vertical temperature profile of the atmosphere are interesting (Figure 16). One reason is that increasing Tropospheric temperatures and decreasing Stratospheric temperatures are two central results of the hypothesis that ascribes global warming to human-induced atmospheric CO_2 increases.

The temperature variations recorded in the lowermost Troposphere are generally reflected at higher altitudes, up to about 10 km altitude, including many individual troughs and peaks, such as the El Niño induced temperature spike of 2015–16, and the new El Niño beginning in 2023.

At high altitudes, near the Tropopause, the

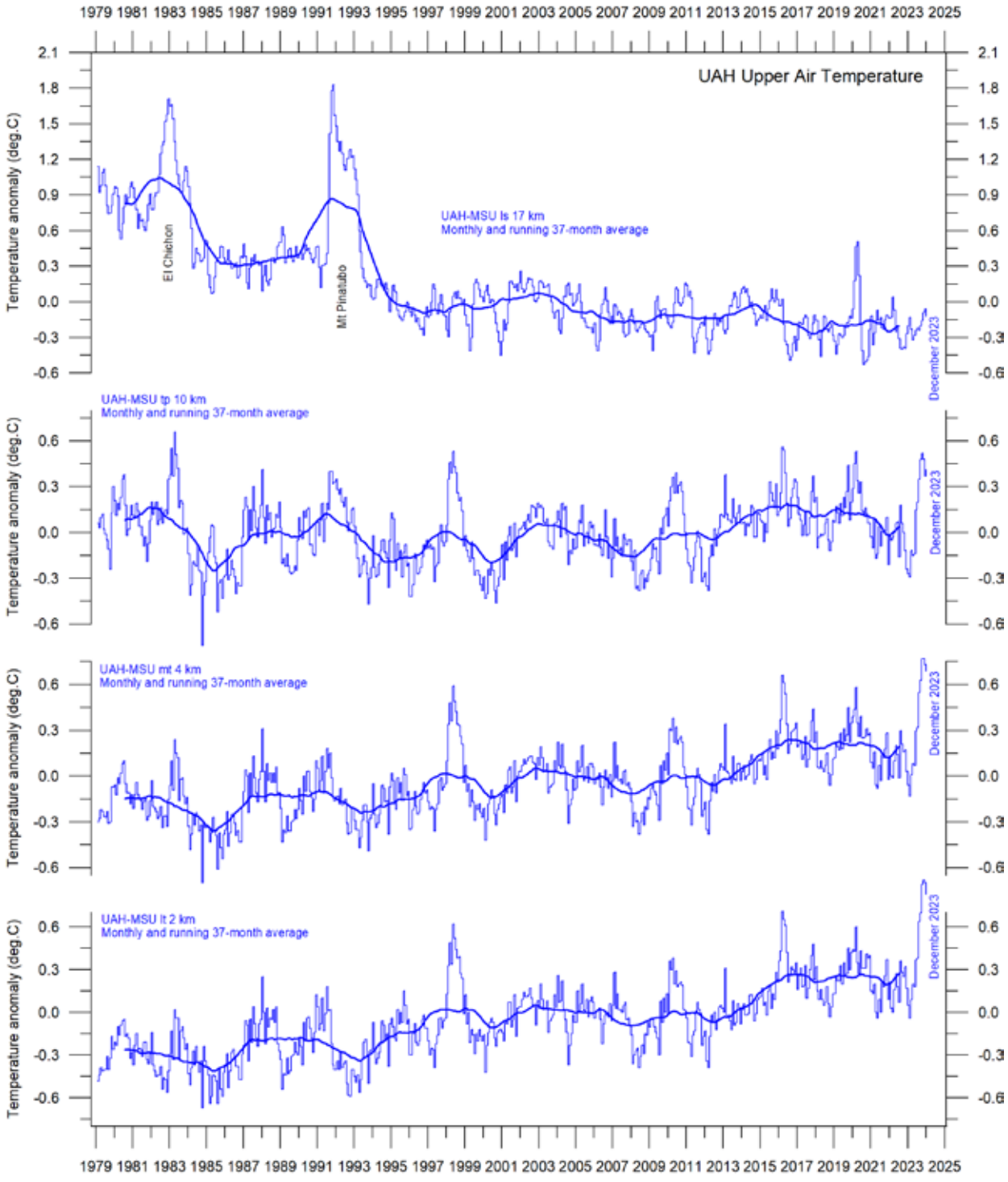

Figure 16: Global monthly average temperature at different altitudes

University of Alabama at Huntsville (UAH), USA. The thin lines represent the monthly average, and the thick line the simple running 37-month average, nearly corresponding to a running 3-year average

pattern of variations recorded lower in the atmosphere can still be recognised, but for the duration of the record (since 1979) there has been no clear trend towards higher or lower temperatures.

Higher in the atmosphere, in the Stratosphere, at 17 km altitude, two pronounced temperature spikes are visible before the turn of the century. Both can be related to major volcanic eruptions, as indicated in the diagram. The spike in 2020 occurs when major wildfires were playing out in Australia. Ignoring such marked spikes, however, until about 1995 the Stratospheric temperature record shows a persistent and marked decline, ascribed by several scientists to the effect of heat being trapped by CO_2 in the Troposphere below. However, the marked Stratospheric temperature decline essentially ends around 1995–96, and a long temperature plateau has characterised the Stratosphere since that time.

A Fourier analysis (not shown here) reveals that Tropospheric temperatures at around 2 and 4 km altitude exhibit a significant 3.6-year cycle. The same periodicity may also be seen at the Tropopause (~10 km altitude), but not in the Stratosphere at 17 km.

4. Atmospheric greenhouse gases

Water vapour

Water vapour (H_2O) is the most important greenhouse gas in the Troposphere. The highest concentration is found within a latitudinal range from 50°N to 60°S. The two polar regions of the Troposphere are comparatively dry. Water vapour is a much more important greenhouse gas than carbon dioxide, both because of its absorption spectrum and its higher concentration.

Figure 17 shows the specific atmospheric humidity to be stable or slightly increasing up to about 4–5 km altitude. At higher levels in the Troposphere (about 9 km), the specific humidity has been decreasing for the duration of the record, but with shorter variations superimposed on the

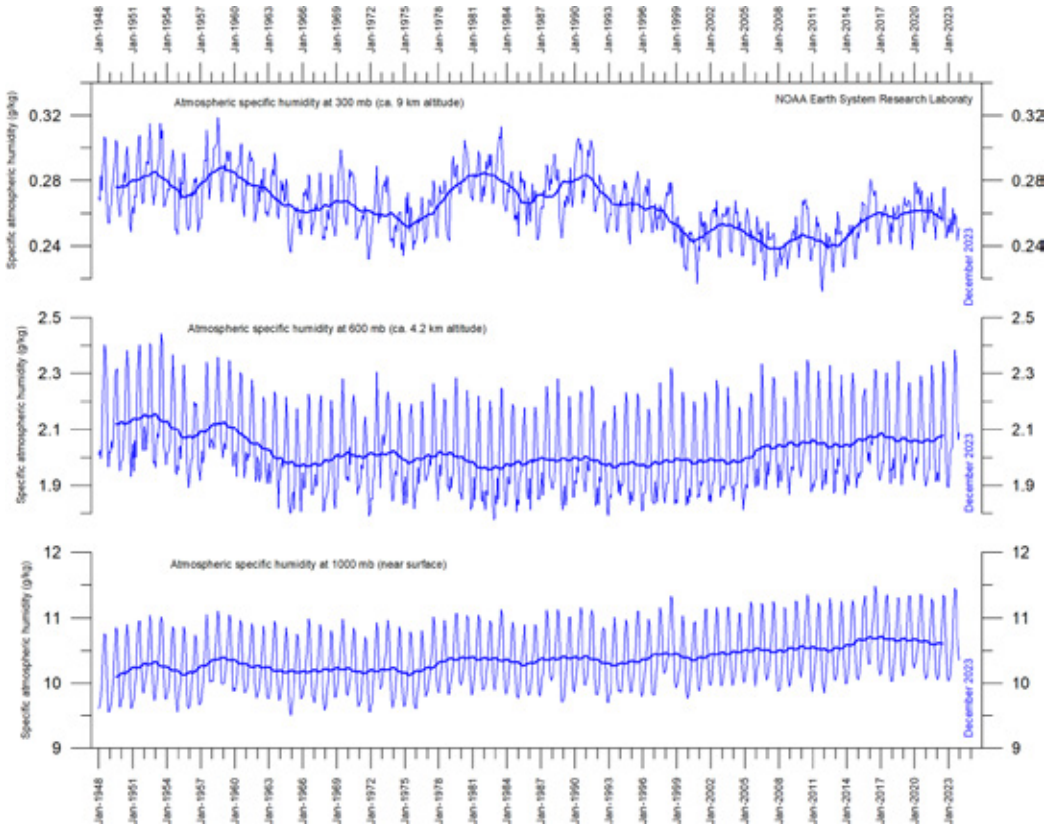

Figure 17: Specific atmospheric humidity in the Troposphere since 1948

The thin blue lines show monthly values, while the thick blue lines show the running 37-month average (about 3 years). Data source: Earth System Research Laboratory (NOAA).

falling trend. A Fourier frequency analysis (not shown here) suggests these changes are influenced, not only by the significant annual variation, but feasibly also by a longer variation of about 35-years' duration.

The overall decrease since 1948 in specific humidity at about 9 km altitude is notable, as this altitude roughly corresponds to the level (the so-called 'characteristic emission level') where the theoretical temperature effect of increased atmospheric CO_2 is expected to be seen first.

Carbon dioxide

Carbon dioxide (CO_2) is an important greenhouse gas, but less important than water vapour. Since 1958, its atmospheric concentration has been increasing, with an annual cycle superimposed on the trend. At the end of 2023, the concentration was nearly 422 ppm (parts per million; Figure 18). The annual change in concentration (Figure 19) has been increasing, from about +1 ppm/year in the early part of the record, to about +2.5 ppm/year towards the end. A Fourier frequency analysis (not shown) suggests the 12-month change of CO_2 has a significant cycle of 3.6-years' period. There is no visible effect of the global COVID-19 lockdown of 2020–22 in the record. The increasing CO_2 concentration enhances photosynthesis and thereby global crop yields.

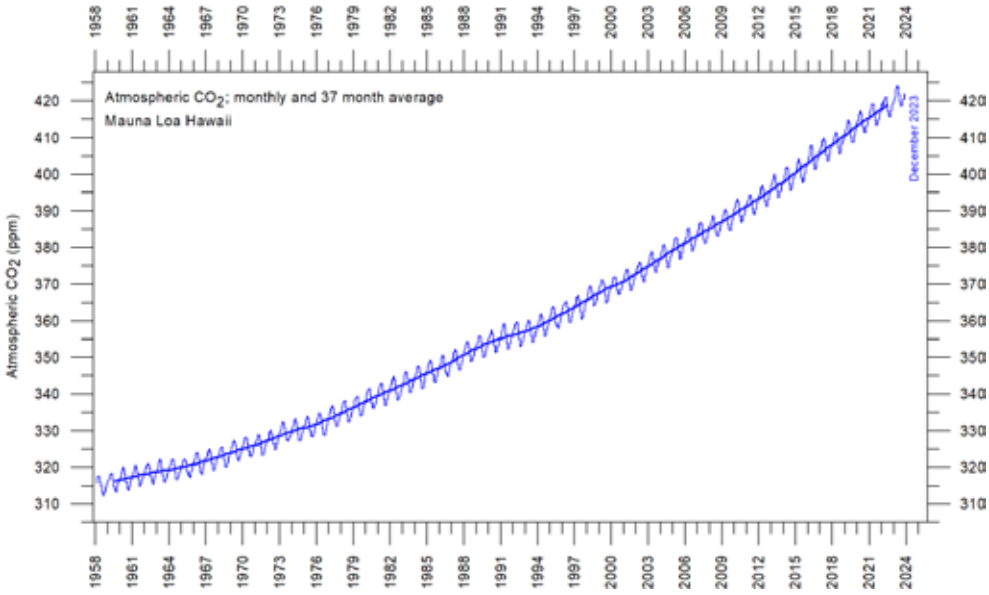

Figure 18: The Mauna Loa CO_2 record

Thin lines: monthly value; thick lines: 37-month running mean.

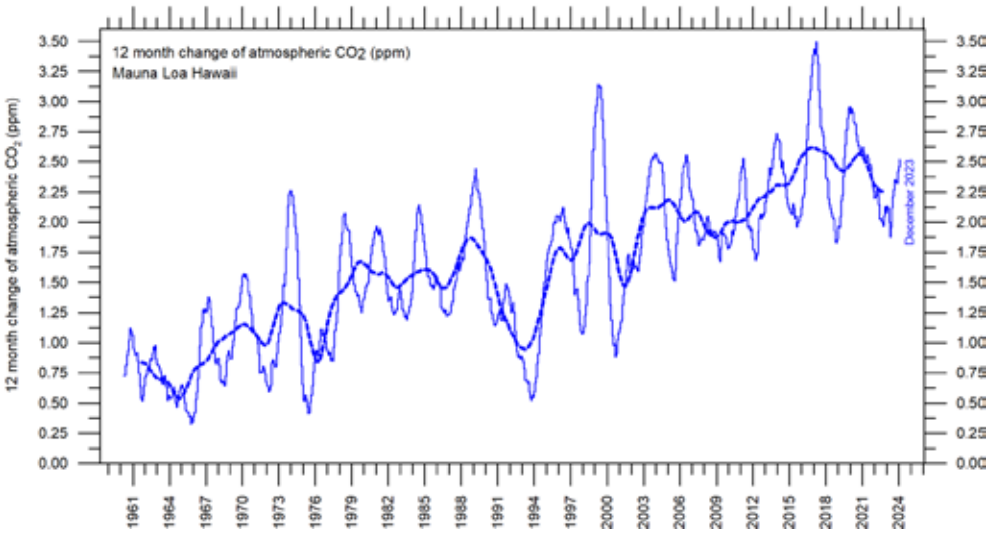

Figure 19: Annual CO_2 change

Difference of two 12-month averages. Thin lines: monthly value; thick lines: 3-year running mean.

It is illuminating to consider the variation of the annual rate of change atmospheric CO_2 against the rates of air and sea-surface temperature change (Figure 20). All three rates vary in concert, but sea-surface temperatures are a few months ahead of air temperatures, and 11–12 months ahead of changes in CO_2 concentrations (Humlum et al. 2012). The ocean surface is evidently the starting point for many important climate-related changes.

Figure 21 shows the visual association between annual change of atmospheric CO_2 and La Niña and El Niño episodes, emphasising the importance of oceanographic dynamics for understanding changes in atmospheric CO_2.

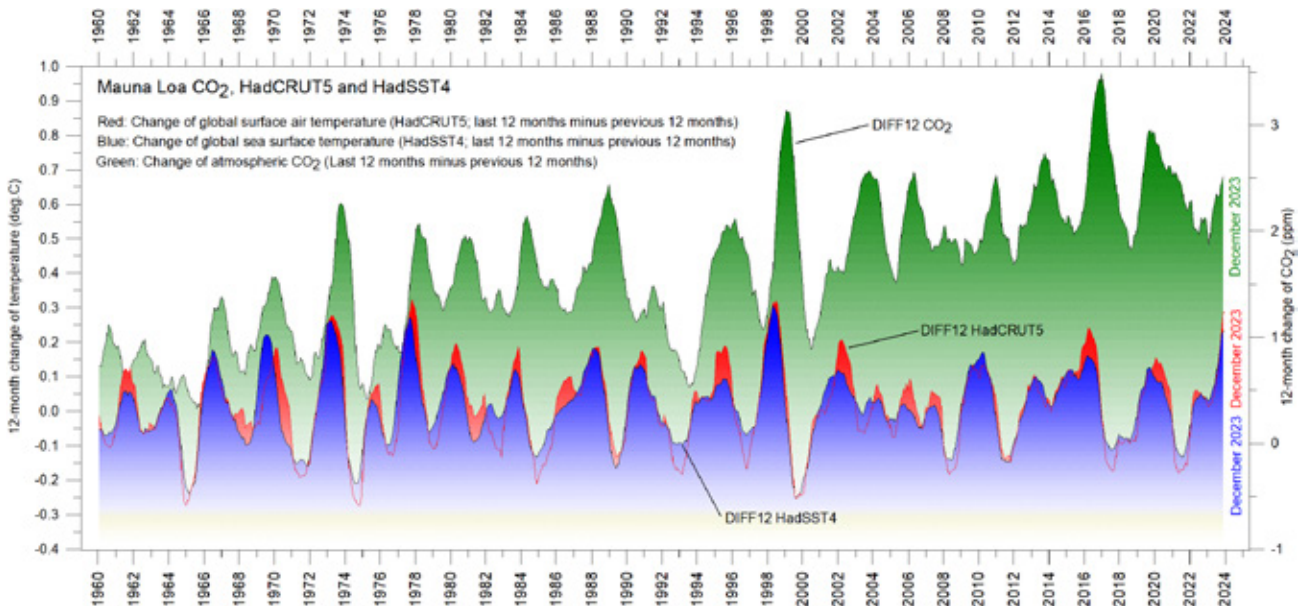

Figure 20: Correlation of carbon dioxide concentrations and temperature records.

Annual (12-month) change of global atmospheric CO_2 concentration (Mauna Loa; green), global sea surface temperature (HadSST4; blue) and global surface air temperature (HadCRUT5; red). All graphs are showing monthly values of DIFF12, the difference between the average of the last 12 months and the average for the previous 12 months for each data series.

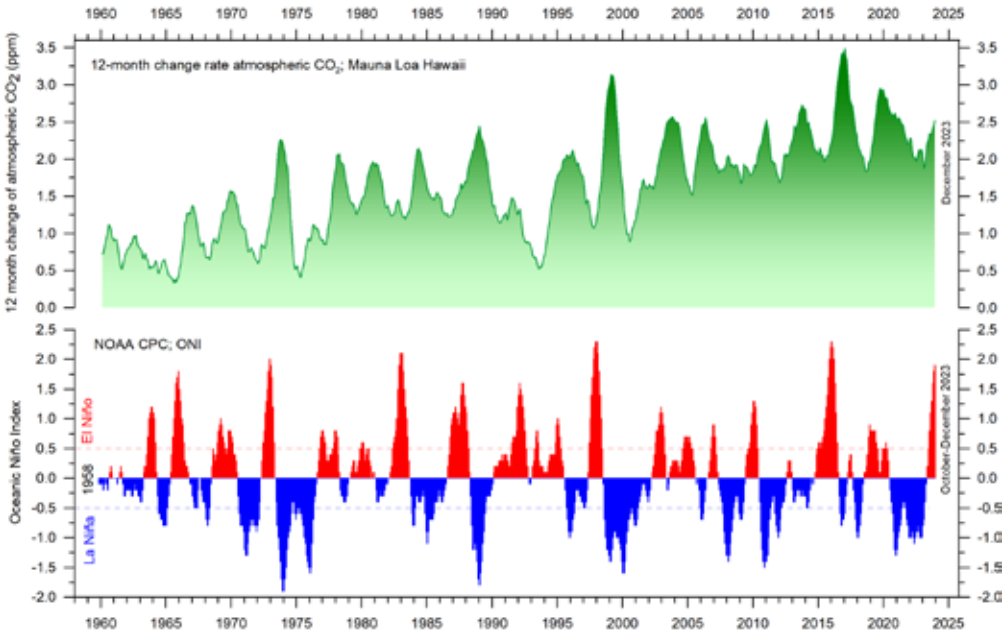

Figure 21: CO_2 growth and El Niño and La Niña episodes

Visual association between annual growth rate of atmospheric CO_2 (upper panel) and Oceanic Niño Index (lower panel).

5. Sea surface temperatures

Recent sea surface temperature anomalies

In the Pacific Ocean, trade winds usually blow west along the Equator, pushing warm water from South America towards Asia. To replace that warm water, cold water rises from the depths near South America. During El Niño episodes, trade winds are weaker than usual, and warm water spreads back east, toward South America. In contrast, during La Niña episodes, trade winds are stronger than usual, pushing more warm water than usual toward Asia, and upwelling of cold water near South America therefore increases.

The three maps in Figure 22 show the moderate La Niña characterising much of 2021 and 2022, and the ongoing strong El Niño episode at the end of 2023. See also the associated global ocean temperature changes shown in Figures 23 and 24, and also Figure 25, where all El Niño and La Niña episodes since 1950 are displayed.

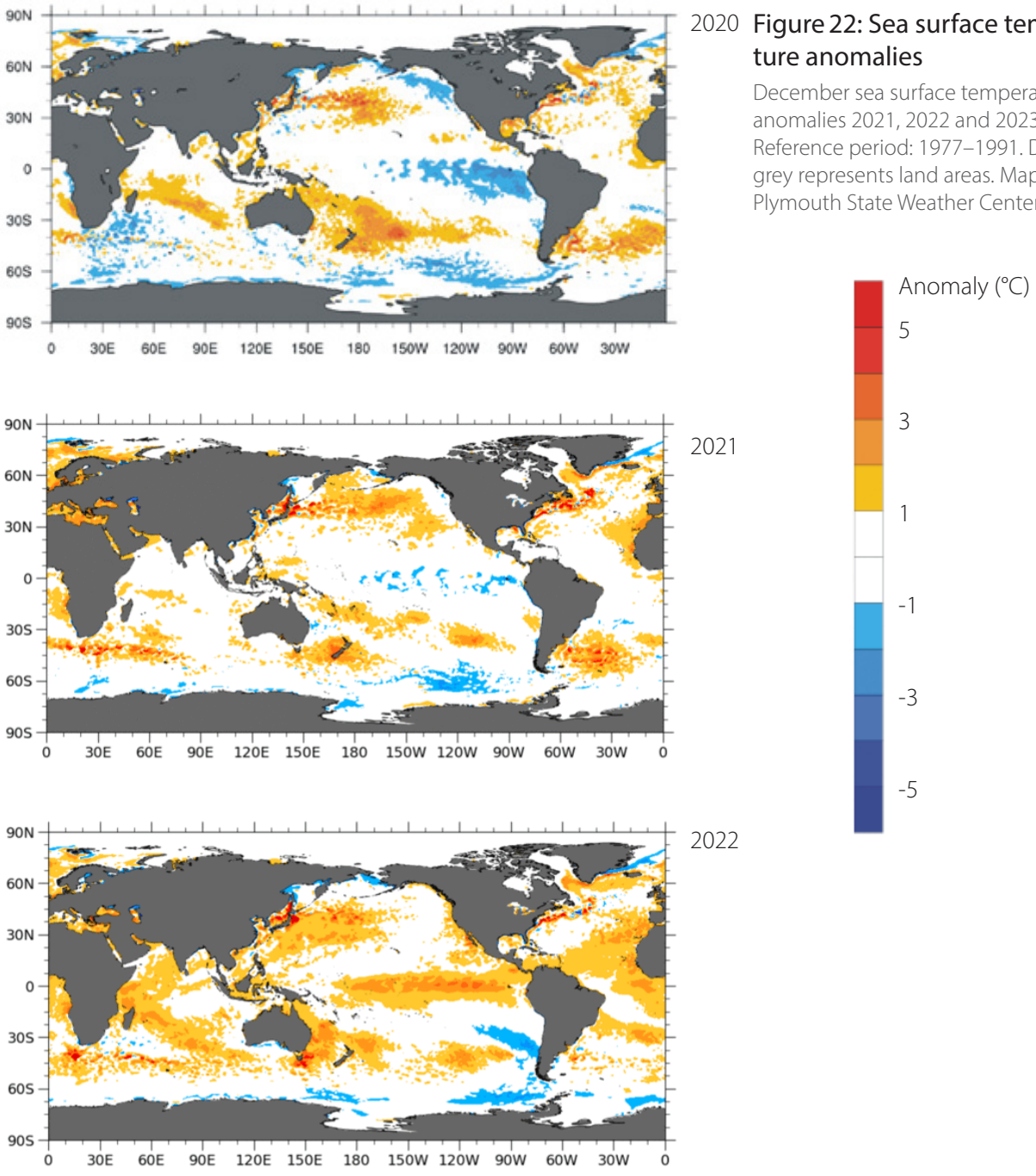

Figure 22: Sea surface temperature anomalies

December sea surface temperature anomalies 2021, 2022 and 2023, (°C). Reference period: 1977–1991. Dark grey represents land areas. Map source: Plymouth State Weather Center.

The 2015–16 El Niños and the ongoing 2023 one are among the strongest seen since the beginning of the record in 1950, and match the recent global air temperature peaks in 2016 and 2023 (Figures 5 and 8). Considering the entire record (Figure 25), however, recent variations between El Niño and La Niña episodes appear to be quite normal.

A Fourier frequency analysis (not shown here) shows the record of El Niño and La Niña episodes since 1950 to be influenced by a significant 3.6-year cycle, and feasibly also by a longer one of 5.6 years' duration.

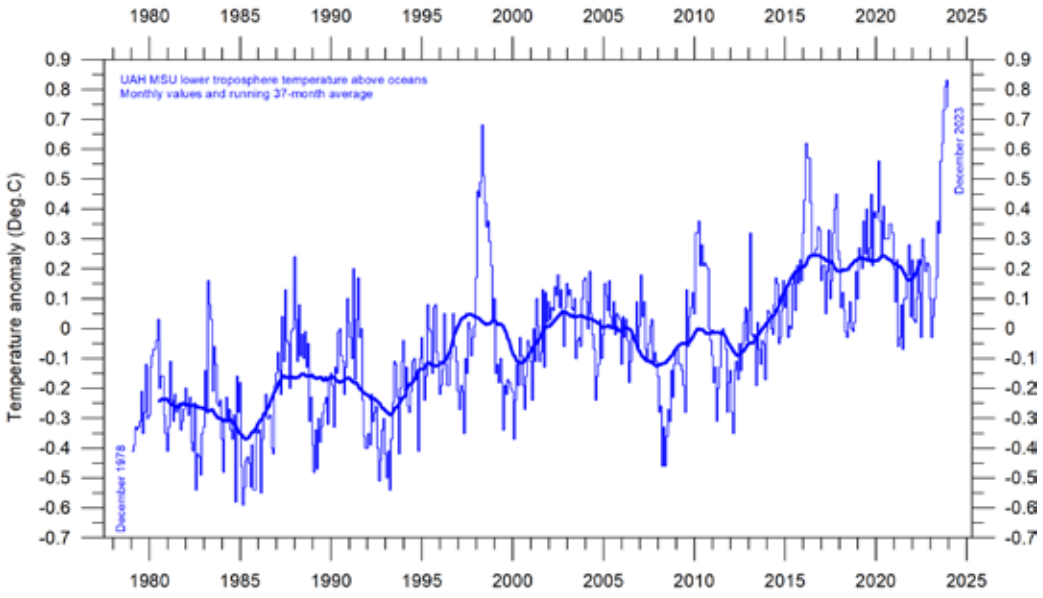

Figure 23: Lower troposphere temperatures above oceans

Global monthly average since 1979, representing conditions at about 2 km altitude. Satellite data interpreted by University of Alabama at Huntsville (UAH), USA. Base period 1981–2010. The thick line is the simple running 37-month average, nearly corresponding to a running 3-year average.

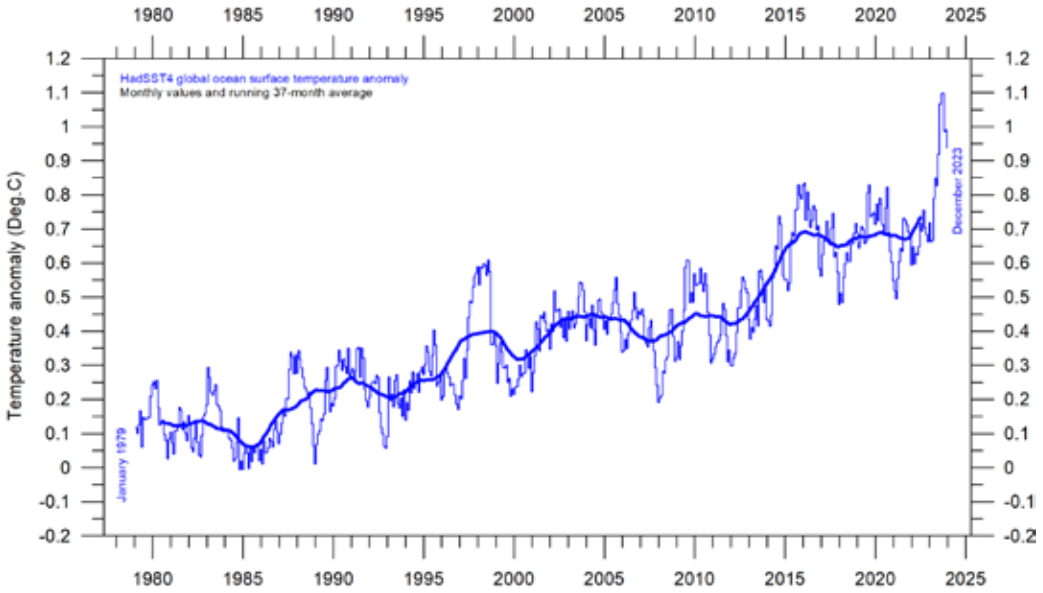

Figure 24: Sea surface temperature anomalies

Global monthly average since 1979, according to the University of East Anglia's Climatic Research Unit (CRU), UK. Base period: 1961–1990. The thick line is the simple running 37-month average, nearly corresponding to a running 3-year average.

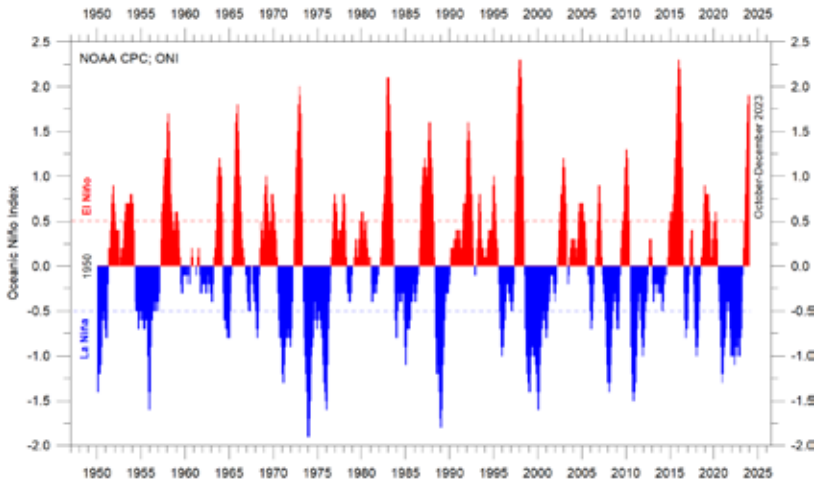

Figure 25: The El Niño index

Warm and cold episodes for the Oceanic Niño Index (ONI), defined as 3-month running mean of ERSST.v5 SST anomalies in the Niño 3.4 region (5°N–5°S, 120°-170°W). Anomalies are centred on 30-year base periods updated every 5 years.

Global ocean average temperatures to 1900 m depth

Figure 26 is based on observations by Argo floats (Roemmich and Gilson 2009), and shows that, on average, the temperature of the global oceans down to 1900 m depth has been increasing since about 2010. It can also be seen that since 2013 this increase has been mainly caused by changes occurring near the Equator, between 30°N and 30°S. In contrast, for the circum-Arctic oceans, north of 55°N, depth-integrated ocean temperatures have been decreasing since 2011. Near the Antarctic, south of 55°S, temperatures have largely been stable. At most latitudes, a clear annual rhythm is seen to play out.

From about 2020, the measurements available hint at the onset of a new regime, with decreasing circum-Equator temperatures, and increasing circum-Arctic temperatures. However, more measurements are needed before firm conclusions can be drawn.

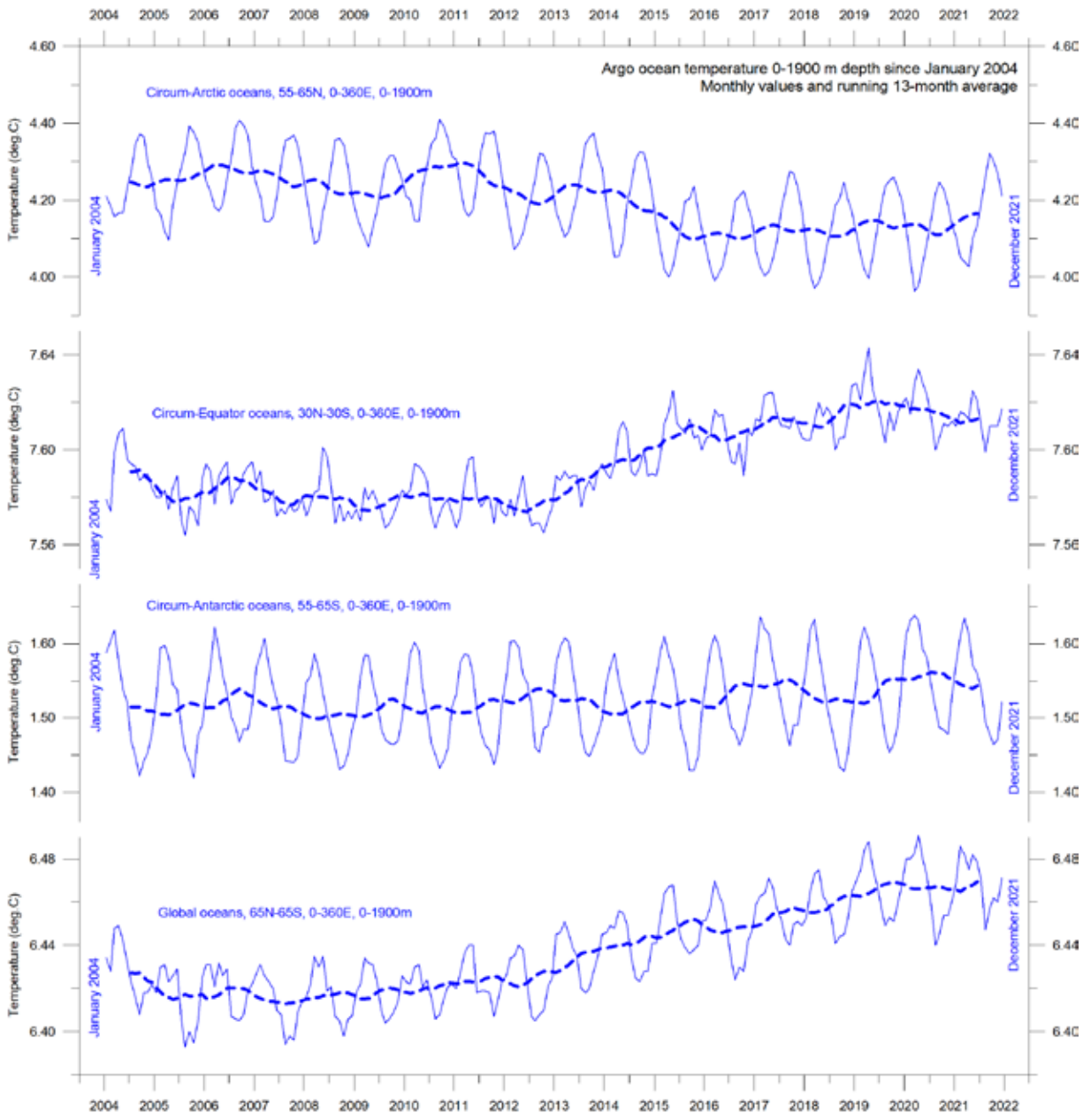

Figure 26: Ocean temperatures to 1900 m

Average ocean temperatures January 2004–December 2021 at 0–1900 m depth in selected latitudinal bands, using Argo data. The thin line shows monthly values, and the thick dotted line shows the running 13-month average. Source: Global Marine Argo Atlas.

Global ocean temperatures at different depths

Figure 27 displays global average oceanic temperatures at different depths. An annual rhythm can be seen down to about 100 m. In the uppermost 100 m, temperatures have increased since about 2011. At 200–400 m, temperatures have exhibited little change during the observational period.

For depths below 400 m, however, global average ocean temperatures have increased over the observational period. Interestingly, the data suggest that this increase commenced at 1900 m depth in around 2009, and from there has gradually spread upwards. At 600 m depth, the present temperature increase began around 2012; that is, about three years later than at 1900 m depth. The timing of these changes shows that average temperatures in the upper 1900 m of the oceans are not only influenced by conditions playing out at or near the ocean surface, but also by

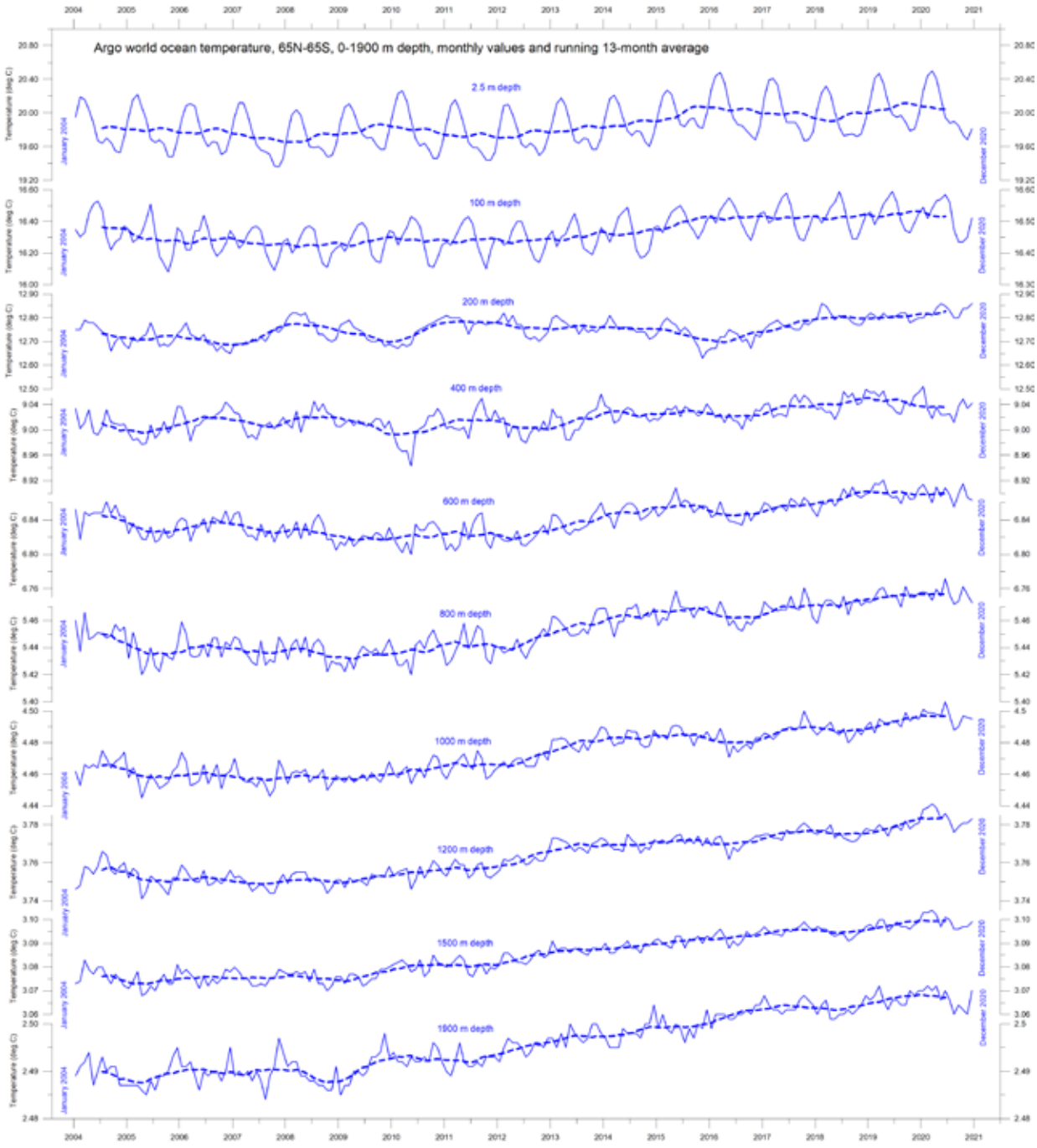

Figure 27: Ocean temperatures at different depths

Ocean temperatures January 2004–December 2021 at different depths between 65°N and 65°S, using Argo data. The thin line shows monthly values, and the dotted line shows the running 13-month average. Source: Global Marine Argo Atlas.

processes operating at depths below 1900 m; in other words, part of the recent warming results from circulation changes, and are therefore not directly related to processes operating at or near the surface.

This development is also seen in Figure 28, which shows changes of global ocean temperatures at different depths, calculated as the net difference between two 12-month averages: for January–December 2004 and January-December 2020. The largest net changes are seen to have occurred in the uppermost 200 m of the water column. However, such average values, although valuable, also hide many interesting regional details. These are considered in the next two sections.

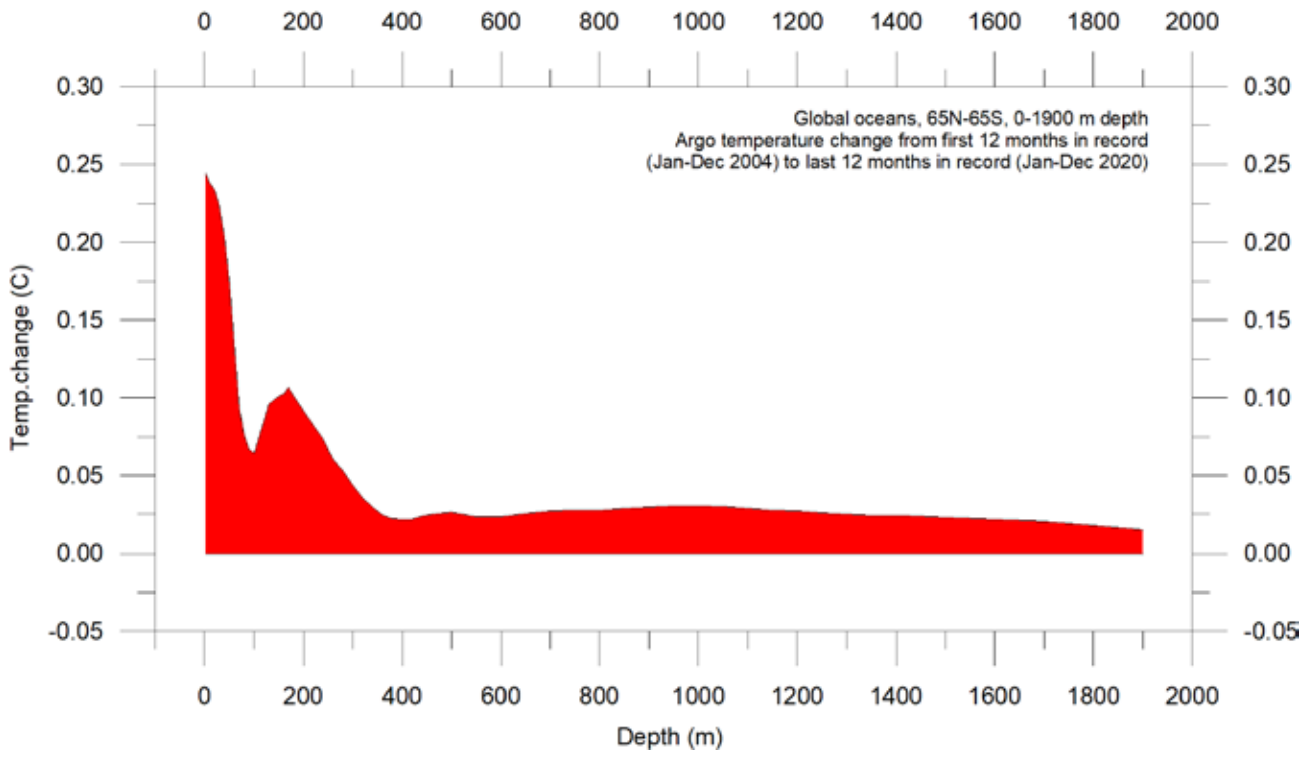

Figure 28: Temperature changes 0–1900 m

Global ocean net temperature change since 2004 from surface to 1900 m depth, using Argo-data. Source: Global Marine Argo Atlas.

Regional ocean temperature changes temperatures 0-1900 m depth

Figure 29 shows the variation of oceanic temperature net changes between the same two 12-month periods as in the last section, for various depths, and for three different latitudinal bands, representing the Arctic Oceans (55–65°N), Equatorial Oceans (30°N–30°S), and Antarctic Oceans (55–65°S), respectively. The global net surface warming displayed is seen to affect the Equatorial and Antarctic Oceans, but not the Arctic Oceans, where net cooling is pronounced down to 1400 m depth. However, a major part of Earth's land area is in the Northern Hemisphere, so the surface area (and volume) of 'Arctic' oceans is much smaller than the 'Antarctic' oceans, which are in turn smaller than the 'Equatorial' oceans. In fact, half of the planet's surface area (land and ocean) is located between 30°N and 30°S.

Nevertheless, the contrast in net tempera-

ture changes for the different latitudinal bands is instructive. For the two polar oceans, the Argo data appear to suggest the existence of a bi-polar seesaw, as described by Chylek et al. (2010). It is no less interesting that the near-surface ocean temperature in the two polar oceans contrasts with the overall development of sea ice in the two polar regions (see Section 8).

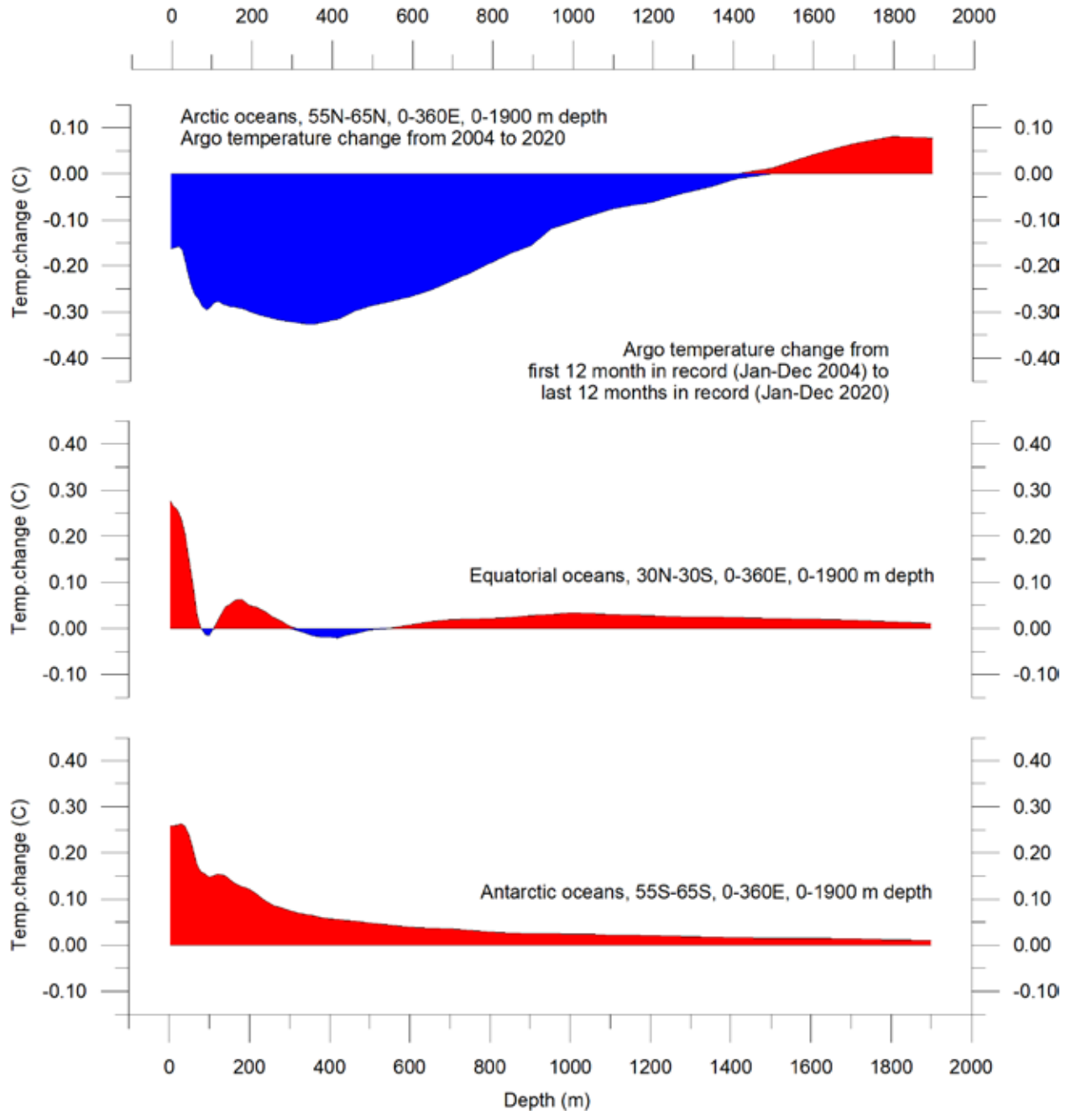

Figure 29: Temperature changes 0–1900 m

Global ocean net temperature change since 2004 from surface to 1900 m depth. Source: Global Marine Argo Atlas.

Ocean temperature net change 2004-2021 in selected sectors

Figure 30 shows net temperature changes for 2004–2021 along 20°W (see Figure 31), representing the Atlantic Ocean. To prepare the diagram, 12-month average ocean temperatures for 2021 were compared to annual average temperatures for 2004, representing the first 12 months in the Argo-record. To give an insight into also the most recent changes, the equivalent 12-month net change from January 2021 to December 2021 is shown in Figure 30b.

Warm colours indicate net warming and blue colours indicate cooling. Due to the spherical shape of the Earth, high latitudes represent smaller ocean volumes than lower latitudes near the Equator. With this reservation in mind, the data along the Atlantic transect nevertheless reveal several interesting features.

The most prominent in the 2004–2021 profile (Figure 30a) is a marked net cooling north of 35-40°N, affecting depths down to 1500–1600 m.

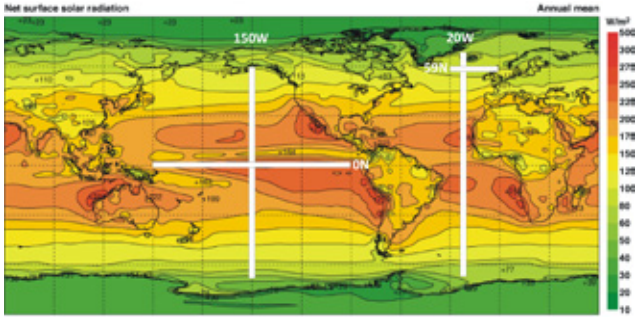

Figure 31: Location of the four profiles

Average annual mean net surface solar radiation (W/m²), and the location of profiles discussed below.

In contrast, warming characterises latitudes further south, especially between 20–50°S, down to about 1100 m depth. At 100–150 m depth, cooling dominates between 10°N and 40°S.

The temperature development over the last 12 months of the record (Figure 30b) shows a more complicated pattern, especially near the surface. Much of the South Atlantic, which displayed net

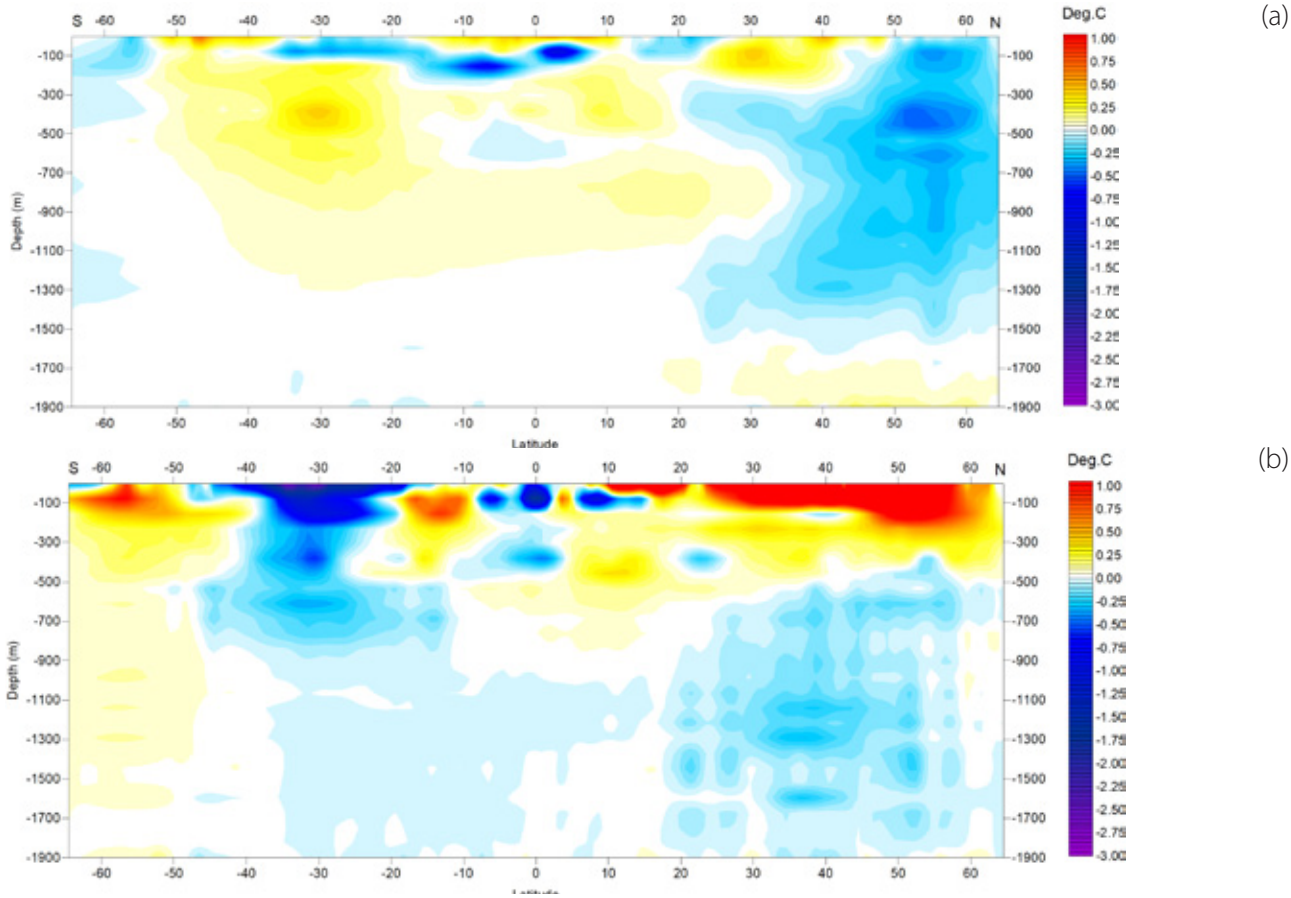

Figure 30: Temperature change along Atlantic profile, 0–1900 m

(a) 2004–2021 and (b) Jan–Dec 21. See Figure 31 for geographical location of transect. Data source: Global Marine Argo Atlas.

warming in 2004–21, is currently undergoing cooling, especially between 20°S and 40°S. In the North Atlantic, the last 12 months on record show warming north of 10°N, affecting depths down to 200 m. At greater depths, cooling still prevails.

Of particular interest for Europe are oceanic temperature changes playing out within a 59°N transect across the North Atlantic current (see Figure 31), just south of the Faroe Islands. This region is important for weather and climate in much of Europe. Figure 32 displays a time series at 59°N, from 30°W to 0°W, and from the surface to 800 m depth. This essentially represents a section across the water masses affected by the North Atlantic current. Ocean temperatures higher than 9°C are indicated by red colours.

This time series, although still relatively short, displays noteworthy dynamics. The prominence of warm water (above 9°C) apparently peaked in early 2006, after which temperatures gradually decreased until 2016. Since then, a partial temperature recovery has taken place. The observed change, from peak to trough, playing out over approximately 11 years, might suggest a 22-year temperature cycle, but we will have to wait until the Argo series is longer before drawing conclusions.

Figure 33 shows the identical time series data (59°N, 330–0°W, 0–800 m depth, 2004–2021) but as depth-integrated average ocean temperature.

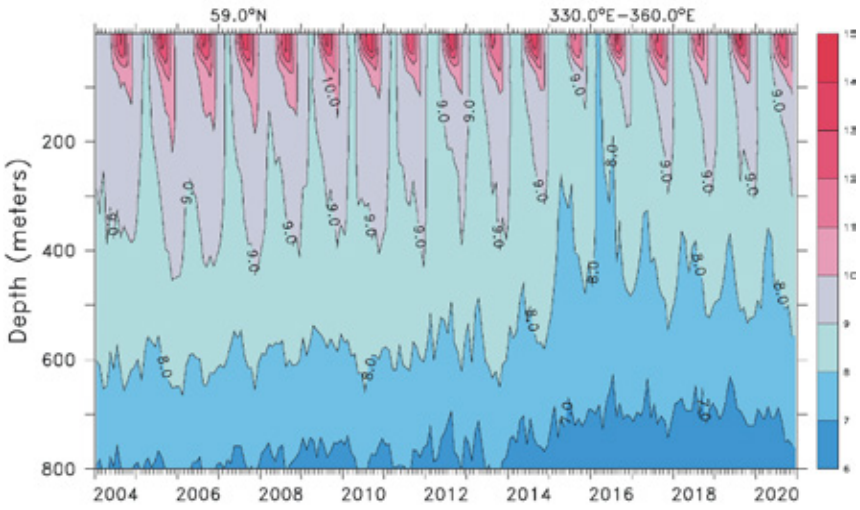

Figure 32: Temperature change along North Atlantic Current profile, 0–800 m

See Figure 31 for geographical location of transect. Data source: Global Marine Argo Atlas.

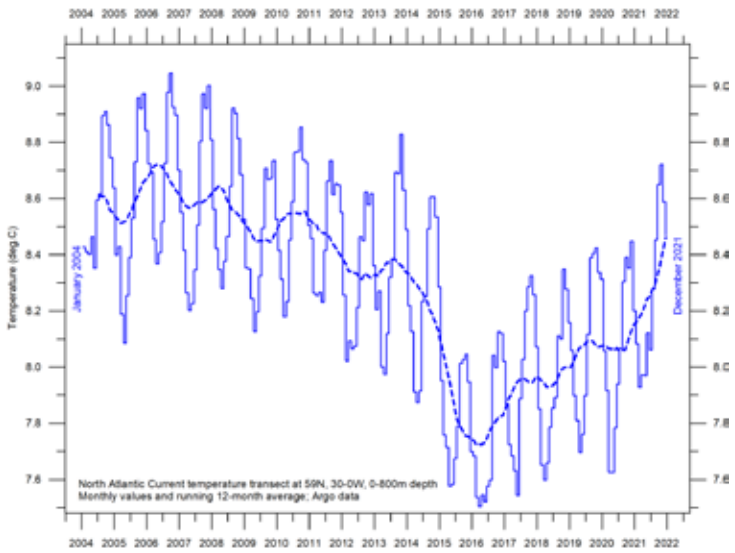

Figure 33: Depth-integrated temperature for the North Atlantic Current profile

See Figure 31 for geographical location of transect. Data source: Global Marine Argo Atlas.

Figure 34 shows the two equivalent Pacific Ocean diagrams, representing net changes for 2004–21 and during 2021, along 150°W. It again uses data obtained by Argo floats, and os prepared in the same way as the two Atlantic diagrams in Figure 30. Recall also that northern, and southern latitudes represent only relatively small ocean volumes compared to latitudes near the Equator.

One interesting feature for 2004–21 (Figure 34a) is net cooling near the Equator (15°S–20°N) down to about 700 m depth. In contrast, two bands (20–40°S and 30–45°N) are characterised by net warming down to 800–900 m. During the last 12 months (Figure 34b) net cooling has been prominent, apart from surface water in 5°S–50°N displaying warming down to 100–200 m depth. This recent (2021) warming at the surface near Equator is likely to be the result of a brief weakening of the La Niña playing out at that time (Figure 32).

Neither the Atlantic nor the Pacific longitudinal diagrams reveal the extent to which the net changes displayed are caused by ocean dynamics operating east and west of the two profiles considered. For that reason, they should not be overinterpreted. They do, however, suggest an interesting contrast, with the Atlantic since 2004 displaying a more dynamic temperature development than the Pacific, except for depths and latitudes affected by El Niño and La Niña episodes in the Pacific.

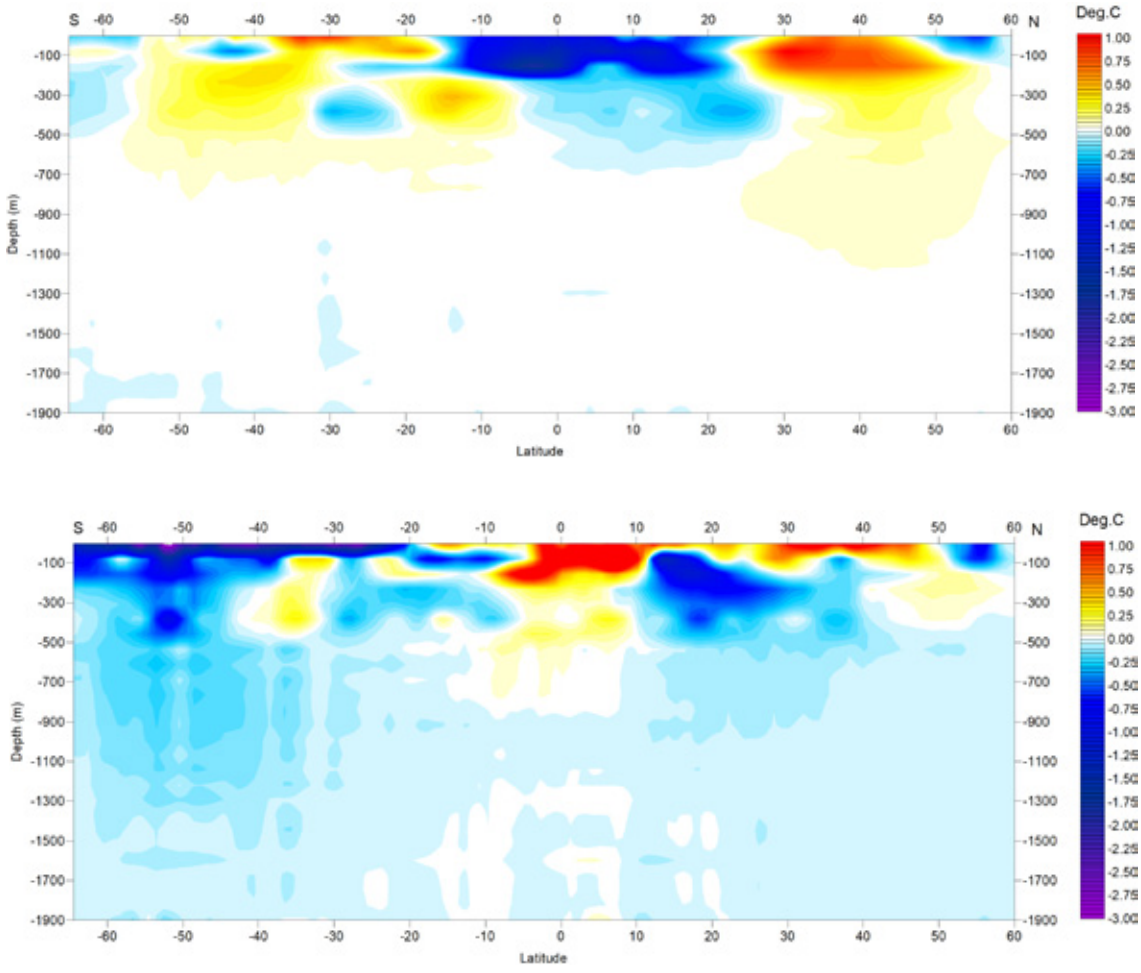

Figure 34: Temperature change along Pacific profile, 0–1900 m

(a) 2004–2021 and (b) Jan–Dec 2021. See Figure 31 for geographical location of transect. Data source: Global Marine Argo Atlas.

Figure 35 shows a time series of sea temperatures from surface to 400 m depth in the El Niño/La Niña region (Pacific Ocean). By comparing with Figure 32 the individual episodes are clearly seen as temperature variations in the upper 150–200 m of the ocean. Below 200–250 m, temperatures are essentially constant, demonstrating that El Niño and La Niña episodes are phenomena mainly driven by variations in surface conditions, with little or no influence from greater depths. See also comments on Figures 22 and 25 for general information on El Niño and La Niña episodes.

Figure 35: Temperature change along Pacific profile, 0–400 m

Sea temperature variations with depth January 2004–December 2020 in the El Niño and La Niña region along the Equator in the Pacific Ocean. See Figure 31 for geographical location of transect. Data source: Global Marine Argo Atlas.

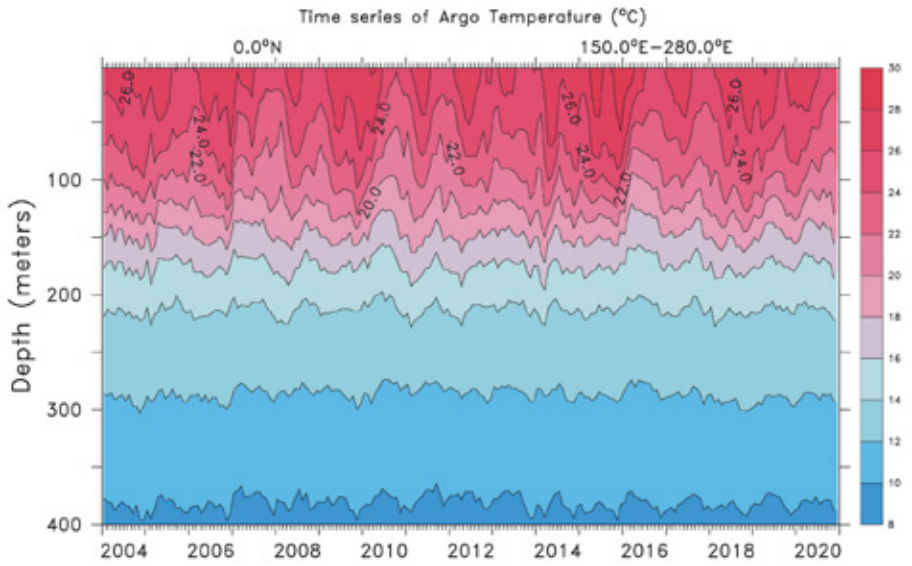

6. Ocean cycles

Southern Oscillation Index

The Southern Oscillation (SOI) may be considered the atmospheric component of El Niño/La Niña episodes. It is a standardised index, based on the observed sea-level pressure differences between Tahiti (French Polynesia) and Darwin (Australia). Smoothed time series of the SOI frequently correspond with changes in ocean temperatures across the eastern tropical Pacific Ocean. The SOI is related to the El Niño–Southern Oscillation (ENSO), which involves coordinated, season-long changes to ocean-surface temperatures and atmospheric circulation in the tropical Pacific Ocean. It tracks the atmospheric part of the pattern, while the Oceanic Niño Index (Figure 25) tracks the ocean part.

Sustained negative values of the SOI (Figure 36) often indicate El Niño episodes. Such negative values are usually accompanied by persistent warming of the central and eastern tropical Pacific Ocean, a decrease in the strength of the Pacific Trade Winds, and a reduction in rainfall over eastern and northern Australia.

Positive values of the SOI are usually associated with stronger Pacific trade winds and higher sea-surface temperatures to the north of Australia, indicating La Niña episodes. Waters in the central and eastern tropical Pacific Ocean become cooler during this time, and eastern and northern Australia usually receive increased precipitation.

A Fourier frequency analysis (not shown here) shows the SOI record to be influenced by a 3.6-year cycle.

Figure 36: Annual SOI anomaly since 1866

The thin line represents annual values, while the thick line is the simple running 5-year average. Source: Climatic Research Unit, University of East Anglia.

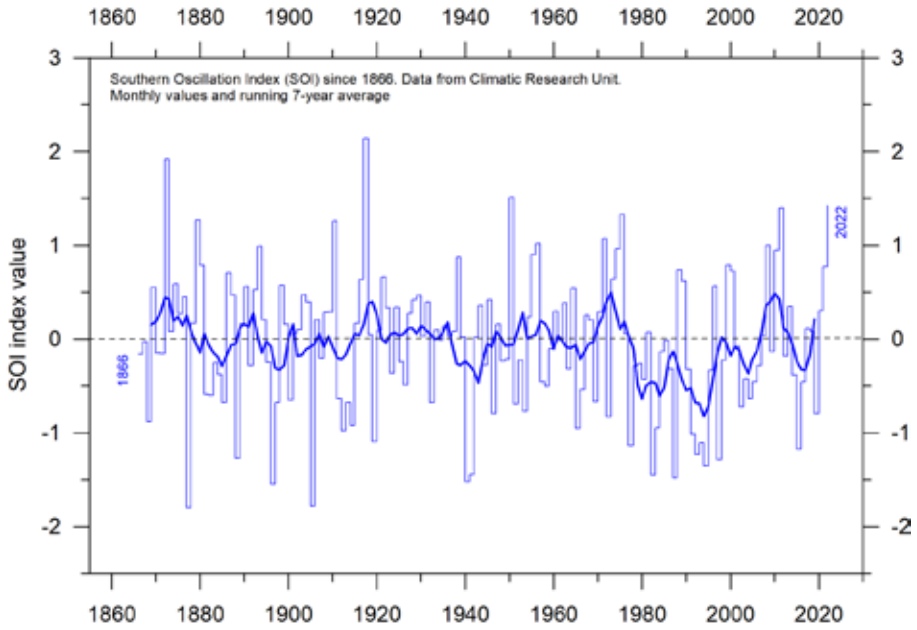

Pacific Decadal Oscillation

The PDO (Figure 37) is a long-lived El Niño-like pattern of Pacific climate variability, with data extending back to January 1854. When sea surface temperatures (SST) are low in the interior North Pacific and high along the North American coast, and when sea-level pressures are below average over the North Pacific, the PDO has a positive value. When this pattern is reversed, with high SST anomalies in the interior North Pacific and low SST anomalies along the North American coast, or above average sea level pressures over the North Pacific, the PDO has a negative value.

Origins for PDO are not currently known, but even in the absence of a theoretical framework, understanding its variability improves season-to-season and year-to-year climate forecasts for

Figure 37: Annual values of the Pacific Decadal Oscillation (PDO) according to the Physical Sciences Laboratory, NOAA.

The thin line shows the annual PDO values, and the thick line is the simple running 7-year average. Source: PDO values from NOAA Physical Sciences Laboratory: ERSST V5 https://psl.noaa.gov/pdo/.

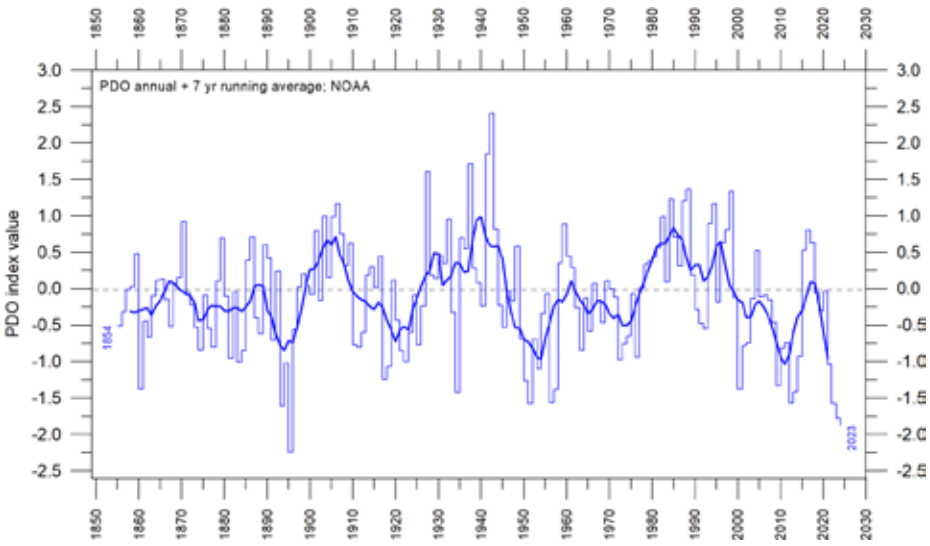

North America because of its strong tendency for multi-season and multi-year persistence. The PDO also appears to be roughly in phase with global temperature changes. Thus, it is important from a societal-impact perspective, because it shows that 'normal' climate conditions can vary over periods comparable to the length of a human lifetime.

The PDO nicely illustrates how global temperatures are – at times, but not always – tied to sea-surface temperatures in the Pacific, the largest ocean on Earth. When sea-surface temperatures are relatively low (negative phase PDO), as they were from 1945 to 1977, global air temperature decreases. When sea-surface temperatures are high (positive phase PDO), as they were from 1977 to 1998, global surface air temperature increases (Figure 8).

A Fourier frequency analysis (not shown here) shows the PDO record to be influenced by a significant 5.6-year cycle, and feasibly also by a longer 18.6-year long period, corresponding to the length of the lunar nodal tide.

Atlantic Multidecadal Oscillation

The Atlantic Multidecadal Oscillation (AMO) is a mode of variability occurring in the North Atlantic Ocean sea-surface temperature field (Figure 38). It is an index of North Atlantic sea-surface temperatures (SST).

The AMO index appears to be correlated to air temperatures and rainfall over much of the Northern Hemisphere. The association appears to be high for rainfall in northeastern Brazil and the African Sahel, and also for North American and European summer climate. The AMO index also appears to be associated with changes in the frequency of North American droughts and the frequency of severe Atlantic hurricanes.

Figure 38: The Atlantic Multidecadal Oscillation

Annual Atlantic Multidecadal Oscillation (AMO) detrended and unsmoothed index values since 1856. The thin blue line shows annual values, and the thick line is the simple running 11-year average. Data source: Earth System Research Laboratory, NOAA, USA.

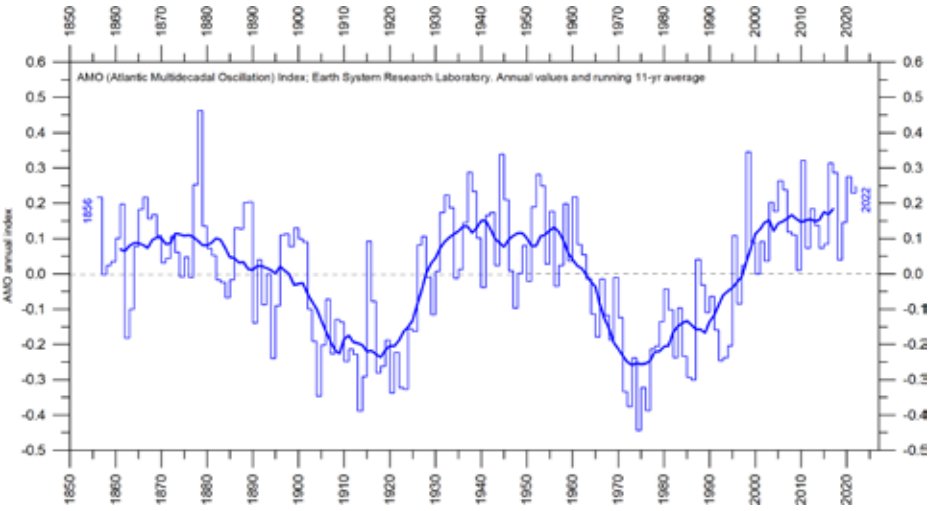

As one example, the AMO index may be related to the past occurrence of major droughts in the US Midwest and the Southwest. When the AMO is high, these droughts tend to be more frequent or prolonged, and vice-versa for low values. Two of the most severe droughts of the 20th century in the US – in the 1950s and the 1930s 'Dust Bowl' – occurred during a time of peak AMO values, which lasted from 1925 to 1965. On the other hand, Florida and the Pacific Northwest tend to experience the opposite effect, high AMO in these areas being associated with relatively high precipitation.

A Fourier analysis (not shown here) suggests the AMO record is influenced by a cycle of around 70 years' duration. This periodicity is also found in the HadCRUT and the NCDC global surface air temperature records (Figures 12 and 13).

7. Sea-level

Global, regional, and local sea levels always change. At the last glacial maximum, about 20–25,000 years ago, the average global sea level was about 120 m lower than today. Since the end of the so-called Little Ice Age, about 100–150 years ago, global sea levels have on average increased by 1–2 mm per year, according to tide-gauge data.

It is well-known that wind (storms) is an important factor in flooding disasters, acting on time scales of hours to days. In this section, however, the focus is mainly on processes operating on longer timescales, of ears to centuries, and longer.

Global sea-level change is measured relative to an idealised reference level, the geoid, which is a mathematical model of planet Earth's surface (Carter et al. 2014). Global sea level is a function of the volume of the planet's surface ocean basins and the volume of water they contain. Changes in global sea level are caused by four main mechanisms (and possibly others):

1. changes in local and regional air pressure and wind, and tidal changes introduced by the Moon;
2. changes in ocean basin volume by tectonic (geological) forces;
3. changes in ocean water density caused by variations in currents, water temperature and salinity;
4. changes in the volume of water, caused by variation in the mass balance of terrestrial glaciers.

There are also some other mechanisms influencing sea level: storage of ground water, storage in lakes and rivers, evaporation, and so on.

Apart from regions affected by the Quaternary glaciations, ocean-basin volume changes occur too slowly to be significant over human lifetimes. In the opinion of the present author, it is therefore mainly mechanisms 3 and 4 that drive contemporary concerns about sea-level rise, although on a local scale mechanism 2 may also be important, in the form of earthquakes, as is discussed below.

Higher ocean-water temperature is only one of several factors contributing to global sea-level rise, because seawater has a relatively small coefficient of expansion and because, over the timescales of interest, any warming is largely confined to the upper few hundred metres (see, e.g., Figure 28).

The growth or decay of sea ice and floating ice shelves has no influence on sea level. However, the melting of land-based ice – including both mountain glaciers and the ice sheets of Greenland and Antarctica – is a significant factor. As already noted, sea-levels were about 120 m lower during the last glacial maximum, and during the most recent interglacial, about 120,000 years ago, global temperatures and thus sea levels were higher than today, because significant parts of the Greenland ice sheet at that time had melted.

On a regional and local scale, however, factors relating to changes in air pressure, wind and the geoid must also be considered. As an example, changes in the volume of the Greenlandic Ice Sheet will affect the geoid in the regions adjacent to Greenland. Should overall mass in Greenland diminish, the geoid surface will be displaced towards the centre of the Earth, and sea level in the region will drop correspondingly. This would happen even though the overall volume of water in the global oceans would have increased as

glacier ice was lost.

In northern Europe and in significant parts of North America, another factor must also be considered when estimating the future sea level. As an example, 20–25,000 years ago, Norway, Sweden, Finland, and Denmark were all totally or partly covered by the European ice sheet. Even today, in these areas, the effect of this ice load is seen in the ongoing isostatic land rise, of several millimetres per year. At many sites this more than compensates for the slow global sea-level rise, so a net sea-level fall relative to the land is recorded.

The enormous mass transfer associated with the growing ice sheets in North America and Europe in the last ice age resulted in viscoelastic mantle flow and elastic effects in the upper crust. Thus, where there was no ice, the planet's surface bulged upwards, while below the ice sheets, the land was compressed. Nowadays, with the ice gone, the latter regions are slowly sinking back, resulting in apparently above-normal rates of sea-level rise. Several locations along the eastern coast of the USA and the west coast of Europe are seeing this process.

Viscoelastic mantle flow not only affects the land surface, but also the volume of adjoining ocean basins. In this way, sea level may change in the affected regions and beyond. This is, however, a slow process, and is not usually important on human timescales. On the other hand, rapid tectonic movement in connection with earthquakes may lead to sudden changes of the local sea level in relation to land.

The relative movement of sea level in relation to land is what matters for coastal planning, and this is termed the 'relative sea-level change'. This is what is recorded by tide gauges.

Sea-level from satellite altimetry

Satellite altimetry is a relatively new type of measurement, providing unique and valuable insights into changes in the detailed surface topography of the oceans, with nearly global coverage. However, it is probably not a precise tool for estimating absolute changes in global sea level due to interpretation issues surrounding the original data.

The most important issue is the Glacial Isostatic Adjustment (GIA), a correction for the large-scale, long-term mass transfer from the oceans to the land that results from the waxing and waning of the large Quaternary ice sheets in North America and northern Europe. This enormous mass transfer causes changes in surface load, resulting in viscoelastic mantle flow and elastic effects in the upper crust, as mentioned above. It is hard to correct the satellite data for this effect, since no single technique or observational network can give enough information. Scientists therefore must resort to modelling, and the answer they get depends upon the type of model used to simulate the last glaciation, and upon the type of crust-mantle model that is assumed. Because of this (and other factors), estimates of global sea-level change based on satellite altimetry vary somewhat.

In Figure 39 the global sea-level rise estimate is about 3.4 mm/year (since 1992), with the estimated GIA effect removed. Linear trends calculated since 2005, 2010 and 2015 do not suggest any recent acceleration, and the lower panel in Figure 39 instead suggests that a peak in sea-level rise may have been passed around 2020. Again, time will tell.

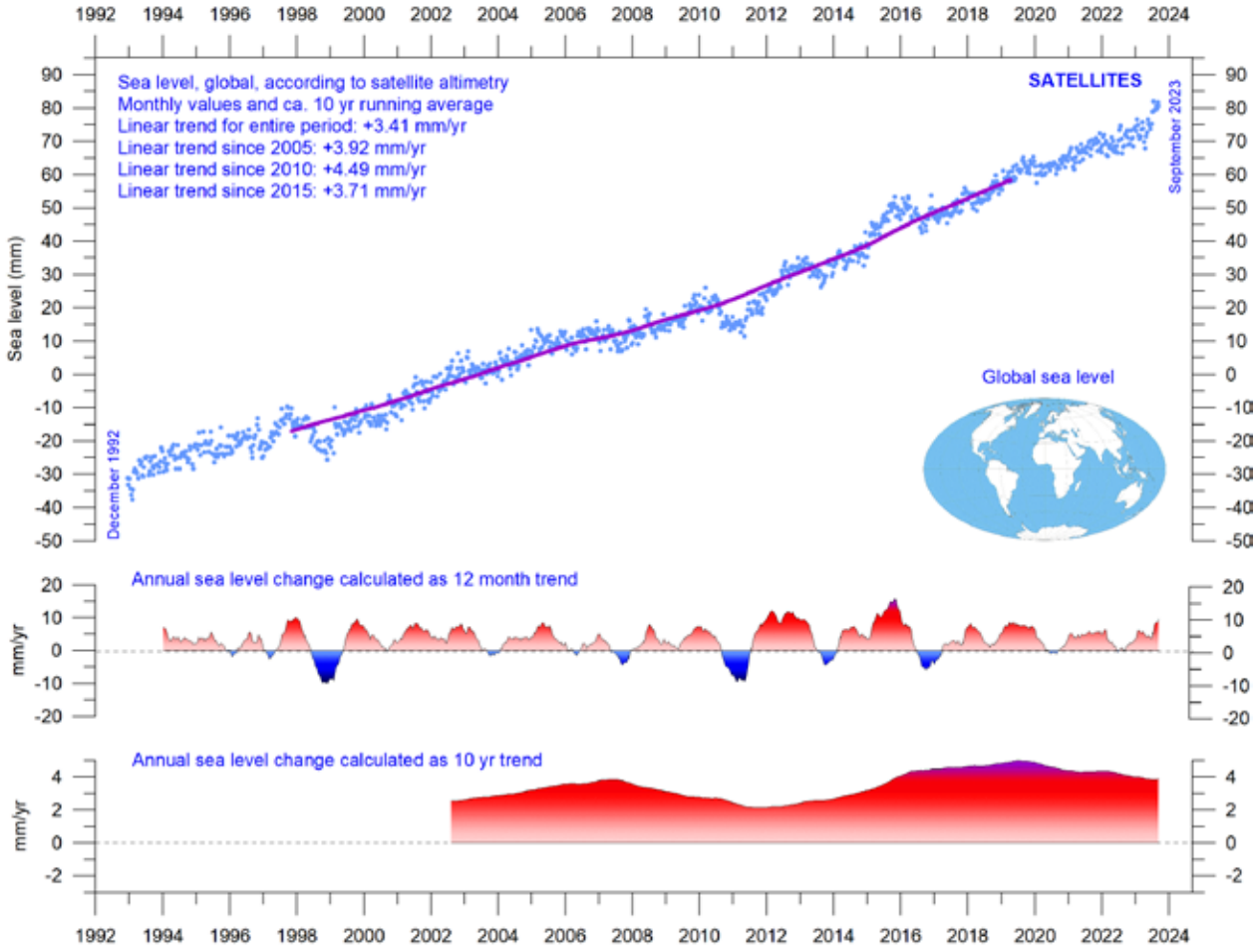

Figure 39: Global sea level change since December 1992

The two lower panels show the annual sea level change, calculated for 1- and 10-year time windows, respectively. These values are plotted at the end of the interval considered. Source: Colorado Center for Astrodynamics Research at University of Colorado at Boulder. The blue dots are the individual observations (with calculated GIA effect removed), and the purple line represents the running 121-month (ca. 10-year) average.

Sea level from tide gauges

Tide gauges are located at coastal sites and record the net movement of the local ocean surface in relation to the land. These measurements are key information for planning coastal installations (Parker and Ollier, 2016 and Voortman 2023), in contrast to satellite altimetry.

At any specific coastal site, the measured net movement of the local sea level comprises two components:

- the vertical change of the ocean surface
- the vertical change of the land surface

For example, a tide gauge may record an apparent sea-level increase of 3 mm/year. If geodetic measurements show the land to be sinking by 2 mm/year, the real sea-level rise is only 1 mm/year (3 minus 2 mm/year). In a global sea-level context, the value of 1 mm/year is relevant, but in a local coastal planning context the 3 mm/year tide-gauge value is the one that is useful for local authorities.

To assemble a time series of sea-level measurements at each tide gauge, the monthly and annual means must be reduced to a common datum. The Revised Local Reference datum at each station is defined to be approximately 7000 mm below mean sea level. This arbitrary choice was made many years ago, to avoid negative numbers in the resulting mean values.

Few places on Earth are completely stable, and most tide gauges are located at sites exposed to tectonic uplift or sinking (vertical change of the land surface). This widespread vertical instability has several causes, and affects the interpretation of data from the individual tide gauges. Much effort is therefore put into correcting for local tectonic movements.

As a result, data from tide gauges located at tectonically stable sites are of special interest. One example of a long, continuous record from such a stable site comes from Korsør, Denmark (Figure 40). This record indicates a stable sea-level rise of 0.83 mm per year since 1897, without any sign of recent acceleration. As the tectonic correction for this particular station is zero, the recorded sea-level rise of 0.83 mm per year is the relevant value for local planning authorities.

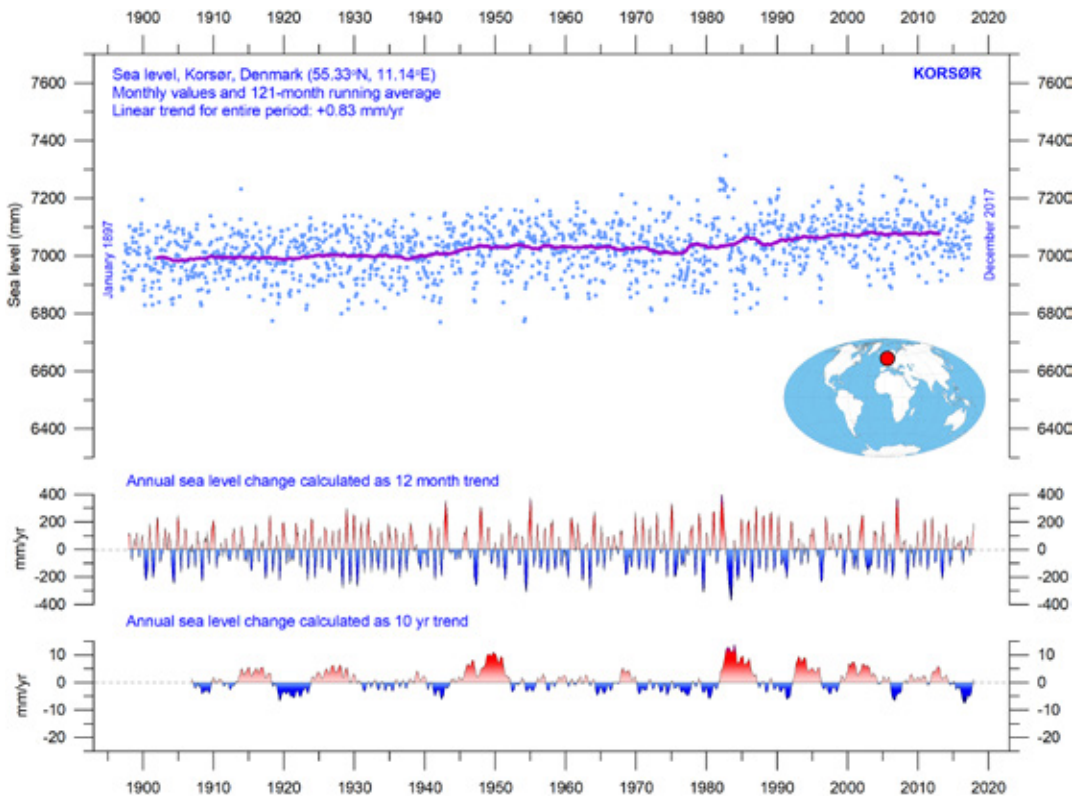

Figure 40: Korsør (Denmark) monthly tide gauge data

From PSMSL Data Explorer. The blue dots are the individual monthly observations, and the purple line represents the running 121-month (ca. 10-year) average. The two lower panels show the annual sea level change, calculated for 1- and 10-year time windows, respectively. These values are plotted at the end of the interval considered.

It is interesting to compare tide-gauge records from different places on the planet. Holgate (2007) suggested nine specific stations that would capture the global variability found in a larger number of stations over the previous half century. However, some of the stations he suggested have not reported values for several years now, leading to the Southern Hemisphere now being seriously underrepresented in his dataset. Therefore, in Figure 48, alternative long tide-gauge series have been included, to provide a more balanced representation of the two hemispheres (15 stations in total).

The early part of the global tide-gauge record has only a small number of stations. For that reason, in this report only observations from 1900 and after are considered. These data, from tide gauges all over the world, suggest an average global sea-level rise of 1–2 mm/year (Figure 41), while, as already noted, the modern satellite-derived record (Figure 39) suggests a rise of about 3.4 mm/year, or more. The difference between the two data sets is remarkable. It is, however, known that satellite observations face several complications in areas near the coast. Vignudelli et al. (2019) provide an updated overview of the current limitations of classical satellite altimetry in coastal regions. An increased rate of sea-level rise since 2015 may be suggested in the composite record in Figure 41, but it remains to be seen if this is the result of one of the recurrent variations displayed in the lower panel of that figure.

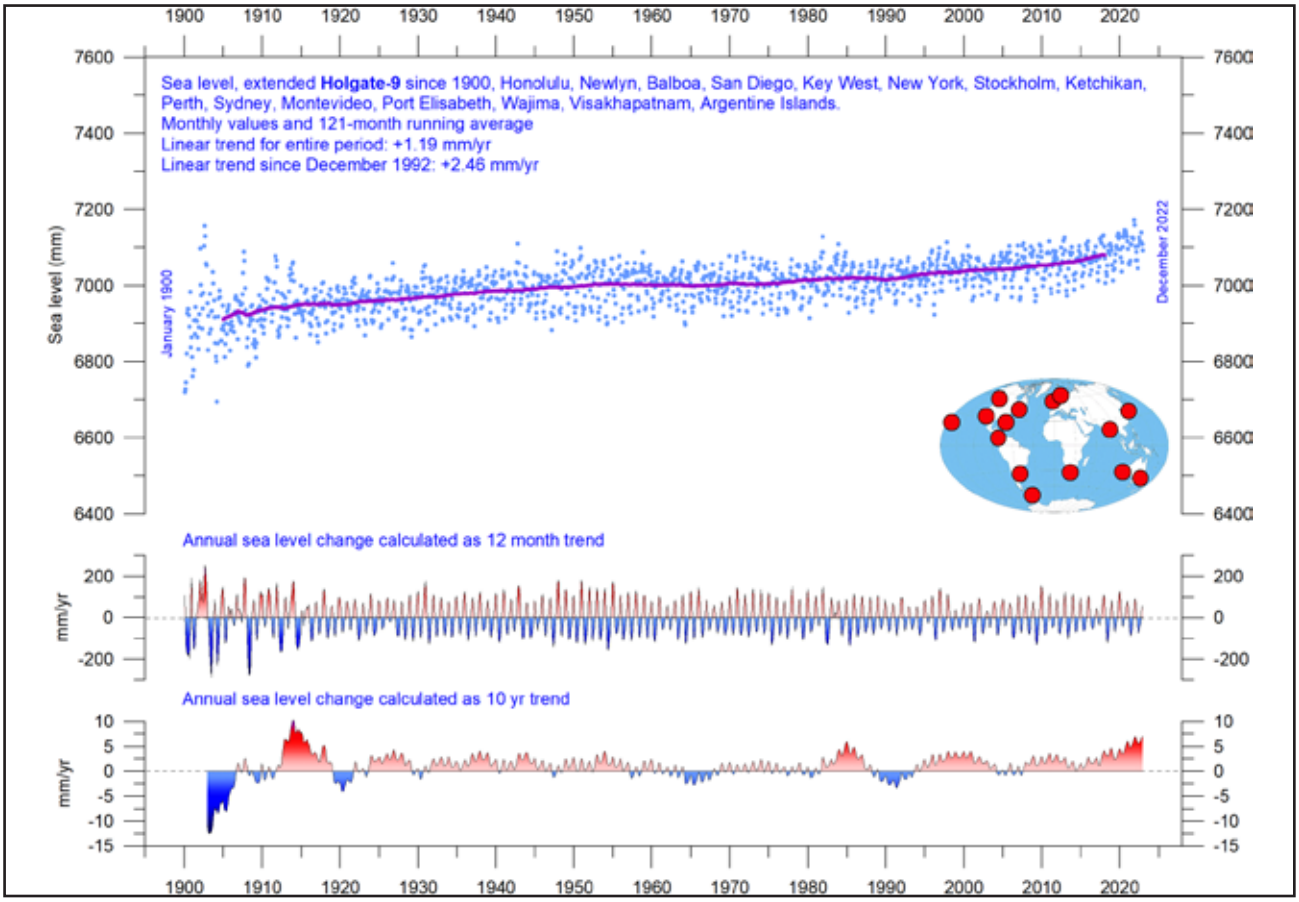

Figure 41: Holgate-9 monthly tide gauge data from PSMSL Data Explorer

The Holgate-9 are a series of tide gauges located in geologically stable sites. The two lower panels show the annual sea level change, calculated for 1- and 10-year time windows, respectively. These values are plotted at the end of the interval considered. Source: Colorado Center for Astrodynamics Research at University of Colorado at Boulder. The blue dots are the individual observations, and the purple line represents the running 121-month (ca. 10-year) average.

Sea level modelled for the future

The issue of sea-level change, and particularly the identification of a hypothetical human contribution to it, is a complex topic. Given the accompanying scientific and political controversy, the great public interest in this area is entirely understandable.

A recent IPCC publication, the Sixth Assessment Report from Working Group I, was released on 9 August 2021. Modelled global and regional sea-level projection data for 2020–2150 were published and are available from the IPCC AR6 Sea Level Projection Tool (link available at the end of this report). The IPCC models the future development of several factors: glacier mass change, vertical land movement, and water temperature and storage. Sea-level projections for different emissions scenarios were calculated relative to a baseline defined by the observations for 1995–2014.

It is enlightening to compare the modelled data with observed sea-level data. Figure 42 shows this for one location, namely Oslo, in Norway. Northern Europe was covered by the European Ice Sheet 20–25,000 years ago, with more than 2 km of ice over the location of the modern city at the maximum glaciation. Today, the effect of this ice load is clearly demonstrated by the fact that southern Norway experiences an ongoing isostatic land rise of several millimetres per year. At many sites in Europe and North America affected by the last (Weichselian/Wisconsin) glaciation, this ongoing isostatic movement more than compensates for the slow global sea-level rise, so a net sea-level decrease in relation to land is recorded.

As Oslo was covered by thick ice during the last glaciation, it is affected by a marked isostatic land rise today. If the observed sea-level change rate at Oslo continues (based on about 110 years of observations), by 2100, the level relative to the

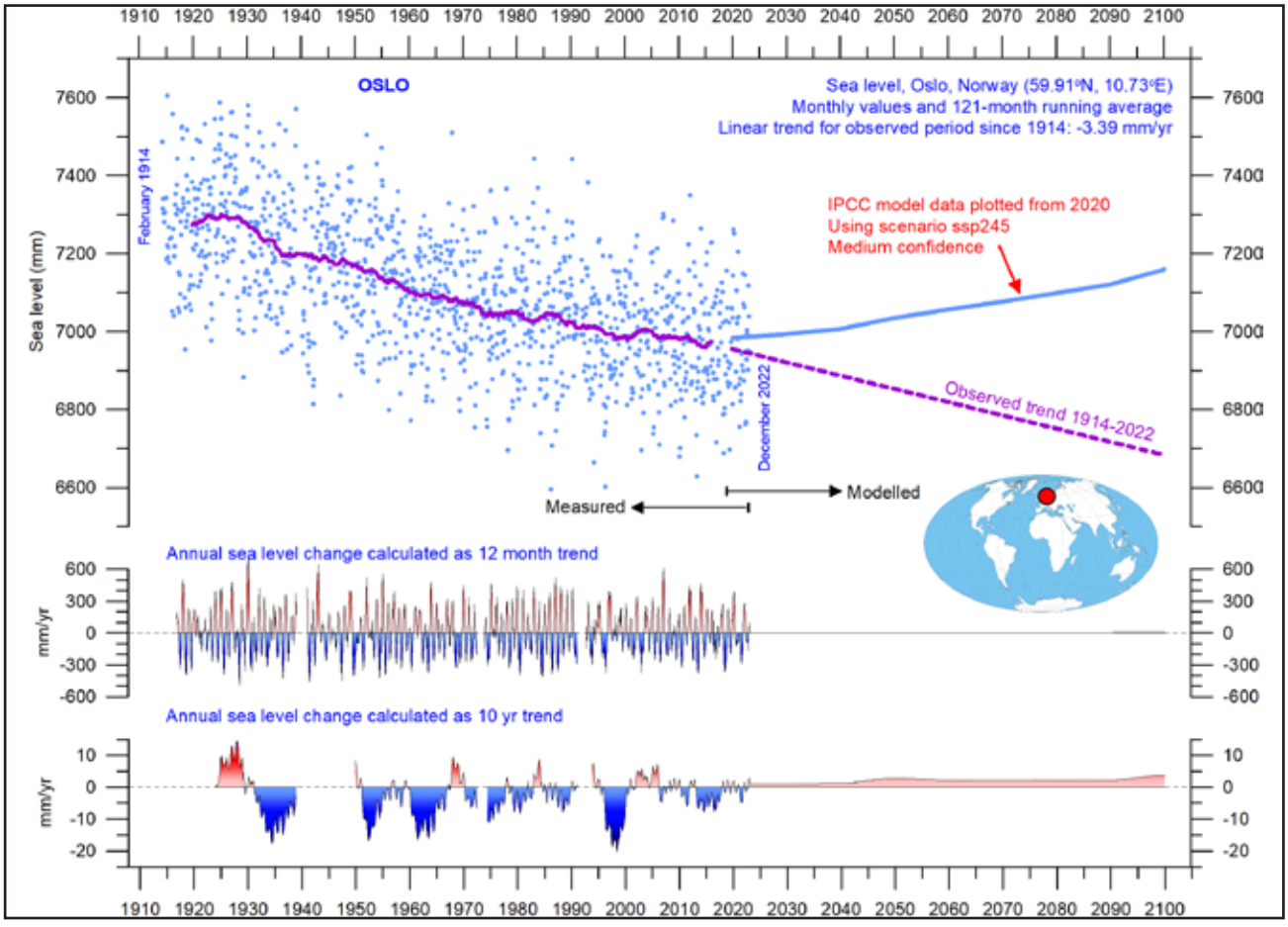

Figure 42: Observed and modelled sea level for Oslo.

The blue dots are the individual monthly tide gauge observations (PSMSL Data Explorer) 1914–2019, and the purple line represents the running 121-month (ca. 10-year) average. The modelled data for the future is shown by a solid blue line 2020–2100, using the moderate SSP2–4.5 scenario (IPCC 2020). The two lower panels show the annual sea-level change, calculated for 1- and 10-year time windows, respectively. These values are plotted at the end of the interval considered.

land will have fallen by about 27 cm relative to 2020 (Figure 42). However, according to the IPCC, it will have increased by about 17.5 cm. The IPCC projects a rather sudden increase in around 2020, which contrasts with the stable sea-level decline of –3.39 mm/year observed since 1914. Observed (measured) and modelled data now have an overlap of three years (Figure 42). The overlap period is still short, and a good comparison is difficult. The observed data, however, seem to suggest an unbroken sea-level decrease at Oslo since 2020, in contrast to the model projection (blue line in Figure 42). Again, time will tell.

A few reflections might be appropriate at this point. The step change in relative sea-level dynamics suggested by the IPCC for Oslo (and for many other coastal sites) in 2020 appears rather implausible and suggests that the modelled data is not describing the real-world dynamics adequately. This is remarkable, as the modelled sea-level projections for the different SSP scenarios are calculated relative to a baseline defined by observations for 1995–2014 for each station. The modelers must therefore have inspected the observed data.

According to the Sixth Assessment Report, human activities are estimated to have caused approximately 1.0°C of global warming above pre-industrial levels, with a likely range of 0.8–1.2°C (Summary for Policymakers, A.1.3). It is therefore particularly surprising that the modelled effect of this change should first affect sea levels in the shape of a step change in 2020. Had the modelers instead calibrated their sea-level data from an earlier date, say 1950, which would have been entirely possible, the contrast between observed and modelled data would immediately have become apparent.

8. Snow and ice

Sea-ice extent

The two 12-month average sea-ice extent graphs in Figure 43 display the contrast between the two poles over the period 1979–2020. The Northern Hemisphere sea-ice trend – towards smaller extent – is clear in the blue line, and so is the simultaneous increase in the Southern Hemisphere until 2016. In many respects, this and previous observations presented in this report suggest that the years 2016–2021 may feasibly mark an important shift in the global climate system (see, e.g., ocean temperatures in Figure 26).

The Antarctic sea-ice extent decreased extraordinary rapidly during the Southern Hemisphere spring of 2016, much faster than in any previous spring during the satellite era (since 1979). This retreat was seen in all sectors of the Antarctic but was greatest in the Weddell and Ross Seas. In these sectors, strong northerly (warm) surface winds pushed the sea ice back towards the Antarctic continent. The background for the unusual wind conditions in 2016 has been discussed by various authors (e.g. Turner et al. 2017 and Phys.org 2019), and appears to be a phenomenon related to natural climate variability. The satellite sea-ice record is still short and does not fully represent natural variations playing out over more than a decade or two.

What can be discerned from the still short record is nevertheless instructive. The two 12-month average graphs in Figure 43 show recurring variations superimposed on the overall trends. These shorter variations are influenced by a 4.3-year periodic variation for the Arctic sea ice, while for the Antarctic sea ice a cycle of about 3.3 years' duration is important.

Figure 44 illustrates the overall extent and thickness of the Arctic sea-ice from the end of 2022 to the end of 2023. Thickness has decreased somewhat along the coast of the Canadian Archipelago, presumably the result of rapid melting during the summer of 2023, while both thickness and extent have been increasing along the east coast of Greenland during 2023. These developments are detailed in Figure 45.

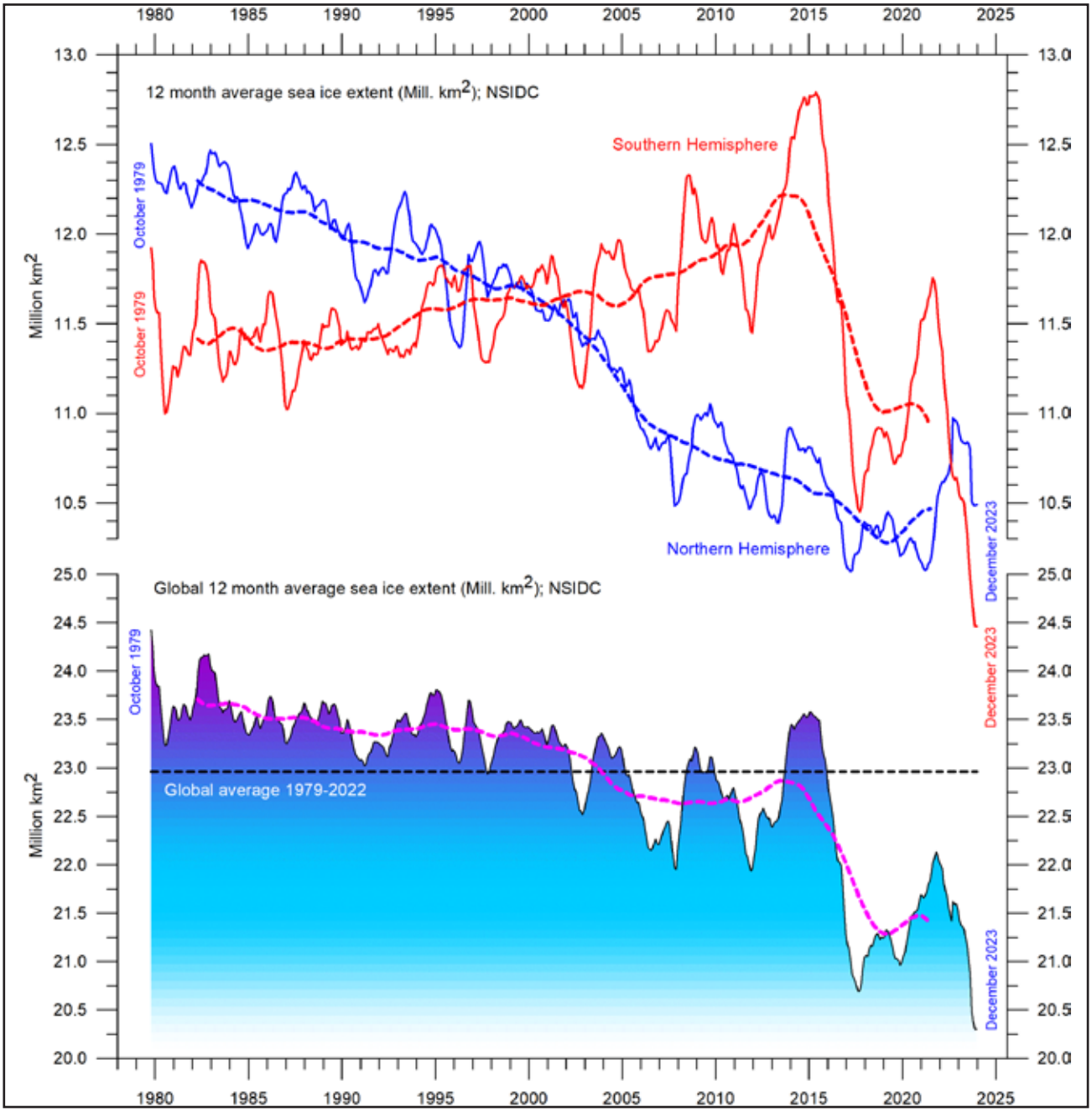

Figure 43: Global and hemispheric sea ice extent since 1979

12-month running means. The October 1979 value represents the monthly average of November 1978–October 1979, the November 1979 value represents the average of December 1978–November 1979, etc. The stippled lines represent a 61-month (ca. 5 years) average. The last month included in the 12-month calculations is shown to the right in the diagram. Data source: National Snow and Ice Data Center (NSIDC).

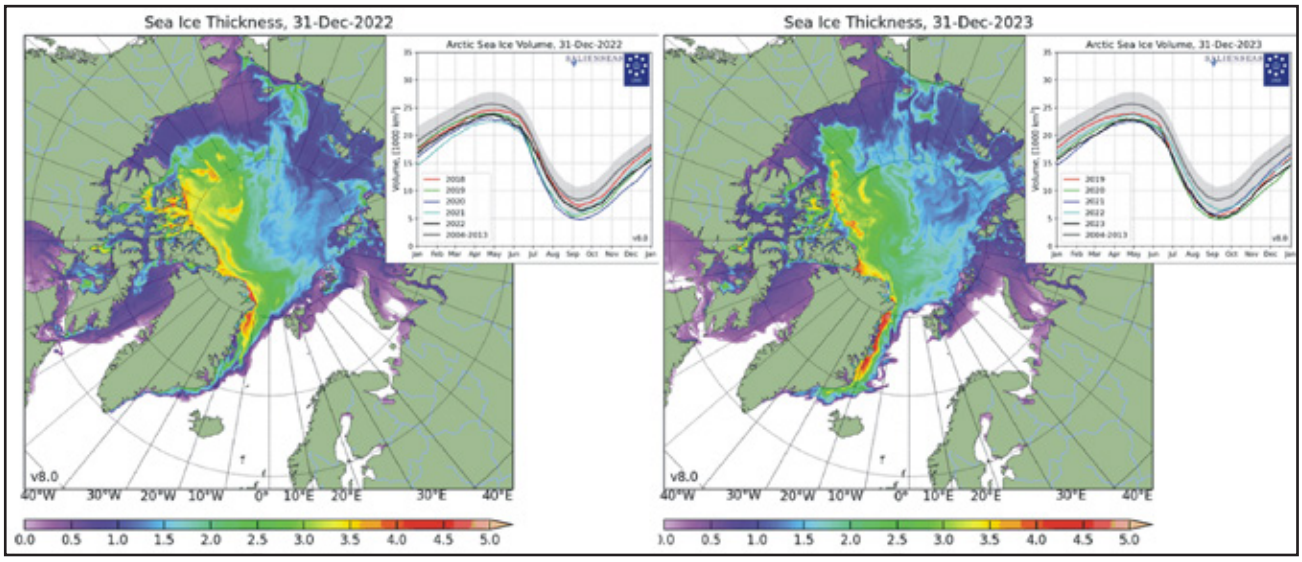

Figure 44: Arctic sea ice 2022 versus 2023

Arctic sea-ice extent and thickness 31 December 2022 (left) and 2023 (right) and the seasonal cycles of the calculated total arctic sea ice volume, according to the Danish Meteorological Institute (DMI). The mean sea ice volume and standard deviation for the period 2004–2013 are shown by grey shading in the insert diagrams.

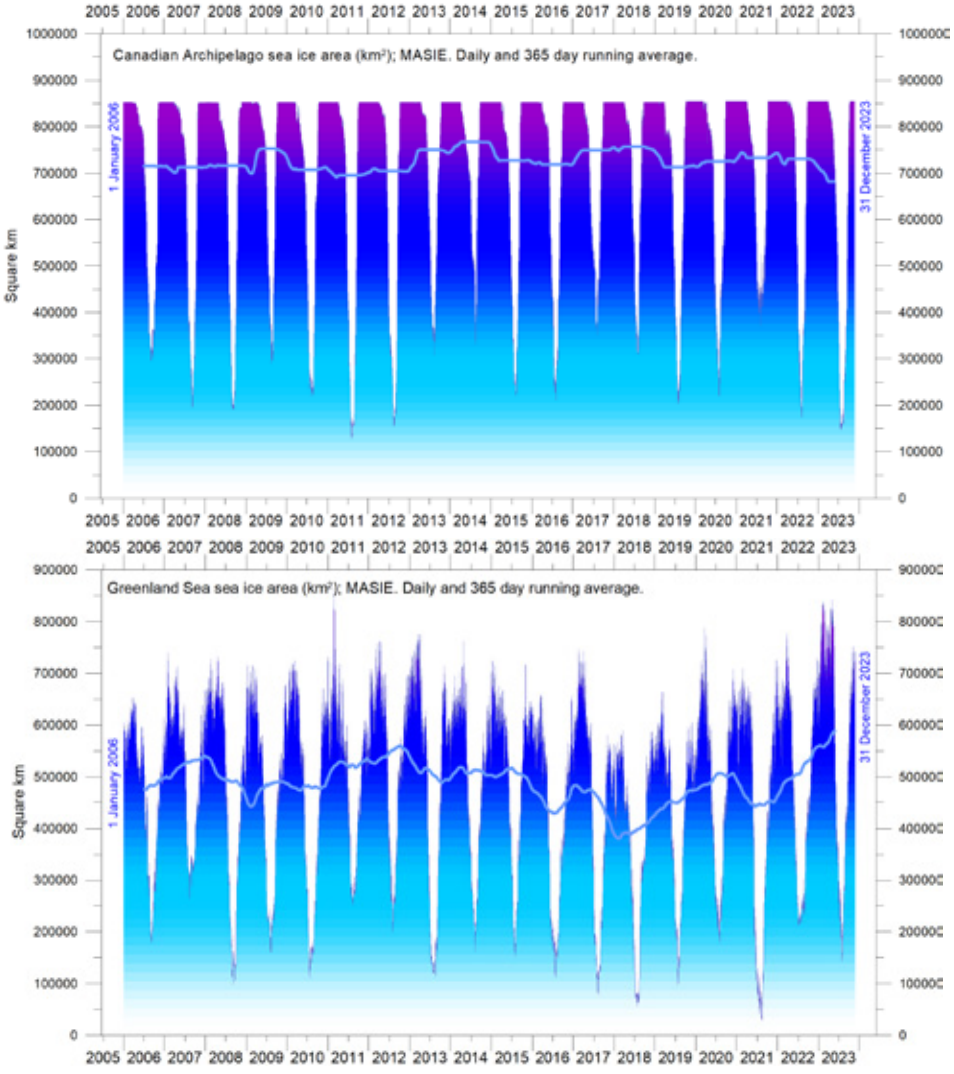

Figure 45: Daily sea ice extent in the Canadian Archipelago and in the Greenland Sea since 2006.

(a) Canadian Archipelago, (b) Greenland Sea. Source: Multisensor Analyzed Sea Ice Extent (MASIE)..

Northern Hemisphere snow cover

Variations in the global snow cover are mainly the result of changes playing out in the Northern Hemisphere (Figure 46), where all the major land areas are located. The Southern Hemisphere snow cover is essentially controlled by the size of the Antarctic ice sheet, and therefore relatively stable.

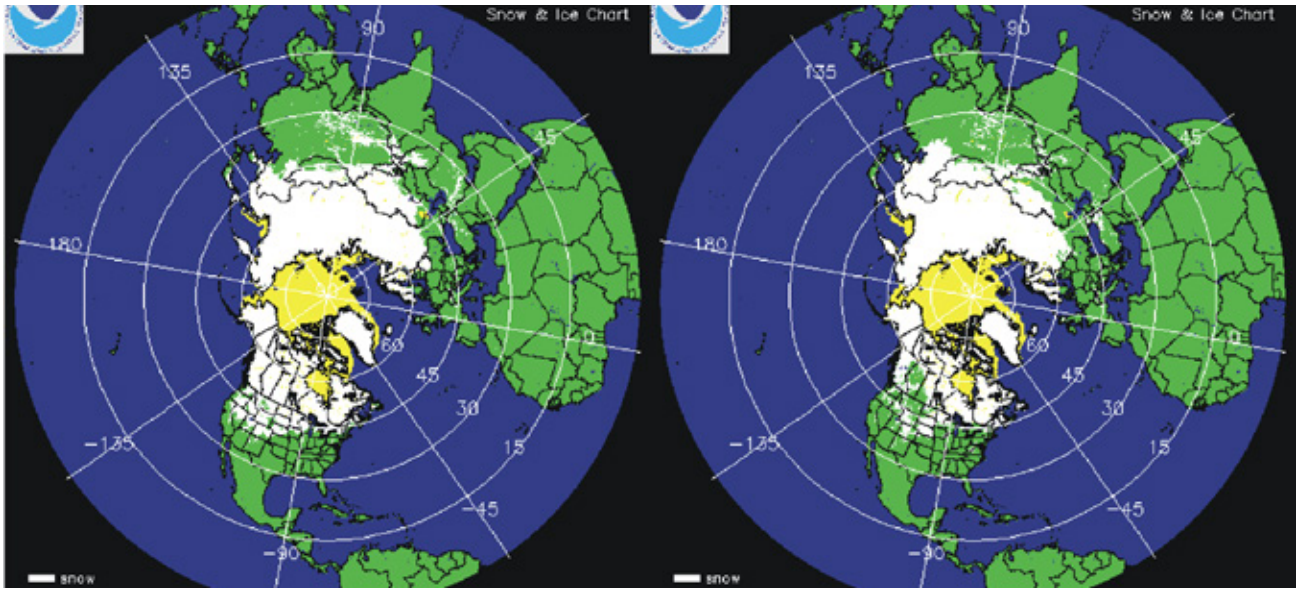

Figure 46: Northern hemisphere snow and sea ice

Snow cover (white) and sea ice (yellow) 31 December 2021 (left) and 2022 (right). Map source: National Ice Center (NIC).

Northern Hemisphere snow cover exhibits large local and regional variations from year to year. However, the overall tendency (since 1972) is towards quasi-stable conditions, as illustrated in Figure 47. During the Northern Hemisphere summer, the snow cover usually shrinks to about 2,400,000 km^2 (principally controlled by the size of the Greenland ice sheet), but during the winter it increases to about 50,000,000 km^2, representing no less than 33% of planet Earth's total land area. Northern Hemisphere maximum snow cover usually occurs in February, and the minimum in August (Figure 47).

A Fourier-analysis (not shown here) suggests the Northern Hemisphere record is influenced, not only by the annual cycle, but probably also by a longer one, of about 6.5 years' duration.

Considering seasonal changes (Figure 48), the Northern Hemisphere snow cover has slightly increased during autumn, is stable at mid-winter, and is slightly decreasing in spring. In 2023, the Northern Hemisphere extent was close to the 1972–2022 average (Figure 47).

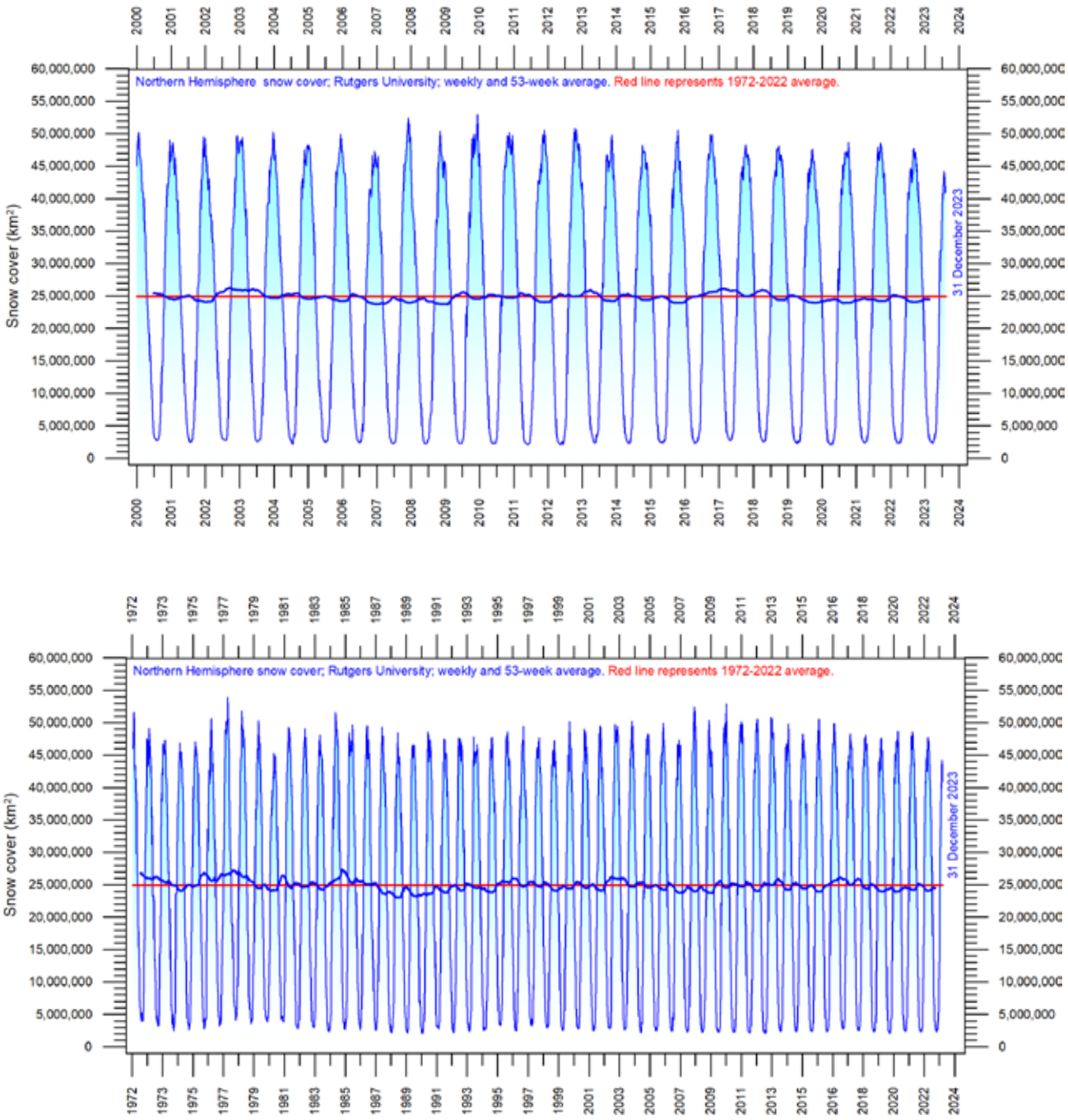

Figure 47: Northern hemisphere weekly snow cover since 2000

(a) Since January 2000 and (b) Since 1972. Source: Rutgers University Global Snow Laboratory. The thin blue line is the weekly data, and the thick blue line is the running 53-week average (approximately 1 year). The horizontal red line is the 1972–2022 average.

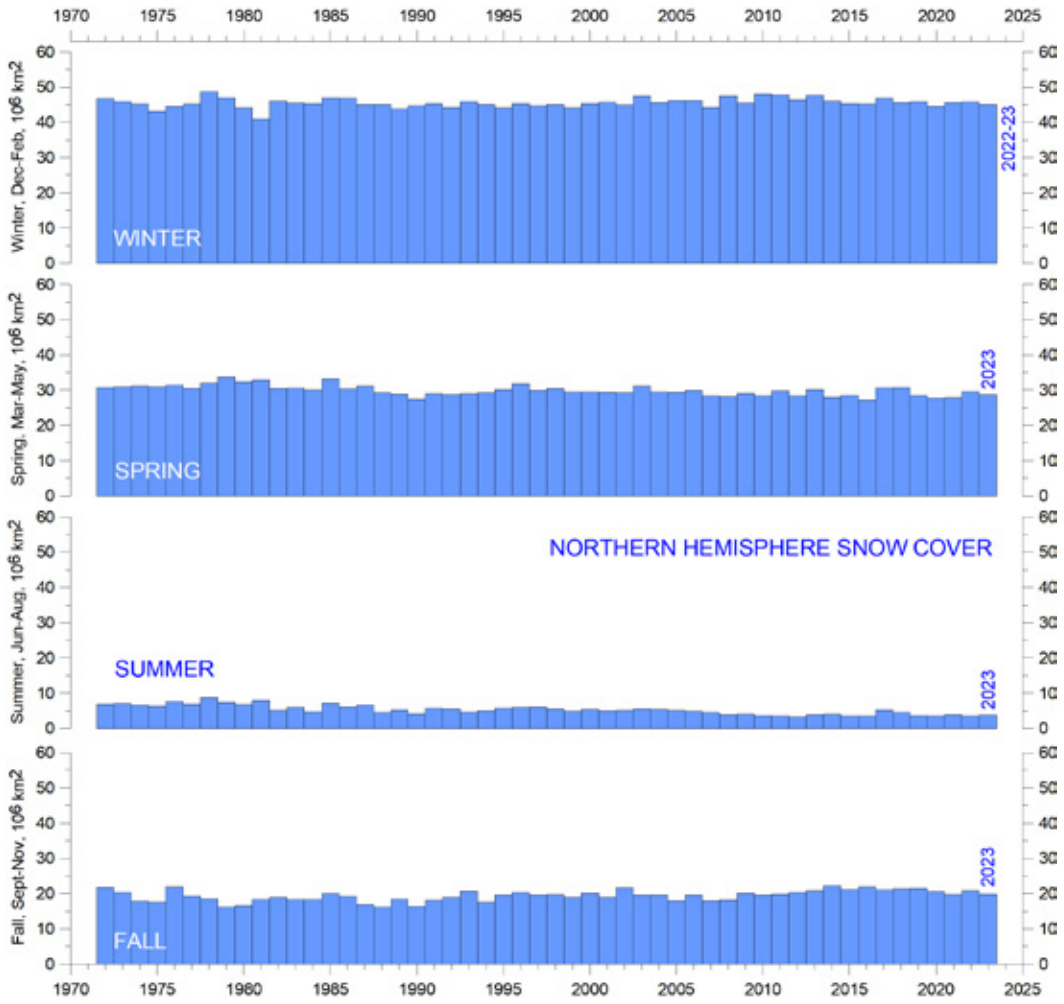

Figure 48: Northern Hemisphere seasonal snow cover since 1972

Source: Rutgers University Global Snow Laboratory. .

9. Precipitation

Annual regional precipitation (rain, snow) varies from more than 3000 mm/year to almost nothing (Figure 49). The global average precipitation undergoes variations from one year to the next, and the calculated annual anomaly in relation to the 1901–2021 average is shown in Figure 50. Annual variations in the global average precipitation up to ±30 mm/year are not unusual. The global precipitation was especially high in 1956, 1973 and 2010, and especially low in 1941, 1965, 1987 and 1992.

A Fourier frequency analysis (not shown here) reveals the global precipitation anomaly (Figure 50) to be influenced by a significant cycle of 5.6 years' duration, and feasibly also by one lasting 3.6 years. The 3.6- and 5.6-year cycles are also found in the SOI and PDO data (Figures 36 and 37, respectively).

Precipitation is part of the global hydrological cycle, and is essential for life on Earth. In addition, the hydrological cycle also transfers huge amounts of energy, so is significant for meteorology and global climate. When snow, ice or water evaporates from the planet's surface and rises as vapour into the atmosphere, it carries heat from the sun-heated surface with it, thereby cooling the surface. Later, when the water vapour condenses to form cloud droplets and precipitation, the heat is released into the atmosphere. This process represents a significant part of Earth's energy budget and climate.

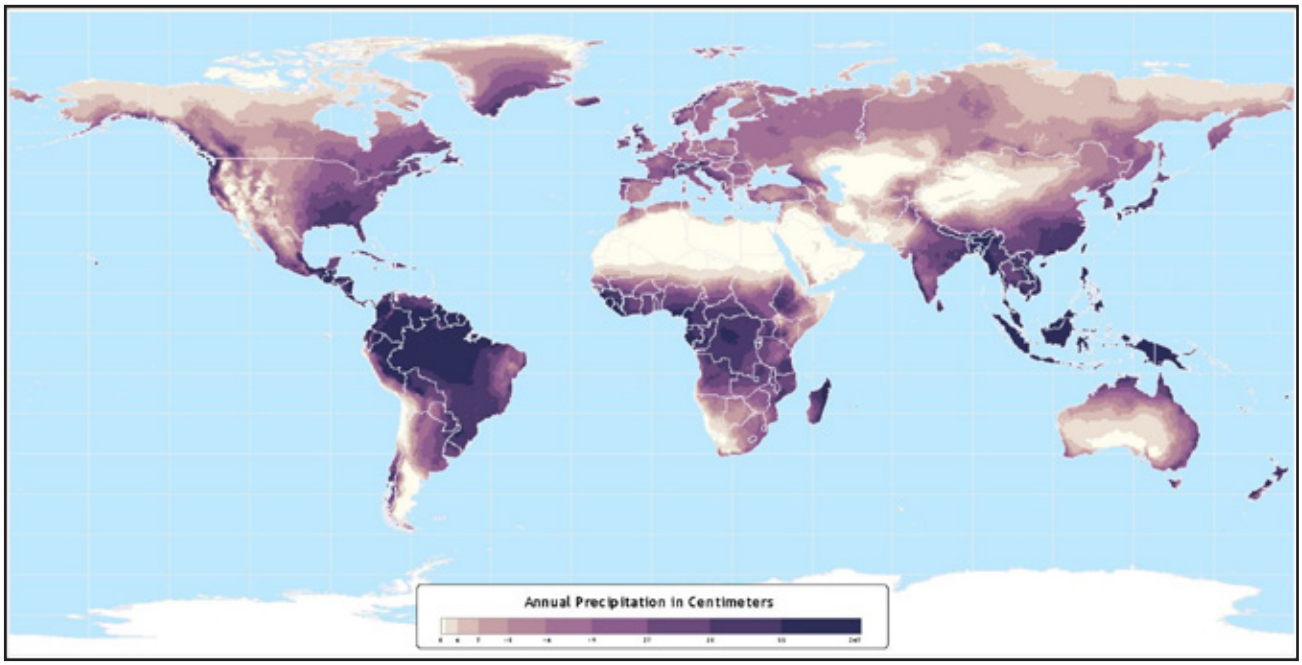

Figure 49: Annual precipitation over land, 1960–90.

Source: NASA/Atlas of the Biosphere. .

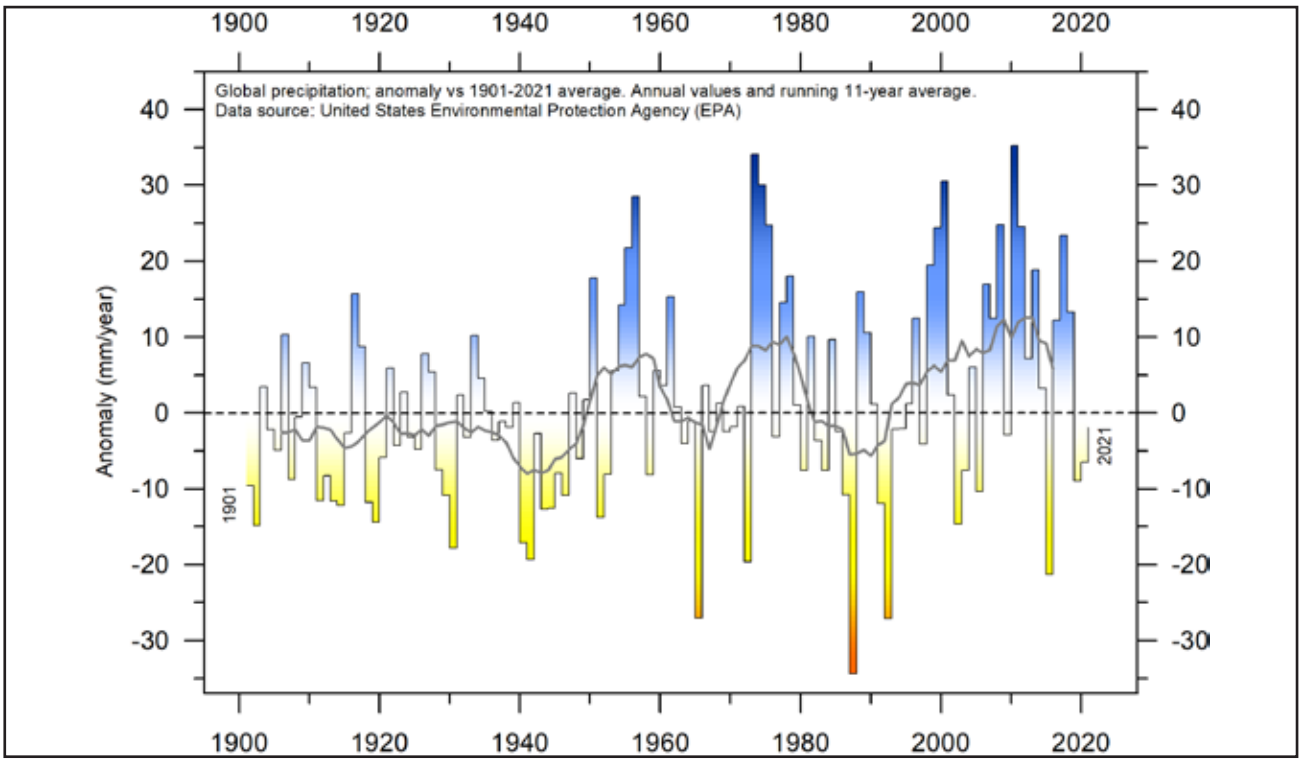

Figure 50: Global precipitation anomalies.

Variation of annual anomalies in relation to the global average precipitation from 1901 to 2021 based on rainfall and snowfall measurements from land-based weather stations worldwide. Data source: United States Environmental Protection Agency (EPA)..

10. Storms and wind

Tropical storm and hurricane accumulated cyclone energy

Accumulated cyclone energy (ACE) is a measure used by the National Oceanic and Atmospheric Administration (NOAA) to express the activity of individual tropical cyclones and entire tropical cyclone seasons. ACE is calculated as the square of the wind speed every six hours and is then scaled by a factor of 10,000 for usability. It is expressed in units of 10^4 knots^2. The ACE of a season is the sum of the ACE for each cyclone, and therefore encapsulates the number, strength, and duration of all the tropical storms in the season. The ACE data and ongoing cyclone dynamics are detailed in Maue (2011).

The damage potential of a hurricane is proportional to the square of the maximum wind speed, and thus ACE is not only a measure of tropical cyclone activity, but also a measure of the damage potential of an individual cyclone or a season.

Existing records (Figure 51) do not suggest any abnormal activity in recent years. The global ACE data since 1970 display a variable pattern over time, but without any clear trend (Figure 51). A Fourier analysis (not shown here) indicates oscillations of about 11.5- and 3.6-years' duration for the global data and suggest a longer one, of about

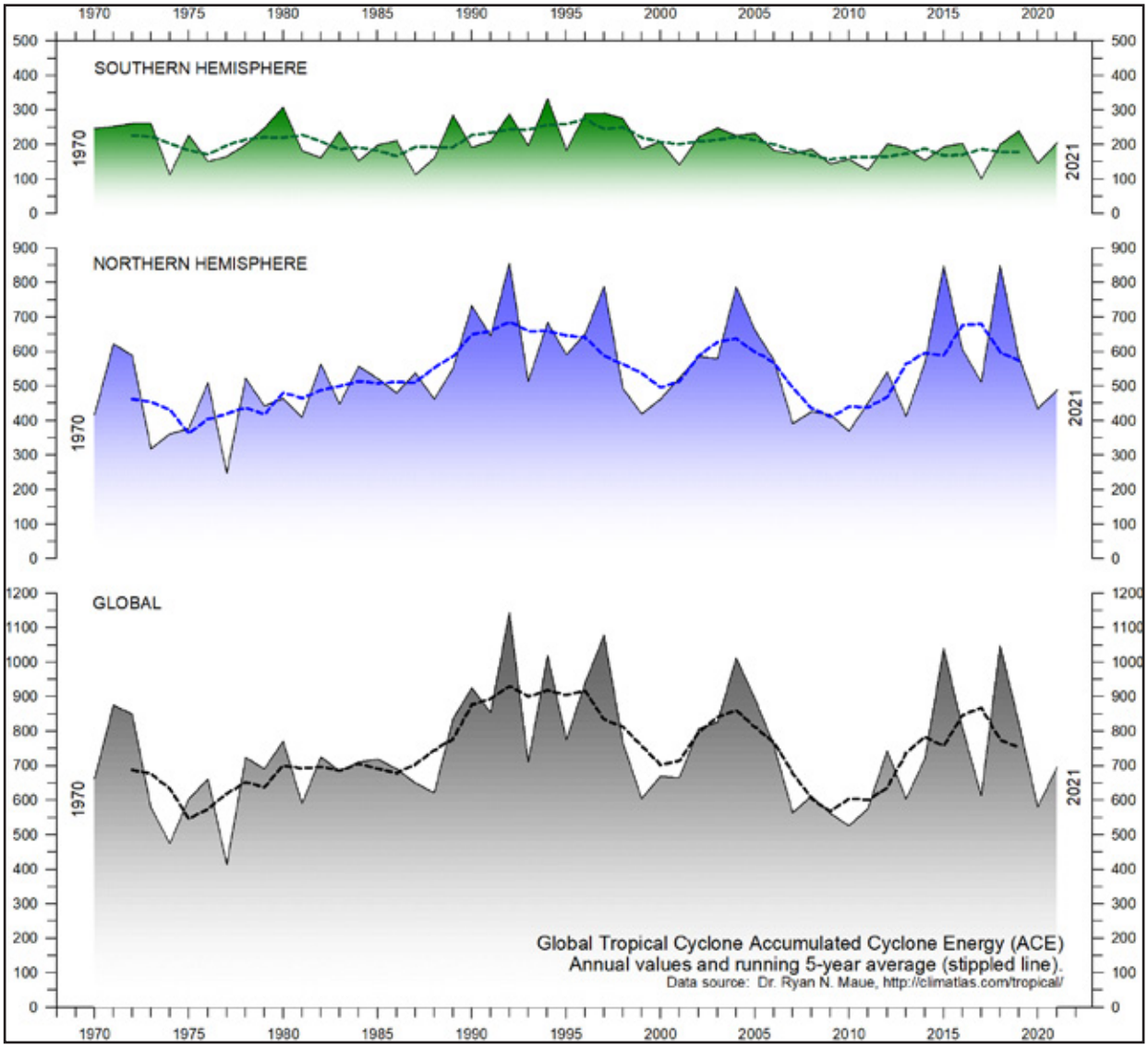

Figure 51: Annual global accumulated cyclone energy

Source: Ryan Maue.

33 years' duration, but the series is too short for firm conclusions to be drawn.

The period 1989–1998 was characterised by high ACE values. Other peaks were seen in 2004, 2015 and 2018. The periods 1973–1988, 1999–2003 and 2006–2014 were characterised by comparatively low activity. The peaks in 1997/98 and 2016 coincide with strong El Niño events in the Pacific Ocean (Figure 25). Northern Hemisphere ACE values (central panel in Figure 51) dominate the global signal (lower panel) and therefore the peaks and troughs are similar to the global data, without any clear trend over the length of the record. The Northern Hemisphere's main cyclone season is June–November. The Southern Hemisphere ACE values (upper panel in Figure 51) are generally lower than for the Northern Hemisphere, and the main cyclone season is December–April.

The Atlantic Oceanographic and Meteorological Laboratory ACE data series goes back to 1850. A Fourier analysis (not shown here) for the Atlantic Basin (Figure 52) shows the ACE series to be influenced by a important cycle of 61.5 years' duration, and feasibly also by one lasting 5.6 years. The Atlantic Basin hurricane season often shows above-average activity when La Niña conditions are present in Pacific during late summer (August–October), as was the case in 2017 (Johnstone and Curry, 2017). The Eastern Pacific Basin data series is shorter, starting in 1971 (Figure 53), and is influenced by an important cycle of 2.4-years' duration, and feasibly also by a longer one of about 28 years. An ACE peak was apparently reached during 2015–18, but future observations will decide if this conjecture is true or not.

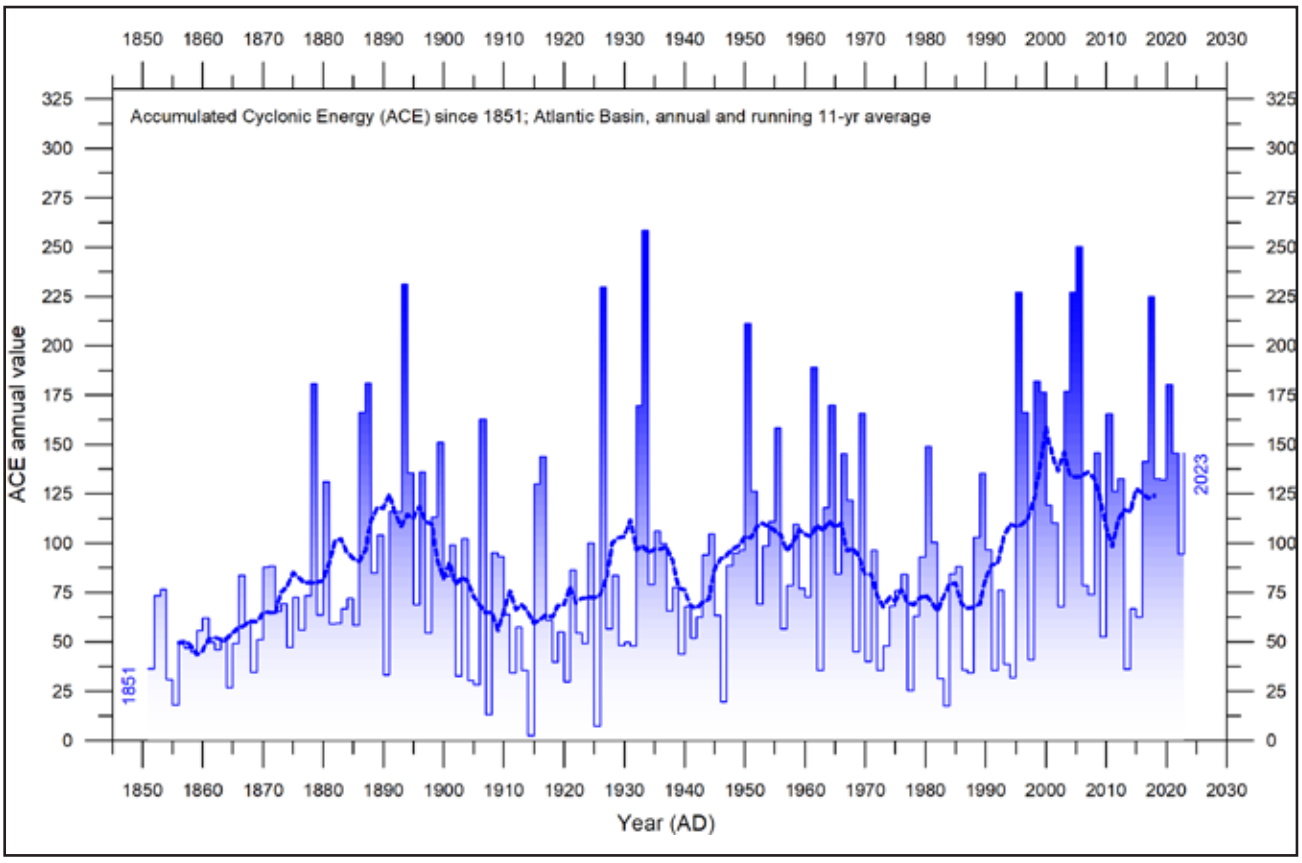

Figure 52: Atlantic Basin ACE since 1851

Thin lines show annual ACE values, and the thick line shows the running 7-year average. Data source: Atlantic Oceanographic and Meteorological Laboratory (AOML), Hurricane Research Division. Please note that these data are not yet updated beyond 2020.

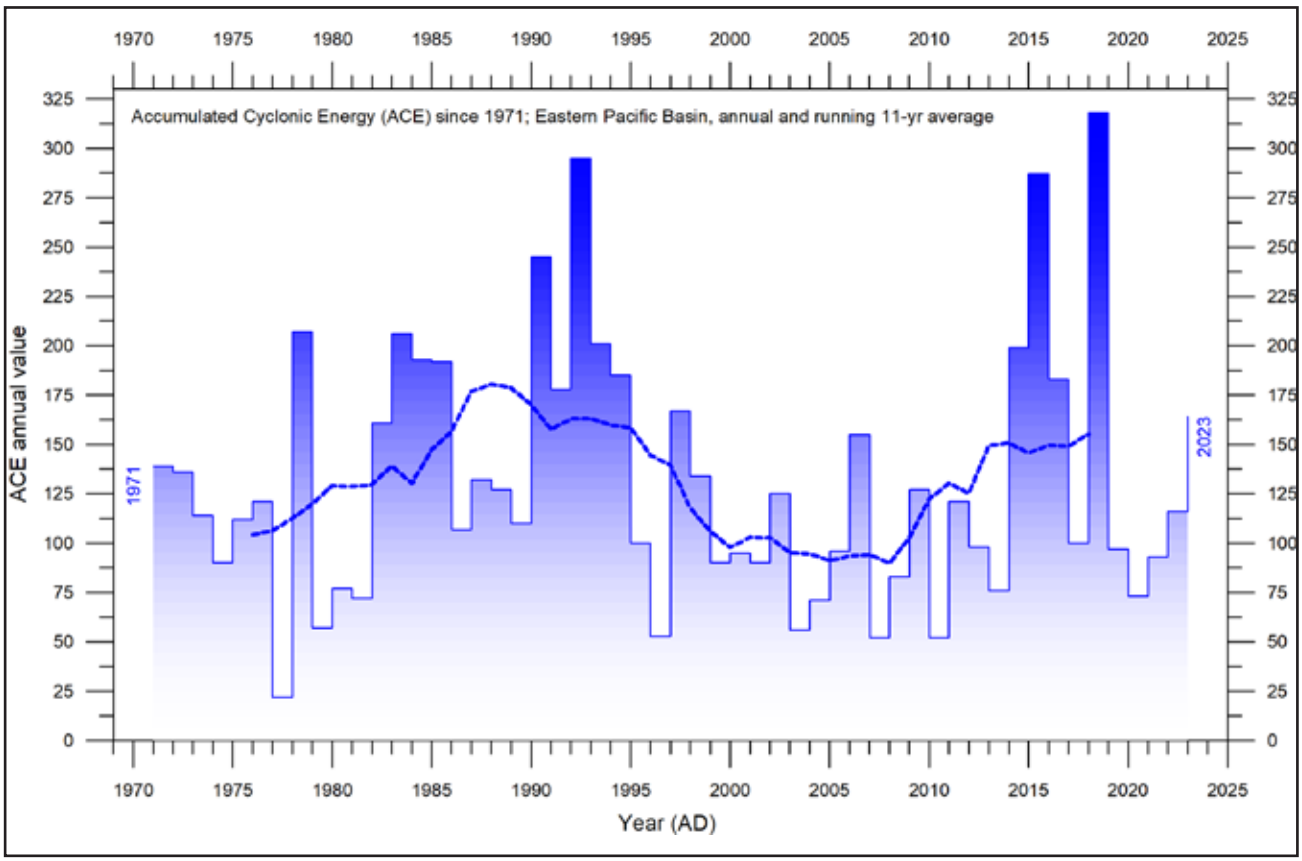

Figure 53: Pacific Basin ACE since 1971

Thin lines show annual ACE values, and the thick line shows the running 7-year average. Pacific Basin ACE-data is not considered reliable before the 1971 season, and therefore not shown here. Data source: ACE data

11. Other storm and wind observations

The number of hurricane landfalls in the continental United States is shown in Figure 54. The series shows considerable variations from year to year, but it is not possible to detect any clear trend over time. A Fourier analysis (not shown here) reveals a statistically significant period of about 3.2 years.

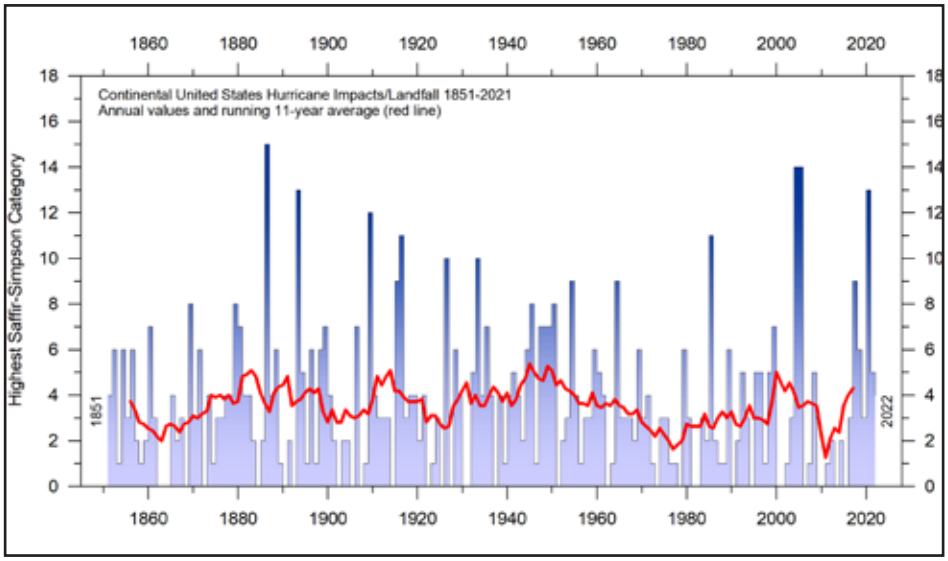

Figure 54: Hurricane landfalls in the continental United States 1851–2022

The highest Saffir-Simpson Hurricane Scale impact in the United States is based upon estimated maximum sustained surface winds produced at the coast. Data source: Hurricane Research Division, NOAA.

An insight into changes in prevailing wind conditions may be obtained from observations carried out at coastal meteorological stations situated at particularly wind-exposed places. One example is Lista Lighthouse, in southernmost Norway. It sits on an exposed cape at the extreme southwestern edge of the mainland of the country, and thus is well suited to register wind conditions in the adjoining North Sea and the European sector of the North Atlantic. It has a monthly wind record going back to January 1931, as displayed in Figure 55. This shows that peak wind strengths were recorded shortly after World War II and have since declined somewhat, to some degree mirroring the record of US hurricane landfalls (Figure 54); that is, on the opposite shore of the North Atlantic.

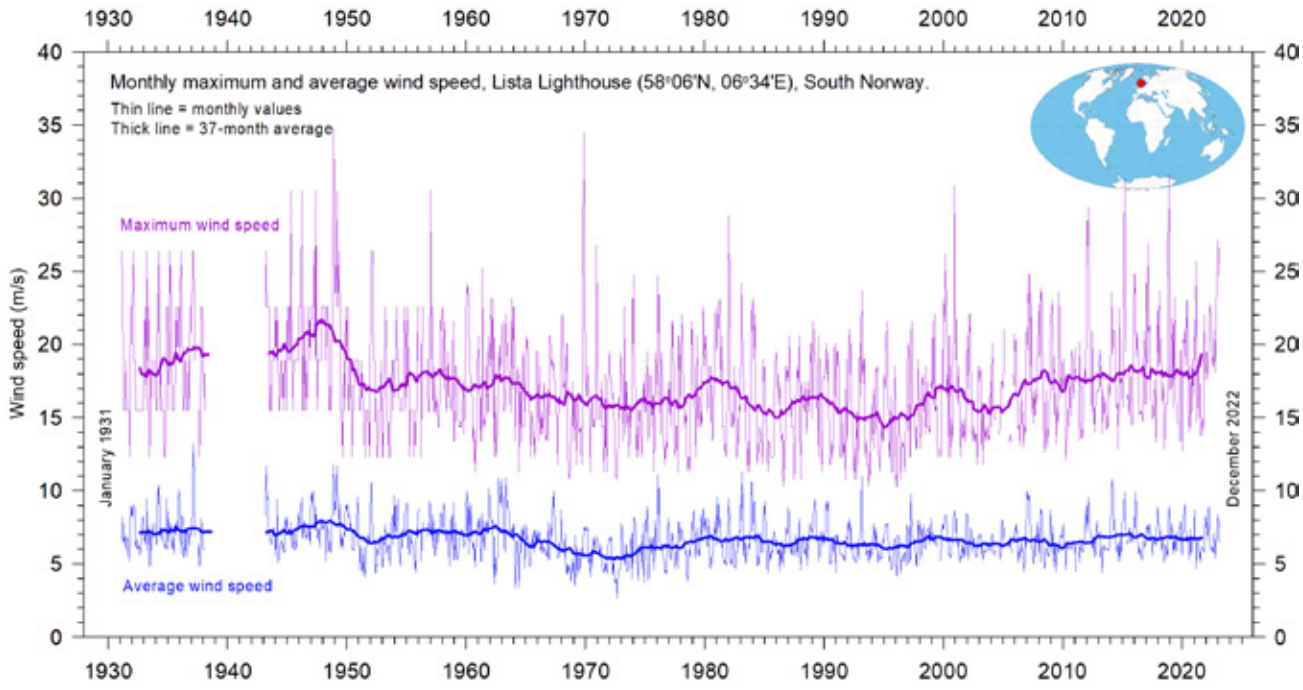

Figure 55: Monthly maximum and average wind speed since January 1931 measured at Lista Lighthouse, South Norway

Lista Lighthouse is situated on an exposed cape located at the extreme southwestern edge of mainland Norway, in a position to register wind conditions in the adjoining North Sea and the European sector of the North Atlantic. Data source: SeKlima.

12. Summary for 2023

Atmosphere

Surface air temperatures, or rather their deviation from the average calculated for a chosen reference period, are central to many climate deliberations. However, the significance of any short-term warming or cooling recorded in these datasets should not be overstated. Firstly, focusing on averages tends to hide the fact that all people deal with much larger temperature variations daily. Secondly, whenever Earth experiences warm El Niño or cold La Niña episodes (Figure 25), major heat exchanges take place between the Pacific Ocean and the atmosphere above, eventually showing up as a signal in the global air temperature. However, this does not reflect similar changes in the total heat content of the atmosphere-ocean system. In fact, global net changes may be small, and such heat exchanges may chiefly reflect redistribution of energy between ocean and atmosphere. Evaluating the dynamics of ocean temperatures is therefore just as important as evaluating changes of surface air temperatures.

Relative to the whole observational period since 1850/1880, 2023 was warm, and all databases used in this report have 2023 as the warmest year on record. A strong El Niño episode established itself during the year, affecting large areas around the Equator (Figures 13 and 22), explaining the high 2023 annual global surface air temperature. This underlines the remarkable importance of ocean-atmosphere exchanges mentioned above.

Since 1979, lower Troposphere temperatures have increased over both land and oceans, but more over land (Figure 12). The most straightforward explanation for this observation is that a significant part of the observed warming is caused by solar insolation, but there may be several supplementary explanations, such as differences in heat capacity and changes in cloud cover and land use.

Many Arctic regions experienced record high air temperatures in 2016, but since then conditions generally have turned toward somewhat cooler conditions (Figure 14). However, this changed again in 2023, possibly marking another temperature peak. Presumably, the Arctic temperature peaks in 2016 and 2023 were affected by ocean heat released from the Pacific Ocean during strong El Niños and subsequently transported towards the North Pole. This highlights how Arctic air temperatures may be affected, not only by variations in local conditions, but also by variations playing out in distant regions.

Many diagrams in this report focus on the time from 1979 and ahead, reflecting the commencement of the satellite era, and the advent of a wide range of observations with nearly global coverage, including temperature. These new data provide a detailed view into temperature changes over time at different altitudes in the atmosphere. Among other phenomena, these observations reveal that a Stratospheric temperature plateau has prevailed since 1995 (Figure 16).

Water vapour is the most important greenhouse gas in the Troposphere. The highest concentration is found within a latitudinal range from 50°N to 60°S. The two polar regions of the Troposphere are comparatively dry. Water vapour is a much more important greenhouse gas than carbon dioxide, both because of its absorption spectrum and its higher concentration. The specific atmospheric humidity since 1948 has been stable or slightly increasing up to about 4–5 km altitude (Figure 17). At higher levels in the Troposphere (about 9 km), the specific humidity has been decreasing for the duration of the record, but with shorter variations superimposed on the falling trend.

The influence of the Hunga Tonga-Hunga Ha'apai eruption January 2022 on atmospheric temperatures 2023 is still uncertain. This eruption released an enormous plume of water vapour into the Stratosphere, but any influence of this on atmospheric temperatures is not apparent (Figure 17).

Carbon dioxide is an important greenhouse gas, although less important than water vapour. Since 1958, there has been an increasing trend in its atmospheric concentration, with an annual cycle superimposed (Figure 18). At the end of 2023, the amount of atmospheric carbon dioxide was close to 422 ppm. The annual change concentration (Figure 19) has been increasing from

about +1 ppm/year in the early part of the record, to about +2.5 ppm/year towards the end of the record. There is no visible effect of the global COVID-19 lockdown 2020–2021 in the atmospheric concentration.The increasing amount of atmospheric carbon dioxide is enhancing photosynthesis and thereby global crop yields.

Oceans

The Argo program has now achieved 20 years of global coverage, growing from a relatively sparse array of 1000 profiling floats in 2004, to more than 3900 in December 2023. Since their inception, these have provided a unique ocean temperature dataset for depths down to 1900 m. The data is currently updated to December 2021. Although the oceans are much deeper than 1900 m, and the dataset is still relatively short, interesting features are now emerging (Figure 26).

Longwave (infrared) radiation penetrates less than 100 microns into the oean (Hale and Querry, 1973), while shortwave solar radiation penetrates much further, down to about 150–200 m. Below 200 m there is rarely any significant light. Ocean surface heating is therefore essentially a Sun-driven process.

Since 2004, the upper 1900 m of the oceans have globally experienced net warming of about 0.037°C. The maximum net warming (about 0.2°C) affects the uppermost 100 m of the oceans (Figure 28). This is seen mainly in regions near the Equator, where the greatest amount of solar radiation is received. At greater depths, a small (about 0.025°C) net warming has occurred between 2004 and 2021.

This development in the global average ocean temperatures is generally reflected across the Equatorial oceans, between 30°N and 30°S, with the exception of a slight cooling at 300–500 m depth. A temperature peak may possibly have been passed around 2019–2020 (Figure 26). Because of the spherical form of the planet, the Equatorial oceans represent a huge surface area, and have a correspondingly significant impact on global surface air temperatures.

Simultaneously, the northern oceans (55–65°N) have on average experienced a marked cooling down to 1400 m depth, and slight warming at below that (Figure 29). At present, a temperature recovery may be in process in parts of the North Atlantic (Figure 33). The southern oceans (55–65°S) have on average seen some warming at most depths since 2004, but mainly near the surface, above 200 m depth. However, averages may be misleading, and quite often better insight is obtained by studying the details, as discussed previously in this report.

The record of El Niño and La Niña episodes since 1950 is influenced by a significant 3.6-year cycle, and feasibly also by a 5.6-year cycle.

Sea level

Sea level is monitored by satellite altimetry and by direct measurements using tide-gauges situated along coasts. While the satellite-derived record suggests a global sea level rise of about 3.4 mm per year or more (Figure 39), data from tide gauges all over the world suggest a smaller average global sea-level rise, of about 1–2 mm per year (Figure 41). The tide-gauge measurements do not indicate any clear recent acceleration (or deceleration), but the record is characterised by recurrent variations. The marked difference (a ratio of about 1:2) between the two datasets still has no universally accepted explanation, but it is known that satellite observations of sea level are complicated in areas near the coast (see, e.g. Vignudelli et al. 2019). Either way, for local coastal planning the tide-gauge data is preferred, as described in this report.

Sea ice

In 2023, the global sea-ice extent remained well below the average for the satellite era (since 1979), but in recent years there has been a stable or even rising global trend (Figure 43). At the end of 2016, the global sea-ice extent reached a marked minimum, at least partly caused by the operation of two different natural variation patterns characterising sea ice in the Northern- and the Southern Hemisphere, respectively. Both variations had simultaneous minima in 2016, with resulting

consequences for the global sea-ice extent. The marked Antarctic 2016 sea-ice reduction was also affected by unusual wind conditions. The opposite development, towards stable or higher ice extent at both poles, may have begun around 2018, and has since been augmented, especially in the Northern Hemisphere.

Snow cover

Variations in the global snow-cover extent is mainly caused by changes in the Northern Hemisphere, where all the major land areas are located. The Southern Hemisphere snow-cover extent is essentially determined by the size of the Antarctic Ice Sheet, and is therefore relatively stable. The Northern Hemisphere average snow cover extent has also been essentially stable since the onset of satellite observations (Figure 44), although local and regional interannual variations may be large. Considering seasonal changes since 1979, the Northern Hemisphere snow-cover in autumn is slightly increasing, the mid-winter extent is basically stable, and the spring extent is slightly decreasing (Figure 48). In 2023, the Northern Hemisphere seasonal snow cover extent was near the 1972–2022 average.

Global precipitation

Annual precipitation (rain, snow) varies from more than 3000 mm/year in wet regions to almost nothing in desert regions (Figure 49). The global average precipitation, however, undergoes variations from one year to the next, and regional annual variations up to ±30 mm/year from the long-term global average are not unusual. The global precipitation was especially high in 1956, 1973 and 2010, and especially low in 1941, 1965, 1987 and 1992 (Figure 50). Fourier frequency analysis shows the global precipitation anomaly to be influenced by 3.6- and 5.6-year cycles. This periodicity is also see in the Southern Oscillation (SOI) and the Pacific Decadal Oscillation (PDO), respectively.

Storms and hurricanes

The most recent data on global tropical storm and hurricane accumulated cyclone energy (ACE) is well within the range recorded since 1970. The global ACE data display a variable pattern over time, but without any clear trend towards higher or lower values (Figure 51). A Fourier analysis indicates oscillations of about 11.5- and 3.6-years' duration for the global data and also suggests a longer one, of about 33-year length, but the data series is to short to allow firm conclusions to be drawn. A longer ACE series for the Atlantic Basin (since 1850), suggests natural rhythms of 61.5 years' duration, and feasibly also one of 5.6 years. Modern data on the number of hurricane landfalls in the continental United States remain within the normal range throughout the entire observational period since 1851 (Figure 54).

Summing up

The global climate system is multifaceted, involving sun, planets, atmosphere, oceans, land, geological processes, biological life, and complex interactions between them. Many components and their mutual coupling are still not fully understood or perhaps not even recognised. Believing that one minor constituent of the atmosphere (CO_2) controls nearly all aspects of climate is naïve and entirely unrealistic. The global climate has remained in a quasi-stable condition within certain limits for millions of years, although with important variations playing out over periods ranging from years to centuries or more, but the global climate has never been in a fully stable state without change. Modern observations show that this behaviour continuese today; there is no evidence of a global climate crisis.

13. Written references

Carter R.M., de Lange W., Hansen, J.M., Humlum O., Idso C., Kear, D., Legates, D., Mörner, N.A., Ollier C., Singer F. & Soon W. 2014. Policy Brief, NIPCC, 24. September 2014, 44 pp. http://climatechangereconsidered.org/wp-content/uploads/2014/09/NIPCC-Report-on-NSW-Coastal-SL-9z-corrected.pdf.

Chylek, P., Folland, C. K., Lesins, G., and Dubey, M. K. 2010. Twentieth century bipolar seesaw of the Arctic and Antarctic surface air temperatures. , 37, L08703, doi:10.1029/2010GL042793.

Hale, G. M. and M. R. Querry, 1973. , Applied Optics, v. 12, no. 3, pp. 555-563. https://doi.org/10.1364/AO.12.000555.

Holgate, S.J. 2007. On the decadal rates of sea level change during the twentieth century. *Geophys. Res. Letters*, 34, L01602, doi:10.1029/2006GL028492.

Humlum, O., Stordahl, K. and Solheim, J-E. 2012. The phase relation between atmospheric carbon dioxide and global temperature. *Global and Planetary Change*, August 30, 2012. http://www.sciencedirect.com/science/article/pii/S0921818112001658?v=s5.

Johnstone, J. and Curry, J. 2017. *Causes and Predictability of the Exceptionally Active 2017 Atlantic Hurricane Season*. Climate Forecast Applications Network (CFAN), 9 pages. https://curryja.files.wordpress.com/2017/11/hurricane_review_2017-final.pdf.

Maue, R.L. 2011. Recent historically low global tropical cyclone activity. *Geophysical Research Letters*, Vol. 38, L14803, doi:10.1029/2011GL047711.

Parker, A. and Ollier, C.D. 2016: Coastal planning should be based on proven sea level data. *Ocean & Coastal Management*, Vol. 124, p.1-9. https://doi.org/10.1016/j.ocecoaman.2016.02.005.

Roemmich, D. and J. Gilson, 2009. The 2004-2008 mean and annual cycle of temperature, salinity, and steric height in the global ocean from the Argo Program. *Progress in Oceanography*, 82, 81-100.

Turner et.al. 2017. Unprecedented springtime retreat of Antarctic sea ice in 2016. *Geophysical Research Letters*, Vol.44(13), p. 6868-6875. https://doi.org/10.1002/2017GL073656.

Vignudelli et al. 2019. Satellite Altimetry Measurements of Sea Level in the Coastal Zone. *Surveys in Geophysics, Vol.* 40, p. 1319–1349. https://link.springer.com/article/10.1007/s10712-019-09569-1.

Voortman, H. 2023: Robust validation of trends and cycles in sea level and tidal amplitude. *Journal of Coastal and Hydraulic Structures*, 3, 32pp. https://doi.org/10.59490/jchs.2023.0032.

14. Links to data sources, accessed January-February 2024

ACE data: https://en.wikipedia.org/wiki/Accumulated_cyclone_energy.

AMO, Earth System Research Laboratory, NOAA, USA: https://www.esrl.noaa.gov/psd/data/timeseries/AMO/.

Atlantic Oceanographic and Meteorological Laboratory, Hurricane research Division: http://www.aoml.noaa.gov/hrd/tcfaq/E11.html.

NASA, Atlas of the Biosphere: https://www.jpl.nasa.gov/edu/teach/activity/precipitation-towers-modeling-weather-data/ Credit: Center for Sustainability and the Global Environment, University of Wisconsin - Madison; Climate Research Unit, University of East Anglia.

Continental United States Hurricane Impacts/Landfalls: https://www.aoml.noaa.gov/hrd/hurdat/All_U.S._Hurricanes.html.

Colorado Center for Astrodynamics Research: http://sealevel.colorado.edu/.

Danish Meteorological Institute (DMI): http://ocean.dmi.dk/arctic/icethickness/thk.uk.php.

United States Environmental Protection Agency (EPA): https://www.epa.gov/climate-indicators/climate-change-indicators-us-and-global-precipitation.

Earth System Research Laboratory (ESRL):https://www.esrl.noaa.gov/psd/map/clim/olr.shtml.

SeKlima: https://seklima.met.no/observations/GISS temperature data: https://data.giss.nasa.gov/gistemp/.

Global Marine Argo Atlas: http://www.argo.ucsd.edu/Marine_Atlas.html.

Goddard Institute for Space Studies (GISS): https://www.giss.nasa.gov/.

HadCRUT temperature data: http://hadobs.metoffice.com/.

Hurricane Research Division, NOAA: http://www.aoml.noaa.gov/hrd/tcfaq/E23.html.

Hurricane Research Division, Continental United States Hurricane Impacts/Landfalls: https://www.aoml.noaa.gov/hrd/hurdat/All_U.S._Hurricanes.html.

Multisensor Analyzed Sea Ice Extent (MASIE): https://nsidc.org/data/masie.

National Ice Center (NIC). http://www.natice.noaa.gov/pub/ims/ims_gif/DATA/cursnow.gif.

National Snow and Ice Data Center (NSIDC): http://nsidc.org/data/seaice_index/index.html.

NCDC temperature data: https://www.ncdc.noaa.gov/monitoring-references/faq/.

Ocean temperatures from Argo floats: http://www.argo.ucsd.edu/.

Oceanic Niño Index (ONI): http://www.cpc.ncep.noaa.gov/products/analysis_monitoring/ensostuff/ensoyears.shtml.

Outgoing long wave radiation (OLR): https://www.esrl.noaa.gov/psd/map/clim/olr.shtml.

PDO, NOAA Physical Sciences Laboratory: https://psl.noaa.gov/pdo/.

Permanent Service for Mean Sea Level: http://www.psmsl.org/.

Phys.org 2019: https://phys.org/news/2019-01-antarctica-sea-ice-climate.html.

Plymouth State Weather Center: http://vortex.plymouth.edu/sfc/sst/.

PSMSL Data Explorer: http://www.psmsl.org/data/obtaining/map.html.

Rutgers University Global Snow Laboratory: http://climate.rutgers.edu/snowcover/index.php.

RSS temperature data: http://www.remss.com/measurements/upper-air-temperature.

Sea level from satellites: https://sealevel.colorado.edu/data/2020rel1-global-mean-sea-level-seasonal-signals-retained.

Sea level from tide-gauges: http://www.psmsl.org/data/obtaining/map.html.

Sea level modelled: IPCC AR6 Sea Level Projection Tool: https://sealevel.nasa.gov/data_tools/17.

Sea ice extent Danish Meteorological Institute (DMI): http://ocean.dmi.dk/arctic/icethickness/thk.uk.php.

Southern Oscillation Index (SOI): http://crudata.uea.ac.uk/cru/data/soi/.

Maue ACE data: climatlas.com/tropical/.

UAH temperature data: http://www.nsstc.uah.edu/data/msu/v6.0/tlt/uahncdc_lt_6.0.txt.

Review process

GWPF publishes papers in a number of different formats, each subject to a more or less formal review process. This helps ensure that any materials published by the GWPF are of a proper academic standard, and will serve the GWPF's educational purpose. As a charity, we recognise that educational material should provide any reader the opportunity to understand, and explore different perspectives on a subject.

Our flagship long-form GWPF Reports are all reviewed by our Academic Advisory Council, and are also made available for pre-publication open peer review. We will publish any substantive comments alongside the main paper, provided we are satisfied they will enhance the educational experience of the reader. In this way, we hope to encourage open and active debate on the important areas in which we work.

GWPF Briefings and Notes are shorter documents and are reviewed internally and/or externally as required.

The enhanced review process for GWPF papers is intended to take the content and analysis beyond a typical review for an academic journal:

- More potential reviewers can be involved
- The number of substantive comments will typically exceeds journal peer review, and
- The identity of the author is known to the potential reviewers.

As an organisation whose publications are sometimes the subject of assertive or careless criticism, this review process is intended to enhance the educational experience for all readers, allowing points to be made and considered in context and observing the standards required for an informed and informative debate. We therefore expect all parties involved to treat the reviews with the utmost seriousness.

Final responsibility for publication rests with the Chairman of the Trustees and the GWPF Director. But In every case, the views expressed are those of the author. GWPF has never had any corporate position beyond that dictated by its educational objectives.

About the Global Warming Policy Foundation

People are naturally concerned about the environment, and want to see policies that enhance human wellbeing and protect the environment; policies that don't hurt, but help.

The Global Warming Policy Foundation (GWPF) is committed to providing a platform for educational research and informed debates on these important issues.

In order to make progress and advance effective policy assessments, it is essential to cultivate a culture of open debate, tolerance and learning.

Our aim is to raise standards in learning and understanding through rigorous research and analysis, to help inform a balanced debate amongst the interested public and decision-makers.

We aim to create an educational platform on which common ground can be established, helping to overcome polarisation and partisanship. We aim to promote a culture of debate, respect, and a hunger for knowledge.

RECENT GWPF REPORTS

24	Curry et al.	Assumptions, Policy Implications and the Scientific Method
25	Hughes	The Bottomless Pit: The Economics of CCS
26	Tsonis	The Little Boy: El Niño and Natural Climate Change
27	Darwall	The Anti-development Bank
28	Booker	Global Warming: A Case Study in Groupthink
29	Crockford	The State of the Polar Bear Report 2017
30	Humlum	State of the Climate 2017
31	Darwall	The Climate Change Act at Ten
32	Crockford	The State of the Polar Bear Report 2018
33	Svensmark	Force Majeure: The Sun's Role in Climate Change
34	Humlum	State of the Climate 2018
35	Peiser (ed)	The Impact of Wind Energy on Wildlife and the Environment
36	Montford	Green Killing Machines
37	Livermore	Burnt Offering: The Biomess of Biomass
38	Kelly	Decarbonising Housing: The Net Zero Fantasy
39	Crockford	The State of the Polar Bear Report 2019
40	Darwall	The Climate Noose: Business, Net Zero and the IPCC's Anticapitalism
41	Goklany	The Lancet Countdown on Climate Change: The Need for Context
42	Humlum	The State of the Climate 2019
43	Alexander	Weather Extremes: Are They Caused by Global Warming?
44	Constable	Hydrogen: The Once and Future Fuel?
45	Kessides	The Decline and Fall of Eskom: A South African Tragedy
46	Goklany	Impacts of Climate Change: Perception and Reality
47	Constable	A Little Nudge with a Big Stick
48	Crockford	The State of the Polar Bear Report 2020
49	Alexander	Weather Extremes in 2020
50	Humlum	The State of the Climate 2020
51	Humlum	The State of the Climate 2021
52	Constable	Europe's Green Experiment
53	Montford	Adaptation: The Rational Climate Policy
54	Alexander	Extreme Weather: The IPCC's Changing Tune
55	Ridd	Coral in a Warming World: Causes for Optimism
56	Humlum	The State of the Climate 2022
57	Porter	Prospects for Nuclear Energy in the UK
58	Lesser	Green Energy and Economic Fabulism
59	Kelly et al.	Improving Science Advice to Governments
60	Alexander	Weather Extremes in Historical Context
61	Humlum	The State of the Climate 2023

For further information about the Global Warming Policy Foundation, please visit our website at www.thegwpf.org.
The GWPF is a registered charity, number 1131448.

GWPF